INFORMATION TO USERS

This manuscript has been reproduced from the microfilm master. UMI films the text directly from the original or copy submitted. Thus, some thesis and dissertation copies are in typewriter face, while others may be from any type of computer printer.

The quality of this reproduction is dependent upon the quality of the copy submitted. Broken or indistinct print, colored or poor quality illustrations and photographs, print bleedthrough, substandard margins, and improper alignment can adversely affect reproduction.

In the unlikely event that the author did not send UMI a complete manuscript and there are missing pages, these will be noted. Also, if unauthorized copyright material had to be removed, a note will indicate the deletion.

Oversize materials (e.g., maps, drawings, charts) are reproduced by sectioning the original, beginning at the upper left-hand corner and continuing from left to right in equal sections with small overlaps.

ProQuest Information and Learning
300 North Zeeb Road, Ann Arbor, MI 48106-1346 USA
800-521-0600

UNIVERSITY OF CINCINNATI

May 15 19 48

I hereby recommend that the thesis prepared under my supervision by Michael Field

entitled Studies in the Physics of Metal Cutting

be accepted as fulfilling this part of the requirements for the degree of Doctor of Philosophy

Approved by:

Harold J. Kersten

L.A. Wells

Form 668—G.S. and T.C.—500—5-45

STUDIES IN THE MECHANICS OF METAL CUTTING

A dissertation submitted to the
Graduate School of Arts and Sciences
of the University of Cincinnati
in partial fulfillment of the
requirements for the degree of

DOCTOR OF PHILOSOPHY

1948

by

MICHAEL FIELD

B.M.E. The College of the City of New York - 1937

M.S. Columbia University - 1938

Table of Contents

INTRODUCTION

The process of metal cutting is a vital link in all stages of manufacturing. It would indeed be difficult to think of any product that did not involve, directly or indirectly, some phase of the metal cutting process, namely turning, drilling, milling, shaping, planing, hobbing or boring. The process seemed simple, at least from the standpoint of utilization, and attracted the attention of ingenious mechanics and engineers who devised ways of expanding its usefulness. Thus metal cutting advanced as an art for many years utilizing the principle of trial and error.

The fundamental study of the metal cutting process naturally centered itself about the study of chip formation, i.e., the mechanism by which the tool produced failure in the work material.

H. Tresca[1] in 1873 first carried out chip formation research by planing lead at low cutting speeds with a tool of zero rake angle. He noted that as the tool progressed the work material started to flow over the tool face in an upward direction. Finally the material sheared along a plane extending from the cutting edge to the original surface. Tresca's tests are significant because he was the first one to conceive the important idea of a two dimensional analysis as a means for facilitating research in chip formation.

I. Thime[2] in 1878 extended Tresca's tests by investigating other materials like zinc, bronze, cast iron, and steel.

He recognized the basic difference between the "shear type chip" occurring in the case of tough materials and rupture type chips encountered in the case of brittle materials.

A Haussner[3] in 1892 considered the three dimensional case of chip formation. He had the concept of the built-up edge when referring to "particles of the work material sticking to the tool face and interferring with the chip flow".

G. Sellegran[4] in 1896 used a tool dynamometer to study the cutting force in the direction of the motion of the workpiece. He noted the existence of the shear plane and also distinguished between a continuous chip and a chip that separates.

F. W. Taylor[5] in 1906 published his classic book "On the Art of Cutting Metals" which presented the results of empirical research on problems of tool life, tool forces and production.

E. G. Coker[6] in 1925 utilized photoelastic methods in the study of chip formation.

Rosenhain and Sturney[7] in 1925 classified chips as "tear" type, "shear" type and "flow" type. The tear and shear type chips refer to discontinuous chips while the flow type refers to the continuous chip. In plunge cutting brass and steel they were able to obtain any of the above mentioned chip types by varying the rake angle and the depth of cut at constant cutting speeds and feeds.

E. G. Herbert[8] in 1926 studied the work hardening properties of metals under cutting conditions. He stated that the built-up edge, when it appeared, actually did the cutting.

The metals are work hardened by deformation in the cutting process. This work hardening was found to be greatly influenced by the temperature at which deformation took place. In most ferrous as well as non-ferrous metals the capacity for work hardening showed a low value at temperatures of about 250 to 300°F.

M. Kronenberg[9, 10] in 1927 published a book "Grundzuge der Zerspanungslehre" in which he analyzed the metal cutting results of many previous investigators. From their combined data he derived two important emperical laws. The cutting speed law $V = \frac{C_v}{E_v \sqrt{1000A}}$, and a cutting force law $F = C_p (1000A)^r$ where V is the cutting speed for some definite tool life, F is the cutting force, A is the chip cross sectional area and the remaining symbols are constants depending upon the work material, tool material, tool angles and cutting fluid. Kronenberg formulated tables for these various constants from data taken from various investigators.

M. Okoshi[11] in 1930 recognized only two types of chips, namely "crack" type and "slip" type. With the first type of chip a gap occurred substantially in the direction of tool motion ahead of the tool. With the second type of chip shear occurred along a shear plane. Okoshi assumed that the friction between the chip and tool was the major cause for the occurrence of either of the two types of chips. When the chip velocity

was small the friction was almost as high as in the case of static friction. Tests on brass showed that a shear type chip could be changed into a crack type chip by roughing the tool face. Okoshi was of the opinion that the shear angle varied with the rake angle of the tool and the work material. He found the shear angle to be a maximum for all materials at a true rake of 30°.

J. Rathja[12] in 1939 simulated "chip formation" by compressing wet sand with profiled tools and also by pulling such tools through sand. A "stagnant" body developed corresponding to Prantl's theory of plastic deformation. The formation of different types of chips was explained by means of slip lines or trajectories. The flow of material is opposed by friction at the tool face and by the resistance of the material. The slip lines form a constant angle with the principal stresses according to the relation $45° - \frac{\tau}{2}$ where τ is the friction angle. Rathja assumed that a shear type chip developed when the slip lines are curved away from the workpiece. On the other hand when the depth of cut is so large that the slip lines are parallel to the work surface or even curved into the work, the stress in these lines excedes the shear strength before the entire chip can flow. In these cases a "rupture" chip develops. The slip lines are directed toward the surface in the cases of large values of true rake which favor formation of the shear type chip.

M. Okoshi and S. Fukui[13] in 1933 made photoelastic

tests, took stationary and moving pictures together with force measurements and also observed the deformation of the material using a network of lines on the workpieces. Okoshi prepared a diagram of the principal shearing stresses. It was found by comparison with motion pictures that the fragments sheared along one of these lines. The shear lines always start at the cutting edge at a slight curve away from the edge towards the work surface.

A. Rupp[14] in 1937 working with A. Schwerd utilized three principal methods for investigating elastic and plastic deformation of the stress field, namely 1) network of lines on the workpiece, 2) photomicrographs and 3) roughness produced on a polished and etched disc when planed on a lathe.

F. Schwerd[15] in 1932 worked with high speed motion pictures using a spark illumination method which allowed exposures of 10^{-7} seconds and time intervals between frames of as little as 1/10 milli-seconds. Schwerd attempted to simplify chip types by using terms indicating the type of stresses which cause the formation of the respective type chip, namely "tensile chip", "shear chip" and "segmental type chip". The tensile type chip is produced by tensile stresses and occurs primarily in the case of brittle materials. The shear type chip develops when the tangential stresses are greater than the tensile stresses. The built-up edge may or may not occur with this type. The segmental type chip differs somewhat from the shear type chip although both result from tangential

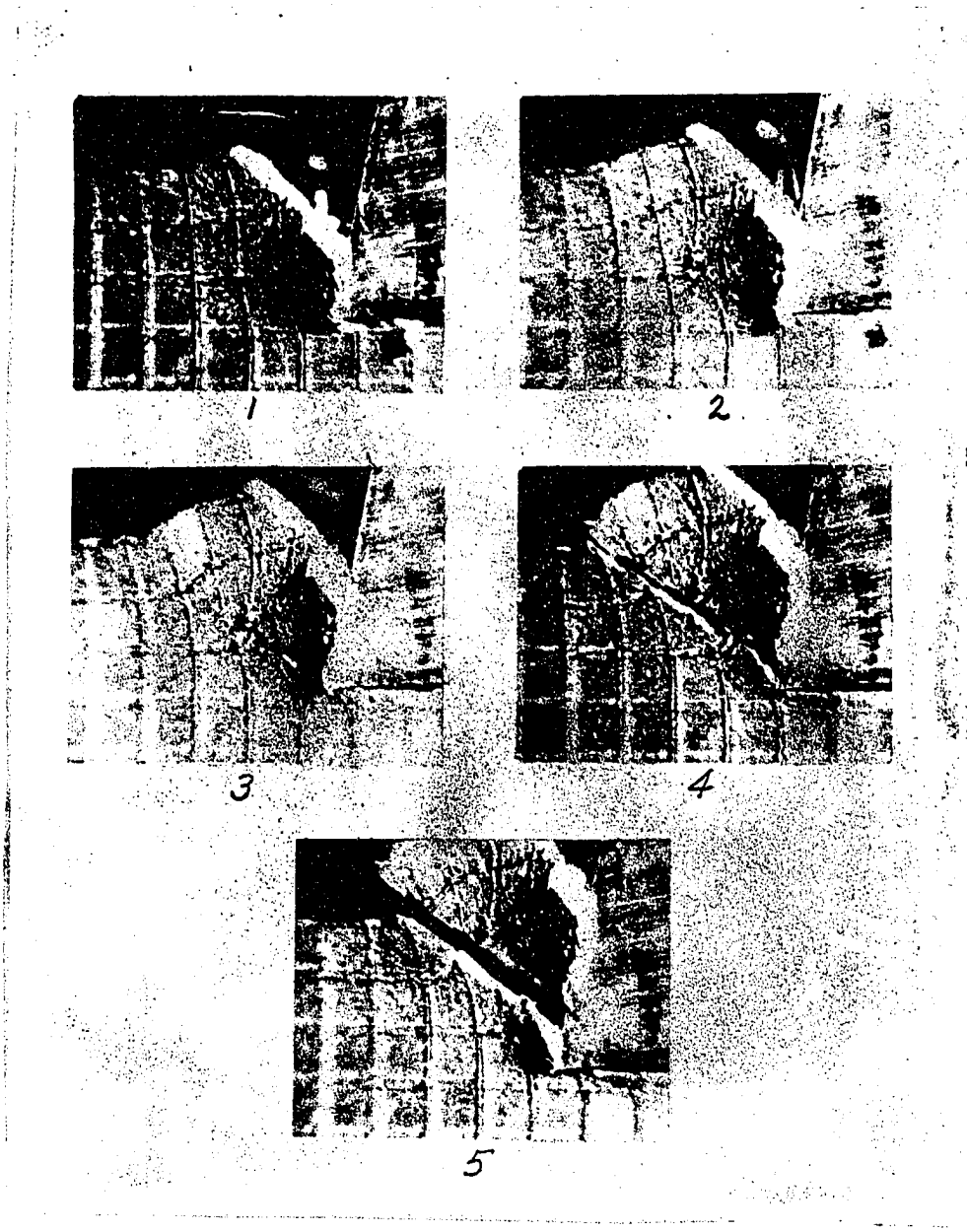

Figure 1

stresses. Segmental type chips are produced when steady flow of the shear type chip is interrupted at regular intervals causing a break in the chip. This type chip is produced by vibrations within a tool or work holding system.

H. Ernst and M. Martellotti[16] in 1935 studied the process of formation of the built-up edge. They took motion pictures of bronze being planed in which a discontinuous chip was produced. These photos, Fig. 1, were used by the author to initiate the study of the discontinuous chip.

H. Ernst[17] in 1938 clearly described and classified what are now considered to be the three basic forms of chips: Type 1, the discontinuous or segmental chip; Type 2, the continuous chip; and Type 3 the continuous chip with the built-up edge, Fig. 2. Ernst stated that a compressed layer or "built-up edge" is formed with all three types of chips. However, with

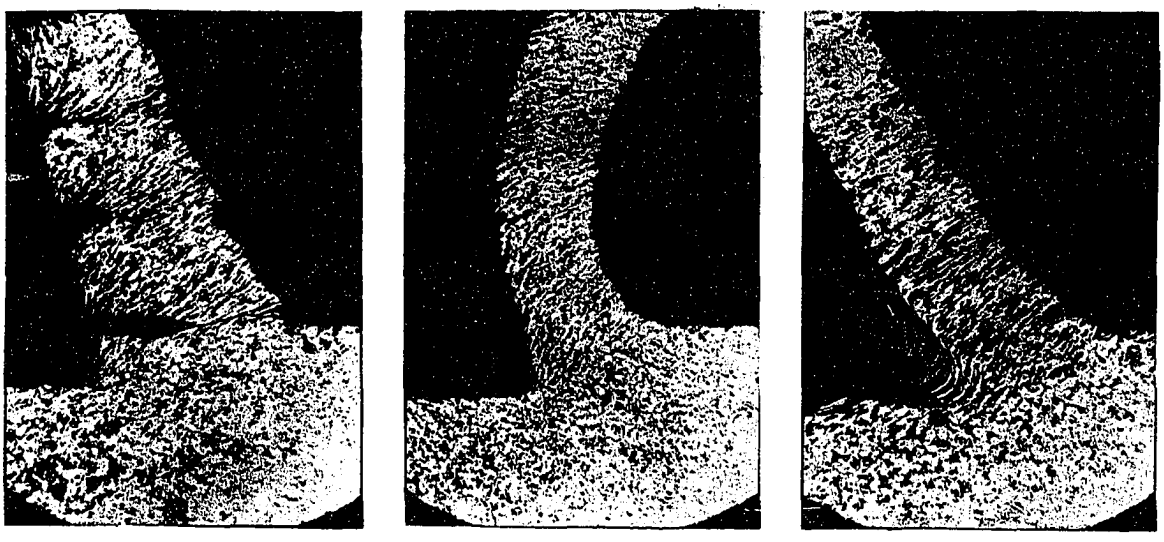

Type 1 Type 2 Type 3

Figure 2

Type 1 chip this initially compressed layer passes off with each segment. With Type 2 chip the layer continuously escapes with the chip. With Type 3 chip this layer remains anchored to the tool face to form a built-up edge while the chip body shears away from it and passes off above. As the stationary pile of compressed material (or built-up edge) increases in size it also becomes more and more unstable. Eventually a point is reached where failure occurs and fragments thereof are torn off and escape both with chip and with workpiece. This intermittent building up and breaking down of the forward end of the built up edge occurs at an extremely rapid rate. Thus the surface of a workpiece finished under these conditions is covered with a multitude of fragments of built-up edge. It is these fragments that constitute the so called "roughness" of a machined surface, the degree of roughness being solely a function of the average size of the fragments; their size in turn being determined by the magnitude of the built-up edge from which they were torn.

H. Ernst and M. E. Merchant[18, 19] in 1940 revealed that extremely high values of coefficients of friction usually exist between chip and tool and that this is responsible for the existence of the built-up edge. A study of friction revealed that the hardness of the mating surfaces and the resistance to shear at their areas of actual contact are the variables of greatest importance in dry friction. For ordinary dry metal surfaces in contact, resistance to shear is low because

of the presence of strongly adsorbed films of low shear strength materials which always cover such surfaces. When under unusual conditions (such as in metal cutting) these films are practically absent, the coefficient of friction rises to very high values because the opposing metal surfaces have united at their points of contact and thus the metal itself must be sheared. Coefficients of friction exceeding one are common in metal cutting.

A simplified force diagram was devised which indicated the relationship of all the forces that existed between the tool and the workpiece. These papers are the start of the quantitative treatment in metal cutting. By utilizing the principle of minimum energy, a relationship between the shear angle ϕ, the friction angle β and the rake angle α was developed: $2\phi + \beta - \alpha = 90°$.

V. Piispanen[20] in 1937 independently presented a mathematical analysis of the factors that determine the shear angle. This angle was assumed to be determined by the condition that the cutting force be a minimum. He also assumed that the shear strength of the work material increased as the compressive load on the shear plane increased and graphically determined the minimum cutting force per given material taking into account the aforementioned increase of shear strength with compressive stress. His analysis was remarkable in view of the lack of experimental work to ascertain his theory.

M. E. Merchant[21] in 1944 made a mathematical analysis of

the geometry and mechanics for two types of metal cutting processes, orthogonal and oblique. He developed expressions for the various forces, velocities, stresses, strains, and energy relationships that exist in metal cutting.

In two later papers Merchant[23, 24] in 1945 completely worked out the mechanics and plasticity conditions that exist in orthogonal cutting with a Type 2 chip. It was shown that if the shear strength of the work material was assumed to be constant then the application of the principle of minimum energy provided the plasticity condition $2\phi + \beta - \alpha = 90°$, which is the same as that presented in a previous paper[19]. This condition was found by experiment to be a poor approximation in a case of polycrystaline metals. A good approximation was obtained, however, if use was made of the fact that the shear strength of the polycrystalline metal is actually a function of the compressive stress on the shear plane. The resulting plasticity condition is $2\phi + \beta - \alpha = C$, where "C" is the complement of the slope angle of the linear curve relating shear strength to compressive stress. "C" turns out to be a constant of the work material.

Such a plasticity condition establishes a relationship between the force system and the geometry of chip formation so that if C and the shear strength is known for the given material, all forces involved in cutting can be calculated with reasonable accuracy directly from chip measurements without the use of the tool dynamometer.

Merchant and Zlatin[24] in 1946 described new experimental

methods for the analysis of the machine processes. They used a tool dynamometer to measure the force system that existed in continuous cutting. The shear angle was determined by measurements on the chip. They prepared nomographs which simplified the evaluation of various stresses, strains, cutting ratio, etc. from their basic measurements.

PART I: THEORY OF THE DISCONTINUOUS CHIP

The geometry, mechanics, and plasticity conditions for the continuous chip have been analyzed by Merchant. His analysis has been found to agree very well with experimental results in actual cases where a continuous chip is obtained. In fact his analysis has been found to be a close approximation for the case of the Type 3 chips, i.e., the continuous chip with the built-up edge.

There remained then the problem of the Type 1 chip; i.e., the discontinuous chip which analysis is treated in the study that follows. The importance of this study can be realized by the fact that probably 80% of all the tonnage machining is performed on cast iron which produces only discontinuous chips.

NOMENCLATURE

The following nomenclature is used in this paper:

A = Instantaneous cross-sectional area of "chip" before removal from workpiece = tw_1

A_o = Cross-sectional area of "chip" before removal from workpiece = $t_1 w_1$

A_c = Cross-sectional area of chip after removal from work-piece = $t_2 w_2$

A_s = Area of the shear plane

C = Machining constant = arc cot k

d = Distance travelled by tool measured from instant of chip rupture

d_1 = Distance travelled by tool at instant shear shifts from shear angle ϕ_2 to ϕ

D = Maximum distance tool can travel at shear angle ϕ_2

F_c = Cutting force; force component acting in direction of motion of tool relative to workpiece.

F_n = Force component acting in direction normal to shear plane.

F_s = Shearing force; force component acting in direction of shear of metal, in shear plane.

F_t = Thrust force; force component acting in direction perpendicular to F_c and to surface generated.

k = Slope of linear curve relating shear stress to compressive stress

L_1 = Arbitrary distance measured in direction of relative motion of cutting tool and workpiece.

L_2 = Distance through which point on chip moves relative to cutting tool, when tool advances distance L_1

N = Normal force; force component acting perpendicular to tool face

R,R' = Resultant forces; forces acting between chip and

tool and between chip and workpiece.

r_c = cutting ratio = r_L

r_L = chip length ratio : L_2/L_1

r_t = chip thickness ratio = t_1/t_2

S_o = Shear strength of metal at atmospheric pressure

S_n = Compressive stress acting perpendicular to shear plane

S_s = Mean shear stress on shear plane

S'_s = Mean shear strength of metal being cut

t = Instantaneous thickness of "chip" in discontinuous cutting

t_1 = Thickness of "chip" before removal from workpiece = maximum depth of cut for discontinuous chip.

t_2 = Thickness of chip after removal from workpiece, as measured in direction perpendicular to face of cutting tool

V_c = Cutting velocity, velocity of tool relative to workpiece

V_f = Chip flow velocity; velocity of chip relative to cutting tool

V_s = Velocity of shear; velocity of chip relative to the workpiece.

w_1 = Width of chip before removal from workpiece

w_2 = Width of chip after removal from workpiece

W_c = work done in cutting, per unit volume of metal removed

W_f = Work done in overcoming friction between chip and

tool, per unit volume of metal removed.

W_s = Work done in shearing of metal, per unit volume of metal removed.

α = Oblique rake angle of tool measured in plane perpendicular to its cutting edge = True rake angle for case of orthogonal cutting

ϵ = Shearing strain undergone by chip under process of removal

ϵ_o = Shearing strain of metal at rupture under atmospheric pressure

K = Slope of linear curve relating shearing strain of metal to compressive stress under rupture conditions

μ = Coefficient of friction acting between sliding chip and tool face = F/N

γ = Friction angle = arc tan μ

ϕ = Shear angle; angle between shear plane and surface being generated measured in plane perpendicular to cutting edge of tool = shear angle to horizontal surface

ϕ_1 = Shear angle at rupture

ϕ_2 = Shear angle to inclined surface

ψ = Direction of crystal elongation in chip

REVIEW OF CONTINUOUS CHIP THEORY

An analysis of the discontinuous chip theory must necessarily be preceded by a review of the geometry, mechanics, and

plasticity conditions that have been developed for the continuous chip. Only the case of orthogonal cutting will be discussed, i.e., cutting with a straight edge tool moving relative to the workpiece in a direction perpendicular to its cutting edge. The mathematical approach for this problem has been carried out by Merchant[21, 22, 23] and his nomenclature will be retained whenever possible.

Geometry of Formation of the Continuous Chip

The tool with rake angle α moves in a direction shown by the arrow, taking a depth of cut t_1, Fig. 3. During the

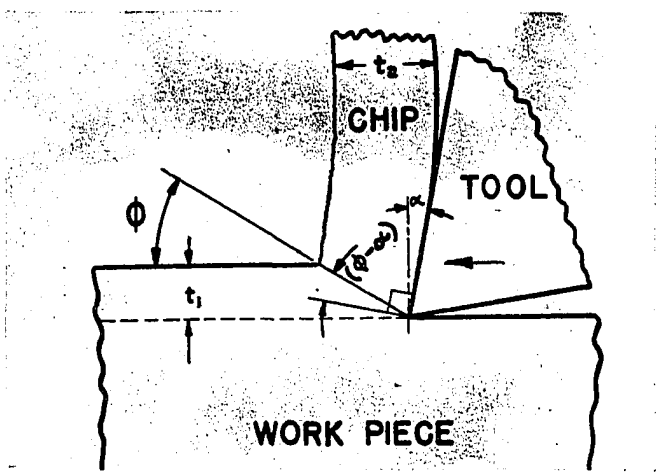

Figure 3

formation of a continuous chip the metal is found to fail by a process of shear confined essentially to a single plane extending from the cutting edge to the horizontal work surface making an angle ϕ with respect to the horizontal surface. The thickness of the chip after removal is designated as t_2, and the ratio of the depth of cut t_1 to the chip thickness t_2 is called the chip thickness ratio, r_t where

$$r_t = \frac{t_1}{t_2} = \frac{\sin \phi}{\cos (\phi-\alpha)} \qquad (1)$$

This ratio is the same as the ratio of the length of chip L_2 to the length of path from which it was cut L_1 which ratio is known as the chip length ratio, r_L. The ratios r_t and r_L are commonly called the cutting ratio r_c.

$$r_L = \frac{L_2}{L_1} = \frac{t_1}{t_2} = r_t = r_c \qquad (2)$$

Shearing strain ϵ occurs in the chip by the displacement of an element of thickness ΔX through a distance ΔS, Fig. 4.

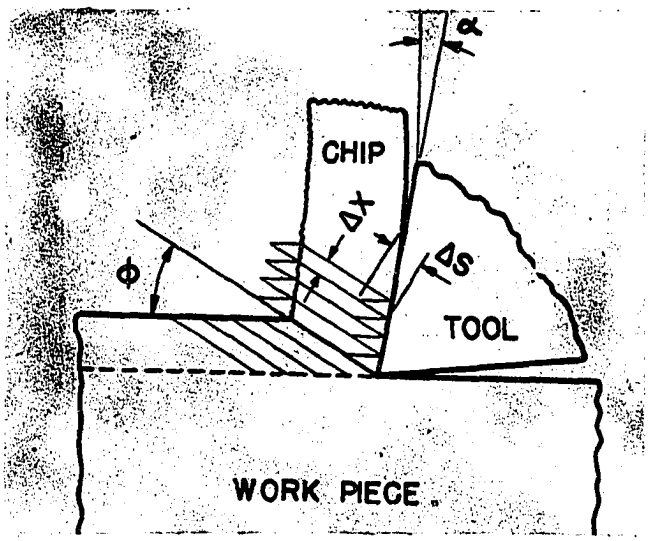

Figure 4

(In actual cutting $\Delta X \rightarrow 0$)

$$\epsilon = \frac{\Delta S}{\Delta X} = \cot \phi + \tan (\phi - \alpha) \qquad (3)$$

The crystal structure of the metal is elongated by the shearing process but at a different direction than the shear angle, Fig. 5. The direction of chip elongation, ψ , is determined by

$$\cot \psi = \cot \phi + \tan (\phi - \alpha) \qquad (4)$$

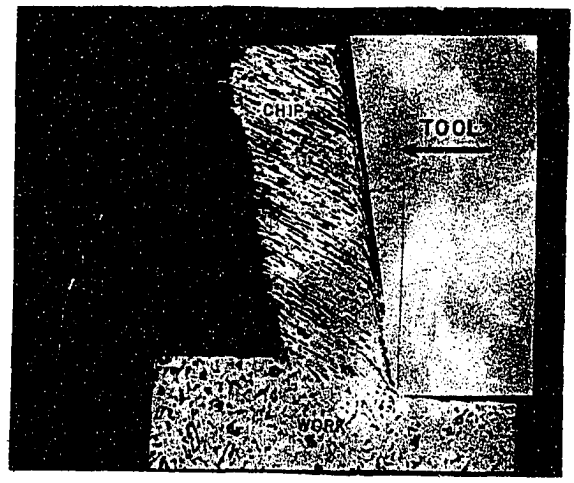

Figure 5

From (3) and (4) it is seen that

$$\epsilon = \cot \psi \tag{3a}$$

The velocity relationships are shown in Fig. 6 where V_c is

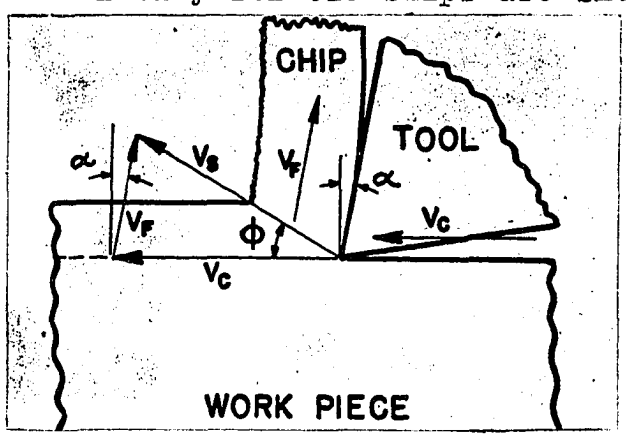

Figure 6

the cutting velocity, V_s the velocity of shear, and V_f the velocity of chip flow up the tool face.

$$V_s = V_c \frac{\cos \alpha}{\cos (\phi - \alpha)} \tag{5}$$

$$V_f = V_c \frac{\sin \phi}{\cos (\phi - \alpha)} = V_c r_c \tag{6}$$

Force Relationships in Orthogonal Cutting

The forces acting between the tool and the work have been conveniently represented by the diagram in Fig. 7 where F_c is

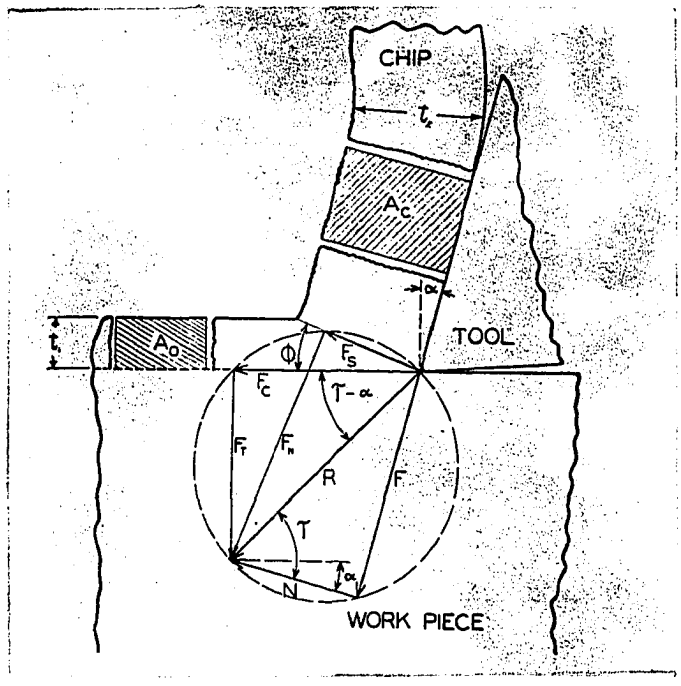

Figure 7

the cutting force acting in the direction of the tool travel, F_t is the thrust force perpendicular to the travel, R is the resultant force, F is the force of friction between the chip and the tool face, N is the force normal to the tool face, F_s is the force tending to shear the metal along the shear plane and F_n is the force perpendicular to the shear plane.

The following relationships have been derived from this diagram:

$$\mu = F/N = \tan \tau \qquad (7)$$

$$F = F_t \cos \alpha + F_c \sin \alpha \qquad (8)$$

$$F_s = F_c \cos \alpha - F_t \sin \alpha \qquad (9)$$

$$S_s = F_s/A_s = (F_c \sin \phi \cos \phi - F_t \sin^2 \phi)/A_o \quad (10)$$

$$S_n = F_n/A_s = S_s \tan (\phi + \gamma - \alpha) \quad (11)$$

$$W_f = F\, r_c/A_o = F/A_c \quad (12)$$

$$W_s = S_s \epsilon \quad (13)$$

$$W_c = S_s \epsilon + F/A_c = W_s + W_f \quad (14)$$

where:

μ = coefficient of friction between chip and tool face

S_s = mean shear strength of material

A_s = area of shear plane = $A_o/\sin \phi$

A_o = cross-sectional area of "chip" before removal = $t_1 w_1$

S_n = mean compressive stress on shear plane

W_f = work expended in friction between chip and tool per unit volume of metal removed

A_c = cross-sectional area of chip after removal = A_o/r_c

W_s = work expended in shearing the metal per unit volume of metal removed.

W_c = total work expended in cutting per unit volume of metal removed.

Attention should be called to the fact that the total work done in cutting is expended at two sources: in overcoming friction between chip and tool and in the shearing process on a shear plane as shown in Equation (14).

Plasticity Conditions in Orthogonal Cutting

In the formation of a continuous chip the shear angle will assume a value so as to make the total work done a minimum. Since the cutting force component F_c is alone responsible for the work done in cutting, the shear angle will take on a value as to make F_c a minimum. F_c can be expressed in terms of S_s, γ, ϕ, and α as

$$F_c = \frac{S_s A_o \cos(\gamma - \alpha)}{\sin\phi \cos(\phi + \gamma - \alpha)} \tag{15}$$

Merchant[23] first assumed that the shear strength along the shear plane was a constant, i.e.,

$$S_s = S_s' = \text{constant} \tag{16}$$

where S_s' = shear strength of the material. Substitution of (16) into (15) gives

$$F_c = \frac{S_s' A_o \cos(\gamma - \alpha)}{\sin\phi \cos(\phi + \gamma - \alpha)} \tag{17}$$

The minimum value of F_c is found by differentiating F_c with respect to ϕ and equating to 0, yielding

$$\cos(2\phi + \gamma - \alpha) = 0$$

$$\text{or:} \quad 2\phi + \gamma - \alpha = 90° \tag{18}$$

Expression (18) was found to be a poor approximation for cutting most polycrystaline materials.

Merchant then made use of the fact that the shear strength of a metal increases when the metal is subjected to high

compressive stresses. Tests made by P. W. Bridgman[25] showed that the relation between the shear strength and the compressive stress to be close to linear for polycrystalline materials.

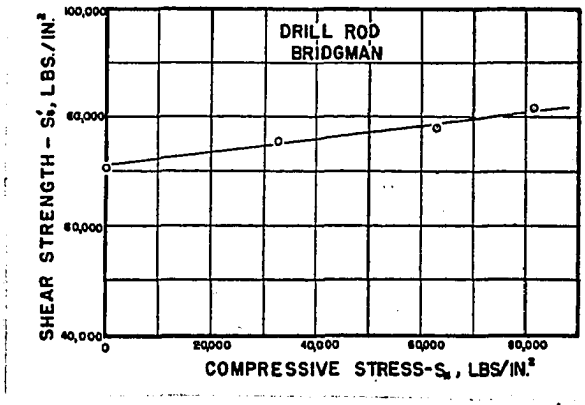

Figure 8

See Fig. 8. The shearing strength of the metal in cutting was, therefore, assumed to be of the form

$$S'_s = S_o + kS_n \tag{19}$$

where S_o is the shear strength of the metal at zero compressive stress, S_n is the compressive stress and k is the slope of the curve relating shear strength to compressive stress.

Substituting (11) into (19) and solving for S'_s

$$S'_s = \frac{S_o}{1 - k \tan (\phi + \gamma - \alpha)} \tag{20}$$

substitute (20) into the expression for F_c in (15)

$$F_c = \frac{S_o A_o \cos (\gamma - \alpha)}{\sin \phi \cos (\phi + \gamma - \alpha) - k \sin \phi \sin (\phi + \gamma - \alpha)} \tag{21}$$

Applying the minimum energy condition to F_c in Equation (21)

gives

$$\cot (2\phi + \gamma - \alpha) = k \tag{22}$$

or

$$2\phi + \gamma - \alpha = C \tag{23}$$

where

$$C = \text{arc cot } k \tag{24}$$

The constant "C" in equation (23) is a physical constant of the work material. Values of "C" have been determined by means of cutting tests for many types of steels. By making use of (23) the force and energy relations that have been previously derived can be transformed to a form that is dependent only on the physical properties of the work material together with the easily measured shear angle.

The Discontinuous Chip and Orthogonal Cutting

The discontinuous chip is produced when cutting inherently "brittle" materials such as cast iron or when machining ductile materials at low cutting speeds in the absence of cutting fluids. In the latter case the discontinuous chip is associated with the high friction that is known to exist between the tool and chip. It was the object of this investigation to formulate an analysis consistent with the above facts.

The cutting action which produced a discontinuous chip was studied by Ernst and Martellotti[16] by taking moving pictures through a microscope of bronze being cut by a planer type tool. As the tool advances with respect to the work, chip segments are produced at approximately a uniform rate.

A complete cycle showing the formation of a segment is illustrated in Fig. 1. The tool advances into the inclined surface which was produced by the ruptured chip. The metal is deformed as indicated by the distortion of the network of scribed lines on the workpiece and eventually a segment ruptures at approximately the same angle as in the previous case.

The analysis of the discontinuous chip was begun by assuming that as the tool first advanced into the workpiece, shear would occur along a plane extending from the cutting edge to the inclined surface as in Fig. 9b. During this time

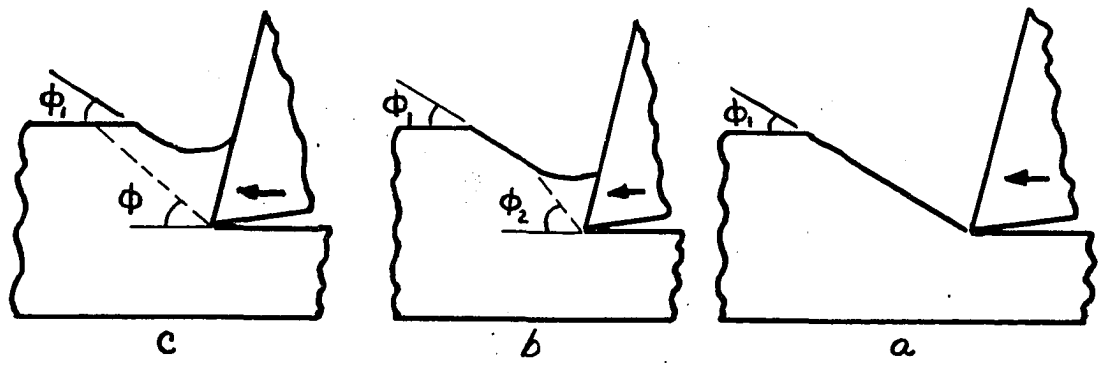

Figure 9

the shear angle would gradually decrease because the friction between the chip and the tool face would gradually increase due to the self cleansing action of the chip sliding up the tool face. It was further assumed that the shear angle decreased until the shear plane eventually extended to the horizontal surface, after which the shear angle was designated as ϕ, Fig. 9c. The continued advance of the tool was

accompanied by a continued decrease in shear angle until the value of the shear angle became so low that rupture occurred.

The criterion for rupture of the work material with decreasing values of shear angle was attributed to be the behavior of the shearing strain. As the shear angle decreased the shearing strain increased in accordance with equation (3). If the work material were ductile and if the friction were not too great, the shearing strain corresponding to the equilibrium shear angle would be less than that necessary for rupture. However, if the material were brittle, a strain would be reached which would cause rupture before the shear angle could seek an equilibrium value.

Several modifications were necessary in these original assumptions to satisfy the actual cutting conditions and they will be brought out later.

A mathematical analysis will be necessary for two conditions: - Condition A when the shear is occurring from the cutting edge to the inclined surface and Condition B when shear is occurring to the horizontal surface. Condition A is the situation that exists during the start of the chip segment formation while Condition B exists during the latter stage of the segment formation.

Condition A - Shear Occurring to the Inclined Surface

Fig. 10 shows the tool with rake angle α after it has advanced a short distance d into the workpiece which originally

had the shape OCE.

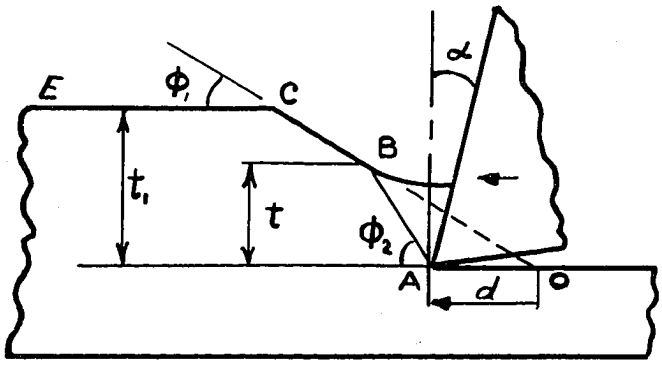

Figure 10

Let t_1 = total depth of cut

t = Instantaneous depth, i.e., vertical distance from machined surface to the intersection of shear plane AB with inclined surface OC.

ϕ_1 = Shear angle of rupture

ϕ_2 = Shear angle while shear plane extends to inclined surface

ϕ = Shear angle while shear plane extends to horizontal surface

d = Distance travelled from point O

w = width of workpiece

t can be expressed in terms of ϕ_1, ϕ_2, and d as follows:

In triangle OAB, angle (ABO) = $(\phi_2 - \phi_1)$

$$\therefore \quad \frac{\sin (\phi_2 - \phi_1)}{d} = \frac{\sin \phi_1}{AB}$$

$$t = AB \sin \phi_2$$

$$= \frac{d \sin \phi_1 \sin \phi_2}{\sin (\phi_2 - \phi_1)} \qquad (25)$$

the instantaneous cross-sectional area A is

$$A = tw = \frac{w\ d\ \sin \phi_1\ \sin \phi_2}{\sin\ (\phi_2 - \phi_1)} \tag{26}$$

the instantaneous cutting force F_c becomes on substituting A from (26) for A_o into equation (5)

$$F_c = S_s\ w\ d\ \frac{\sin \phi_1\ \cos\ (\gamma - \alpha)}{\sin\ (\phi_2 - \phi_1)\ \cos\ (\phi_2 + \gamma - \alpha)} \tag{27}$$

where ϕ_2 indicates that shear is occurring to the inclined surface rather than the horizontal surface. The value of the shear angle ϕ_2 will be determined again by the minimum energy principle, or since the force F_c is responsible for the total work then F_c must be a minimum.

Case I - Assume the shear strength S_s' of the work material to be invariant with respect to ϕ and γ, i.e., $S_s = S_s' =$ constant Then (27) becomes

$$F_c = \frac{S_s'\ w\ d\ \cos\ (\gamma - \alpha)\ \sin \phi_1}{\sin\ (\phi_2 - \phi_1)\ \cos\ (\phi_2 + \gamma - \alpha)} \tag{28}$$

Differentiate F_c with respect to ϕ_2 and equate to 0.

$$\frac{d\ F_c}{d\ \phi_2} = - S_s'\ w\ d\ \cos\ (\gamma - \alpha)\ \sin \phi_1$$

$$\times\ \frac{\cos(\phi_2-\phi_1)\cos(\phi_2+\gamma-\alpha)-\sin(\phi_2-\phi_1)\sin(\phi_2+\gamma-\alpha)}{\left[\sin\ (\phi_2-\phi_1)\cos(\phi_2+\gamma-\alpha)\right]^2} = 0$$

$$\cos\left[(\phi_2-\phi_1) + (\phi_2+\gamma-\alpha)\right] = 0$$

$$\cos\ (2\phi_2 + \gamma-\alpha-\phi_1) = 0$$

or $$2\phi_2+\gamma-\alpha-\phi_1 = 90° \tag{29}$$

Equation (29) would not be expected to provide an accurate evaluation for ϕ_2 since the shear strength of polycrystaline materials are known to be a function of the compressive stresses acting on the shear plane.

Case II - Assume that the shear strength S_s' is a linear function of the compressive stress acting on the shear plane or

$$S_s' = S_o + k\, S_n \tag{19}$$

and as with the continuous chip

$$S_s' = \frac{S_o}{1 - k \tan(\phi_2 + \gamma - \alpha)} \tag{30}$$

where ϕ_2 has replaced ϕ of equation (20). Substitute (30) into (28).

$$F_c = \frac{S_o\, w\, d \sin\phi_1 \cos(\gamma-\alpha)}{\sin(\phi_2-\phi_1)\cos(\phi_2+\gamma-\alpha) - k \sin(\phi_2-\phi_1)\sin(\phi_2+\gamma-\alpha)} \tag{31}$$

apply the minimum energy principle to (31) and get

$$\cos(2\phi_2+\gamma-\alpha-\phi_1) = k \sin(2\phi_2+\gamma-\alpha-\phi_1)$$

$$\cot(2\phi_2+\gamma-\alpha-\phi_1) = k \tag{32}$$

$$2\phi_2+\gamma-\alpha-\phi_1 = C \tag{33}$$

whereas before:

$$C = \text{arc cot } k \tag{24}$$

Condition B - Shear Occurring to the Horizontal Surface

As the tool advances into the workpiece eventually the shear plane is observed to extend to the horizontal surface instead of to the inclined surface. Under this condition the

depth of cut becomes t_1 and the shear angle is called ϕ instead of ϕ_2.

The continuous chip theory is assumed to hold for this condition up to the time of rupture. The shear angle ϕ is thus expressed as in previous equations.

$$2\phi + \gamma - \alpha = 90° \tag{18}$$

for the assumption that the shear strength of the material remains constant and

$$2\phi + \gamma - \alpha = C \tag{23}$$

for the more general case where the shear strength of the material is assumed to be a linear function of the compressive stress acting on the shear plane.

Changeover of Shear from Inclined Surface to Horizontal Surface

At first it was assumed that the shear angle ϕ_2 gradually decreased as the tool advanced until some position of the tool was reached when the depth $t = t_1$, and ϕ_2 became coincident with ϕ. In fact it was thought that the shape of the upper surface of the chip was produced during the time that shearing was occurring at angle ϕ_2 to the inclined surface. This trend of thought was influenced by the rounded concave-down appearance of the chip segment of Fig. 1. However, a graphical analysis of the chip shape that would result from shear to the inclined surface indicated that the upper surface of the chip segment would be concave-up as in Fig. 11b rather than

concave-down as in Fig. 11a. The analysis for the upper

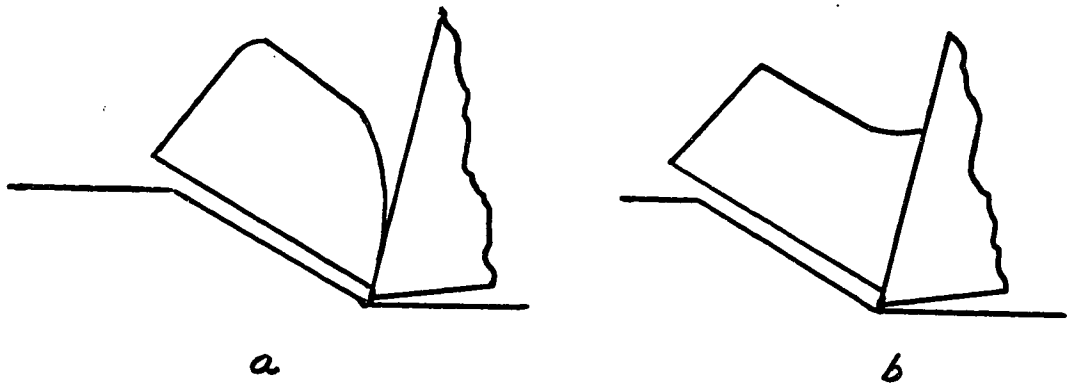

Figure 11

surface of the chip shape when shear is occurring to the inclined surface is as follows:

When the tool edge, Fig. 12, advances from its starting

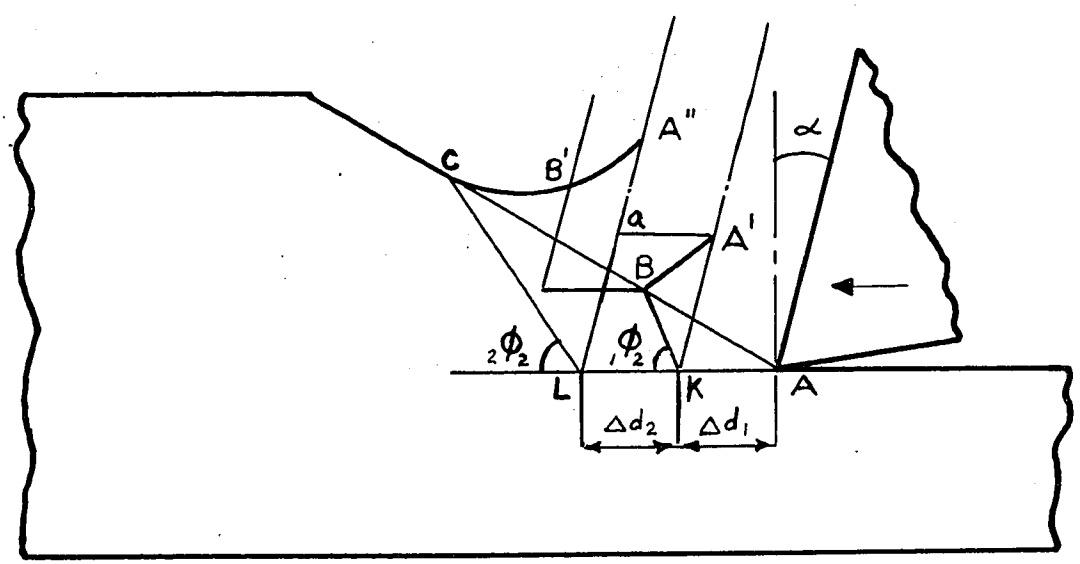

Figure 12

point A to point K through a distance Δd_1 then the increment of the workpiece at point A moves up the tool face to point A' by an amount A'K where

$$\frac{A'K}{\Delta d_1} = \frac{\sin {}_1\phi_2}{\sin ({}_1\phi_2 - \alpha)} = \text{average cutting ratio during travel } d_1.$$

When the tool edge is thus at point K the shear plane at this instant is KB making an angle ${}_1\phi_2$ with the machined surface. The shape of the upper surface of the chip at this instant would be A'B. After the tool moves through another increment Δd_2 $(= \Delta d_1)$ so that the cutting edge reaches point L, then the particle of the workpiece at A' moves still farther up the tool face to A'' where

$$\frac{aA''}{aA'} = \frac{aA''}{d_2} = \frac{\sin {}_1\phi_2}{\cos ({}_2\phi_2 - \alpha)} = \text{cutting ratio during}$$

movement Δd_2. Furthermore the previous upper surface of the chip represented by the line A'B moves parallel to itself to position A''B'. Thus when the cutting edge is at point L the shear angle at this instant is ${}_2\phi_2$ and the upper surface of the chip is A''B'C. Now the shear angle continually decreases as the tool advances, i.e., ${}_1\phi_2 > {}_2\phi_2 > {}_3\phi_2 > \cdots$ since the friction angle β continaully increases. By making graphical analysis in this manner and taking into consideration the fact that the shear angle decreases as the tool advances the upper surface of the chip segment always turned out to be concave up as indicated in Fig. 11b and also by the line A''B'C' of Fig. 12.

If shear were to occur to the inclined surface during an appreciable portion of the tool travel this concavity would have been plainly visible in the final chip shape. However,

no such concavity was observed on the upper surface of the chip. It was, therefore, concluded that the shearing process must shift from the inclined surface to the horizontal surface after a very short tool travel. Such a shift could only occur if the energy required to shear to the inclined surface were greater than that necessary to shear to the horizontal surface, i.e., the shear angle would at all times be determined by the minimum energy principle.

Determination of Distance Tool Travels When Energy to Shear to Inclined Surface Becomes Equal to Energy to Shear to Horizontal Surface

Shear will change over from the inclined surface to the horizontal surface when the energy per unit distance travelled by the tool to shear to the horizontal surface becomes equal to the energy per unit distance travelled by the tool to shear to the inclined surface, i.e., when

$$\left[\frac{F_c V_c}{V_c}\right]_{\phi} = \left[\frac{F_c V_c}{V_c}\right]_{\phi_2} \qquad (34)$$

or when $$\left[F_c\right]_{\ell} = \left[F_c\right]_{\phi_2}$$

where $[\ ]_{\phi}$ and $[\ ]_{\phi_2}$ indicate shear at angles ϕ and ϕ_2 respectively.

From equation (21)

$$\left[F_c\right]_{\phi} = \frac{S_o\, t_1\, w \cos(\gamma-\alpha)}{\sin\phi\cos(\phi+\gamma-\alpha)-k\,\sin\phi\sin(\phi+\gamma-\alpha)} \qquad (35)$$

Where A_o has been replaced by $t_1 w$, and from equation (31)

$$\left[F_c\right]_{\phi_2} = \frac{S_o \, w \, d \sin \phi_1 \cos (\tilde{\gamma}-\alpha)}{\sin(\phi_2-\phi_1)\cos(\phi_2+\tilde{\gamma}-\alpha)-k \sin(\phi_2-\phi_1)\sin(\phi_2+\tilde{\gamma}-\alpha)} \qquad (31)$$

As seen in Fig. 13 changeover occurs when the tool reaches

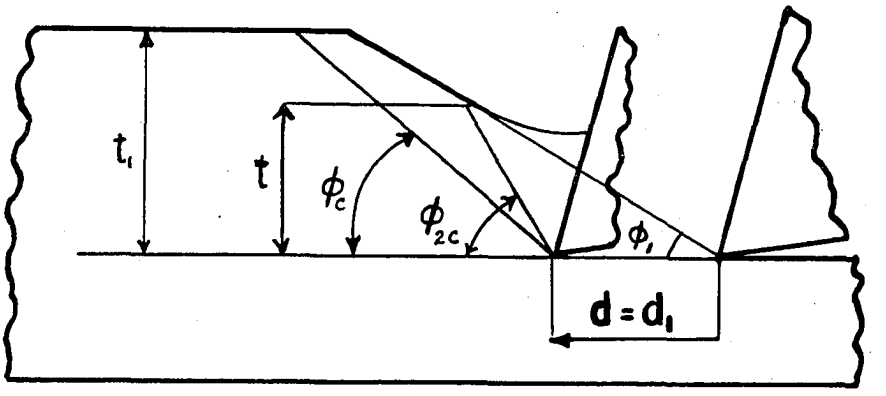

Figure 13

some position where $d = d_1$. At this instant let $\phi = \phi_c$ and $\phi_2 = \phi_{2c}$, the subscript c indicating the instant of changeover.

Now equate (35) and (31) and solve for d_1.

$$d_1 = \frac{t_1 \sin (\phi_{2c} - \phi_1)}{\sin \phi_1 \sin \phi_c}$$

$$\times \frac{\cos(\phi_{2c}+\tilde{\gamma}-\alpha)-k \sin(\phi_{2c}+\tilde{\gamma}-\alpha)}{\cos(\phi_c+\tilde{\gamma}-\alpha)-k \sin (\phi_c+\tilde{\gamma}-\alpha)} \qquad (36)$$

Equation (36) expresses the distance d_1 that the tool travels at which time the energy to shear at angle ϕ_2 equals the energy to shear at angle ϕ.

However, as seen in Fig. 14 the shear to the inclined surface could possibly continue until d = D, i.e., until the shear plane reached the intersection of the inclined and the

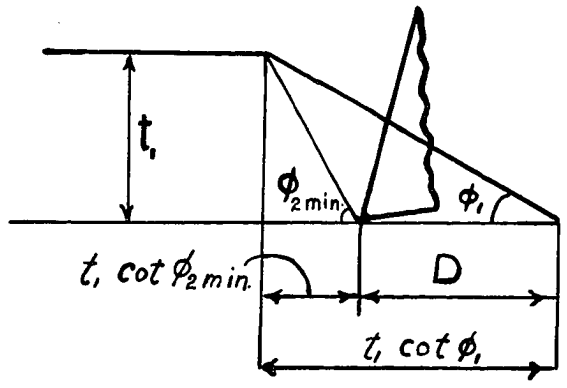

Figure 14

horizontal surface. The angle ϕ_2 at this instant would be the minimum value ϕ_2 could attain. Call this value ϕ_2 minimum. From Fig. 14 it is seen that

$$D = t_1 \ (\cot \phi_1 - \cot \phi_{2\,min.}) \tag{37}$$

Thus shear would shift abruptly from angle ϕ_2 to angle ϕ if $D > d_1$, i.e., if the distance d_1 from equation (36) is less than the distance D. Applying this condition to equations (36) and (37)

$$(\cot \phi_1 - \cot \phi_{2\,min}) > \frac{\sin (\phi_{2c} - \phi_1)}{\sin \phi_1 \sin \phi_c}$$

$$\times \frac{\cos(\phi_{2c}+\gamma-\alpha)-k \sin (\phi_{2c}+\gamma-\alpha)}{\cos (\phi_c+\gamma-\alpha)-k \sin (\phi_c+\gamma-\alpha)} \tag{38}$$

but by trigonometry

$$(\cot \phi_1 - \cot \phi_{2\,min}) = \frac{\sin (\phi_{2\,min.} - \phi_1)}{\sin \phi_1 \sin \phi_{2\,min.}} \tag{39}$$

substitute (39) into (38)

$$\frac{\sin(\phi_{2\,\min} - \phi_1)}{\sin \phi_{2\,\min}} > \frac{\sin(\phi_{2c} - \phi_1)}{\sin \phi_c}$$

$$\times \frac{\cos(\phi_{2c}+\gamma-\alpha)-k\sin(\phi_{2c}+\gamma-\alpha)}{\cos(\phi_c+\gamma-\alpha)-k\sin(\phi_c+\gamma-\alpha)} \qquad (40)$$

in equation (40)

$$\text{let } M \equiv \frac{(\cos \phi_{2c}+\gamma-\alpha)-k\sin(\phi_{2c}+\gamma-\alpha)}{\cos(\phi_c+\gamma-\alpha)-k\sin(\phi_c+\gamma-\alpha)} \qquad (41)$$

$$\text{but } k = \cot(2\phi_c+\gamma-\alpha) = \frac{\cos(2\phi_c+\gamma-\alpha)}{\sin(2\phi_c+\gamma-\alpha)}$$

$$\therefore M = \frac{\sin(2\phi_c+\gamma-\alpha)\cos(\phi_{2c}+\gamma-\alpha)-\cos(2\phi_c+\gamma-\alpha)\sin(\phi_{2c}+\gamma-\alpha)}{\sin(2\phi_c+\gamma-\alpha)\cos(\phi_c+\gamma-\alpha)-\cos(2\phi_c+\gamma-\alpha)\sin(\phi_c+\gamma-\alpha)}$$

but at the instant of changeover

$$2\phi_c + \gamma - \alpha = 2\phi_{2c} + \gamma - \alpha - \phi_1 = C \text{ .}$$

(C may not actually be the same for both ϕ_2 and ϕ because of strain hardening of the material surrounding the zone of deformation. However, its variation is neglected as a first approximation.)

$$\therefore M = \frac{\sin(2\phi_{2c}+\gamma-\alpha-\phi_1)\cos(\phi_{2c}+\gamma-\alpha)-\cos(2\phi_{2c}+\gamma-\alpha-\phi_1)\sin(\phi_{2c}+\gamma-\alpha)}{\sin \phi_c}$$

$$= \frac{\sin(\phi_{2c} - \phi_1)}{\sin \phi_c} \qquad (41a)$$

Substitution of (41a) into (40) gives

$$\frac{\sin(\phi_{2\,\min} - \phi_1)}{\sin \phi_{2\,\min}} > \frac{\sin^2(\phi_{2c} - \phi_1)}{\sin^2 \phi_c} \qquad (42)$$

Equation (42) is the condition necessary for abrupt changeover of shear plane from inclined surface to horizontal surface.

As a limiting case of changeover consider the condition when the shear plane gradually moves up the inclined surface to the horizontal surface. At this instant $\phi_c = \phi_{2c} = \phi_{2\ \min.}$

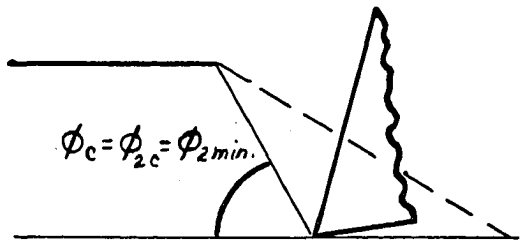

Figure 15

(Fig. 15) and equation (42) becomes

$$\frac{\sin(\phi_c - \phi_1)}{\sin \phi_c} \geq \frac{\sin^2(\phi_c - \phi_1)}{\sin^2 \phi_c}$$

$$\text{or} \quad 1 \geq \frac{\sin(\phi_c - \phi_1)}{\sin \phi_c}$$

If ϕ_1 has any positive value the right hand side is always less than 1. Hence the equal sign will never hold. This means that the condition indicated by Fig. 15 can never occur or that shear plane ϕ_2 can never gradually blend into the shear plane ϕ. In other words, the shear angle abruptly shifts from the inclined surface to the horizontal surface.

Another proof of this is as follows: at the instant of changeover from shear to the inclined surface to shear to the horizontal surface equations (23) and (33) must simultaneously

be satisfied, i.e.,

$$2\phi_c + \gamma - \alpha = C = 2\phi_{2c} + \gamma - \alpha - \phi_1$$

but γ is the same on both sides of this equation

$$\therefore \quad 2\phi_c = 2\phi_{2c} - \phi_1$$

$$\text{and } \phi_{2c} = \phi_c + \frac{\phi_1}{2} \tag{43}$$

but if γ is an increasing function as the tool advances to form the segment,

$$\phi_c \geq \phi_1 \tag{44}$$

$$\phi_{2c} \geq \frac{3}{2}\phi_1 \tag{45}$$

Equation (43) indicates that an abrupt changeover must occur without the shear plane extending to the intersection of the inclined and horizontal surface, i.e., $\phi_{2c} \neq \phi_c$. It should be noted that if $\phi_{2c} = \frac{3}{2}\phi_1$, the segment would immediately rupture at the instant of changeover.

The above analysis which shows that the changeover of shear planes is abrupt is based on the assumption that at both planes of changeover the following factors are equal: the friction angle γ, the shear stress at zero compressive load S_o, and the machining constant "C".

The assumption that γ is the same for both shear planes is quite accurate. However, S_o and C are affected by the work hardening of the material which is known to surround the region of shear. Hence these values may not be the same on

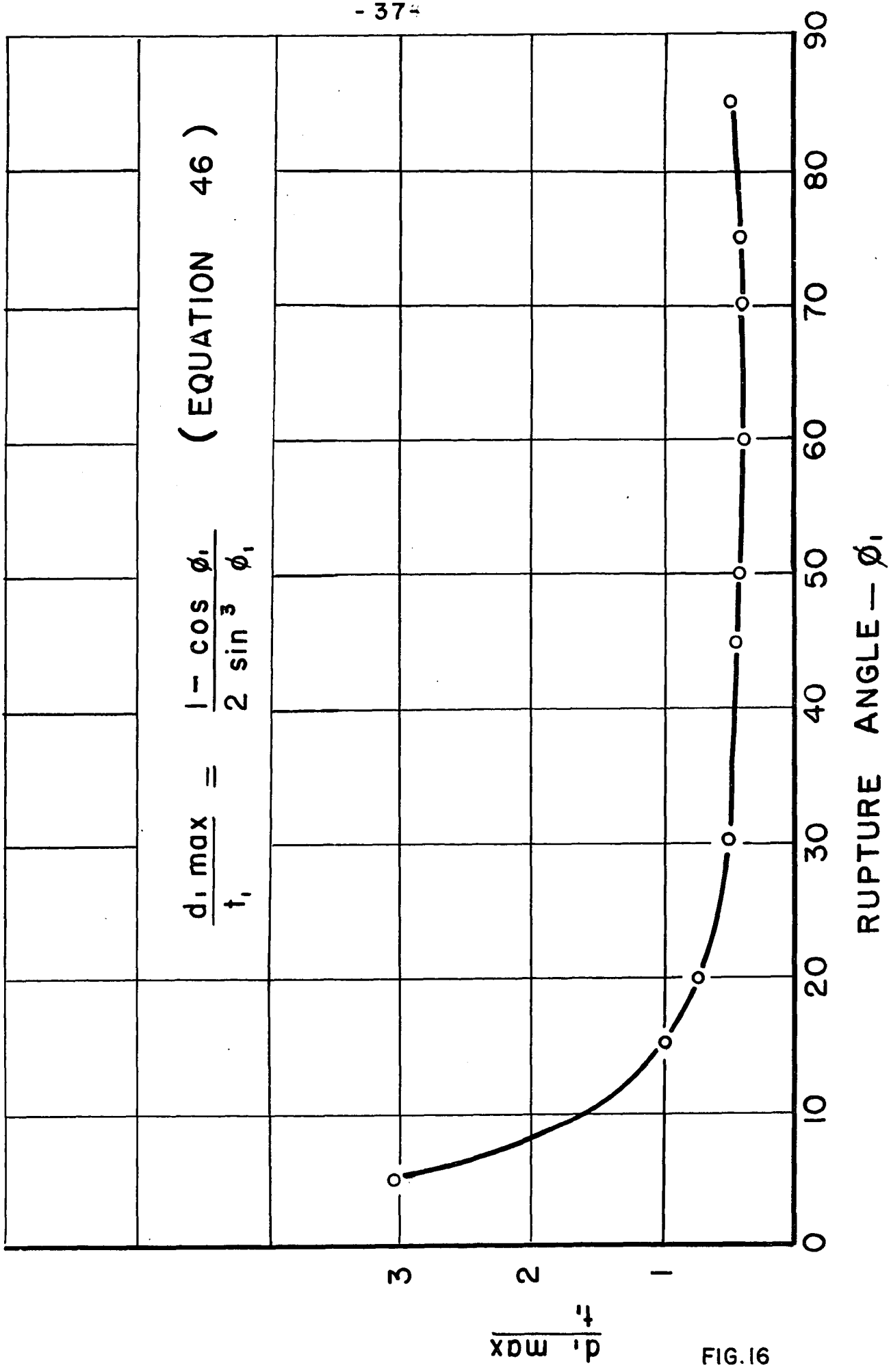

FIG. 16

the two possible planes of shear ϕ_{2c} and ϕ_c, with the result that in actual metal cutting the shear plane may gradually decrease rather than abruptly changeover from shear to the inclined surface to shear to the horizontal surface.

Maximum Value of d_1

By making use of equation (41a), (36) can be written as

$$d_1 = \frac{t_1}{\sin \phi_1} \quad \frac{\sin^2 (\phi_{2c} - \phi_1)}{\sin^2 \phi_c} \tag{36a}$$

The maximum possible value of d_1 can be determined by using the condition of equations (44) and (45) that

$$(\phi_{2c})_{min} = \frac{3}{2} \phi_1 \quad \text{and} \quad (\phi_c)_{min} = \phi_1$$

$$\text{or} \quad d_1 \text{ max} = \frac{t_1}{\sin\phi_1} \quad \frac{\sin^2(\frac{\phi_1}{2})}{\sin^2 \phi_1}$$

$$\text{or} \quad d_1 \text{ max} = \frac{t_1 (1 - \cos \phi_1)}{2 \sin^3 \phi_1} \tag{46}$$

Equation (46) is plotted in Fig. 16. It is seen that at rupture angles greater than 25°, $d_1 \text{ max} \approx 1/2\ t_1$. From experimental results taken from Ernst and Martellotti[16] and our own tests the total distance that the tool travelled to form a chip is of the same order of magnitude as the depth of cut t_1. Therefore, shear occurs to the inclined surface less than half the total distance of tool travel.

Conditions for Rupture of Chip Segment

Both the theoretical development as well as experimental evidence assures that the metal is shearing at angle ϕ to the horizontal plane prior to rupture. In fact both offer evidence that shear occurs to the horizontal surface during the major portion of the chip segment formation. It is thus possible to apply the continuous chip theory to the cutting action during this time keeping in mind, however, that the friction angle τ, and the shear angle ϕ are constantly changing, i.e., τ continues to increase and ϕ continues to decrease. At any instant ϕ and τ are related by the plasticity condition:

$$2\phi + \tau - \alpha = C \qquad (23)$$

As previously discussed the chip is assumed to rupture when the shearing strain developed in the chip reaches a value at which rupture must occur. The shearing strain in the chip is given by equation (3)

$$\epsilon = \cot\phi + \tan(\phi - \alpha) \qquad (3)$$

However, the shearing strain necessary to produce rupture within a polycrystalline material has been shown by P. W. Bridgman[26] to increase with the application of compressive stress.

As an approximation assume that a linear relation holds for the behavior of ϵ with compressive stress, i.e., assume

$$\epsilon = \epsilon_o + K S_n \tag{47}$$

where K = the slope of the ϵ vs. S_n curve and ϵ_o = shearing strain at zero compressive strain.

From equation (11)

$$S_n = S_s' \tan (\phi + \gamma - \alpha) \tag{11a}$$

but $$S_s' = \frac{S_o}{1 - k \tan (\phi + \gamma - \alpha)} \tag{20}$$

where as before S_s' is the shear strength of the material under compressive stress and S_o is the shear strength of the material at zero compressive stress.

Combining (11a) and (20)

$$S_n = \frac{S_o \tan (\phi + \gamma - \alpha)}{1 - k \tan (\phi + \gamma - \alpha)}$$

or $$S_n = \frac{S_o}{\cot (\phi + \gamma - \alpha) - k} \tag{48}$$

Inserting (48) into (47) and changing ϕ to ϕ_1

$$\left[\epsilon\right]_{\text{rupture}} = \epsilon_o + \frac{K S_o}{\cot (\phi_1 + \gamma - \alpha) - k} \tag{49}$$

Using the plasticity conditions

$2 \phi_1 + \gamma - \alpha = C$ and $k = \cot C$, (49) becomes

$$\left[\epsilon\right]_{\text{rupture}} = \epsilon_o + \frac{K S_o}{\cot (C - \phi_1) - \cot C} \tag{49a}$$

The chip segment will rupture when the shearing strain

in the chip as determined by equation (3) reaches the value necessary for rupture as determined by equation (49) or when

$$\cot \phi_1 + \tan(\phi_1 - \alpha) = \epsilon_o + \frac{K S_o}{\cot(\phi_1 + -\alpha) - k} \qquad (50)$$

or inserting the plasticity conditions

$$\cot \phi_1 + \tan(\phi_1 - \alpha) = \epsilon_o + \frac{K S_o}{\cot(C - \phi_1) - \cot C} \qquad (50a)$$

Equation (50a) makes possible the determination of the shear angle at rupture ϕ_1 from the physical properties of the work material.

Geometry of the Discontinuous Chip

In general the chip is observed to have the trapezoidal shape OPQR, Fig. 17. The long leg of the trapazoid OP is an

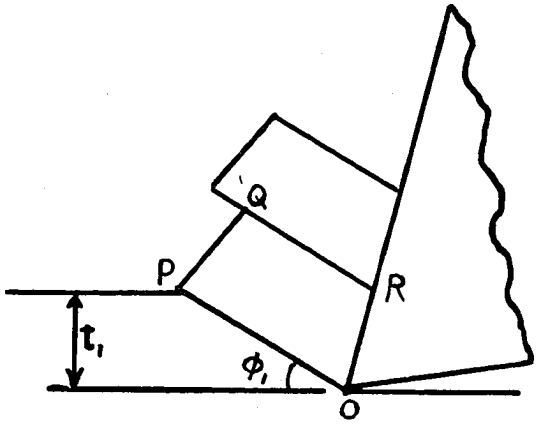

Figure 17

accurate indication of the length of the shear plane at rupture. Hence the shear angle at rupture can be determined

from the relation

$$\sin \phi_1 = \frac{t_1}{OP} \tag{51}$$

OP can be measured fairly accurately on the chip by using a Brinell microscope. A better method, however, is to first mount the chip in a plastic and then polish the surface to give better definition to the cross-sectional area.

The dimension OR on the chip divided by the average tool travel for chip rupture is a measure of the average cutting ratio. The distance the tool travels to rupture a chip may be determined in some cases by counting the number of chip segments per inch of tool travel, either by counting the number of "clicks" as the rupture occurs or by noting the distance between rupture marks on the workpiece.

Another method of determining the average cutting ratio is to use the weight-length method described by Merchant and Zlatin[24] for continuous chips. However, the voids between the chip segments must be deducted from the overall length of the chip if this method is used.

Experimental Study of Discontinuous Chip Formation

A thorough study of the discontinuous chip makes necessary the simultaneous determination of the forces acting between tool and work as well as the conditions of shear within the workpiece.

The arrangement shown in Fig. 18 was used in this study.

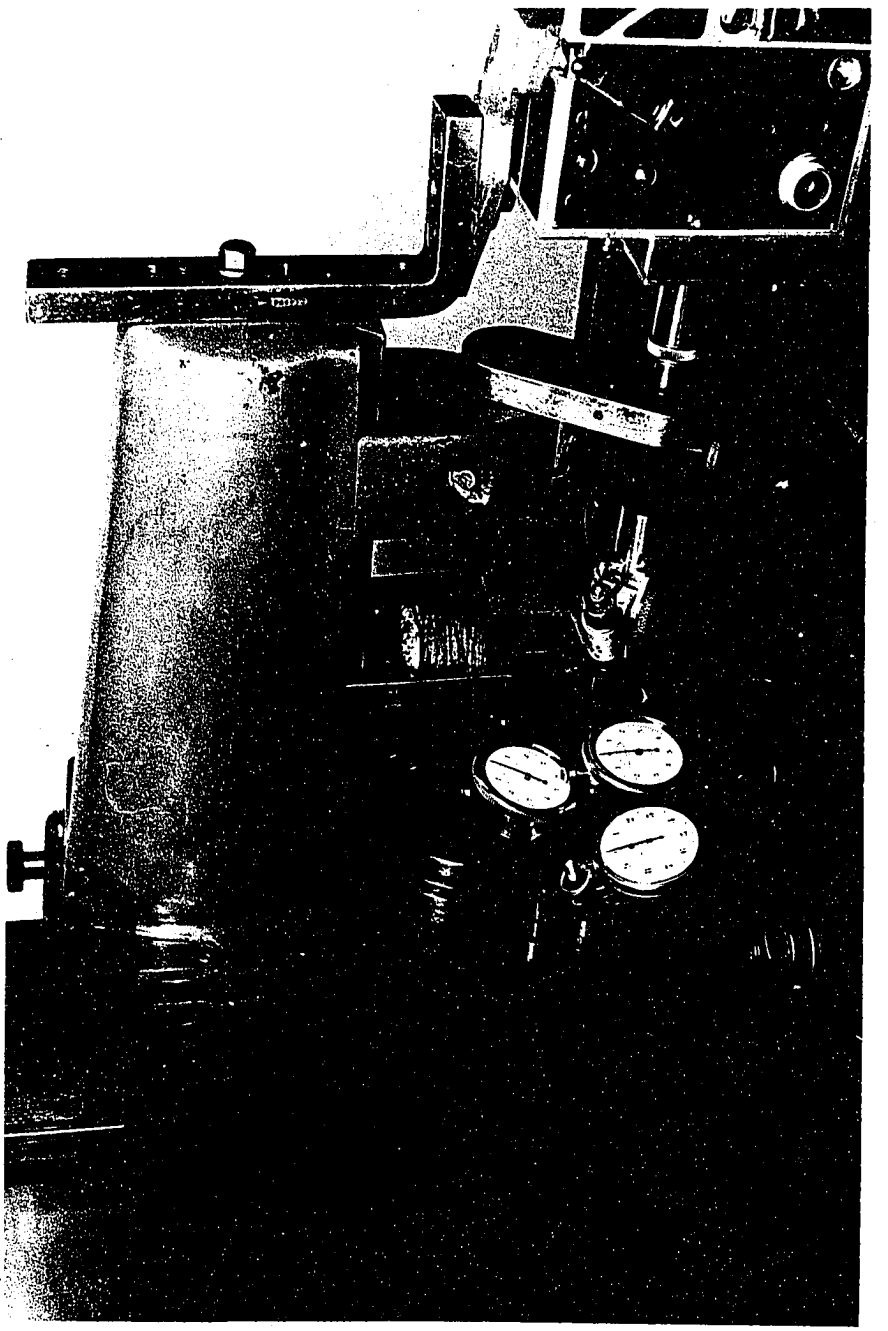

Figure 18

The workpiece was clamped in a dynamometer which deflected under load. The deflection was amplified by an integral mechanical lever arrangement and the amplified deflection was measured by a 1/10,000" dial indicator. The tool was carried in another dynamometer attached to the overarm of a milling machine. This dynamometer measured the horizontal deflection of the tool by means of another 1/10,000" dial indicator. By suitable calibration the deflections of the tool and work dynamometers gave the cutting force F_c and the thrust force F_t respectively.

The two orthogonal force readings F_c and F_t were sufficient to determine the entire force system of Fig. 7, and together with the knowledge of the depth of cut, width of cut and cutting velocity provided all the data necessary for the determination of the velocities, coefficient of friction, etc.

The deformation of the workpiece while cutting was observed through a low power microscope which was likewise attached to the overarm, Fig. 18. Through this microscope the shear angle at rupture was easily discernable. However, the instantaneous shear angle during the formation of the segment was difficult to observe. After attempting many procedures it was found that the shearing zone could be approximately determined in the following manner. The side of the workpiece which faced the microscope was roughened by hand polishing on 120 grit abrasive cloth so as to produce vertical scratches on the workpiece. The workpiece was illuminated by oblique lighting from a pen light placed two inches from the tool (with power

supplied by a 3 volt transformer), and also from a No. 2 photo flood lamp placed 30" from the workpiece. As the work advanced into the tool, the deformed metal bulged sideways slightly so as to smooth out the scratches in that region. The deformed zone was thus observable by the increase in its reflectivity.

Various types of bronzes and cast irons were cut and it was found that the best material for observation was Ampco No. 15 Bronze having a composition of 87% Cu, 10% Al and 3% Fe. This material has a tensile strength 80,000 lbs. per square inch, a yield point of 45,000 lbs. per square inch and a hardness of 175 Brinell.

The workpiece was 1/2" long, 3/16" thick and 3/4" high. The top of the workpiece was machined as shown in Fig. 19

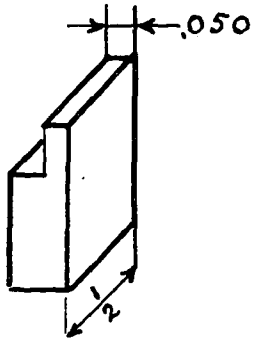

Figure 19

so that the actual width of cut was 0.050". Various depths of cuts from 0.005" to 0.020" were used. The cutting velocity was held constant at 0.515" per minutes. This speed was obtained by feeding the table toward the tool.

The cutting tool was made of high speed steel and had a true rake of +14° and a clearance angle of 6°.

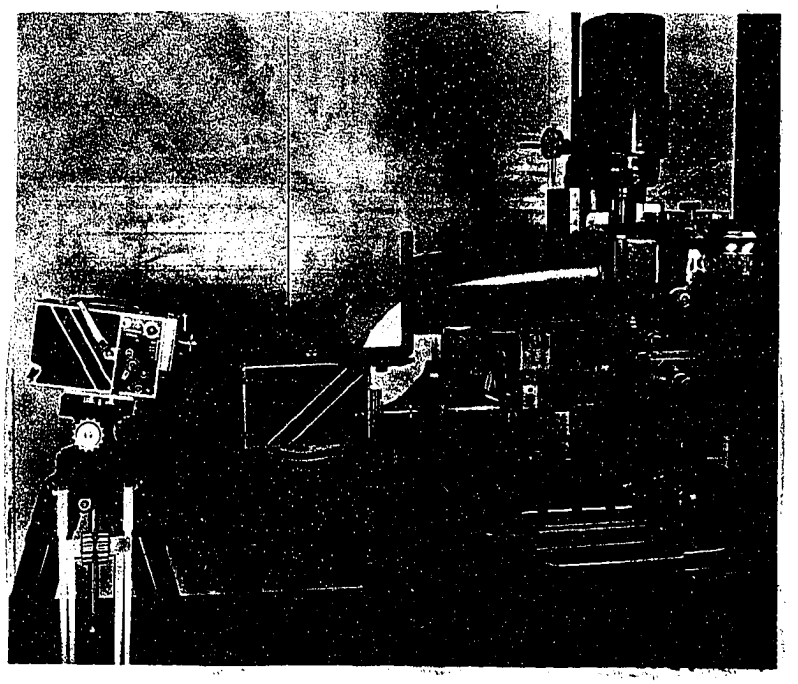

Figure 20a

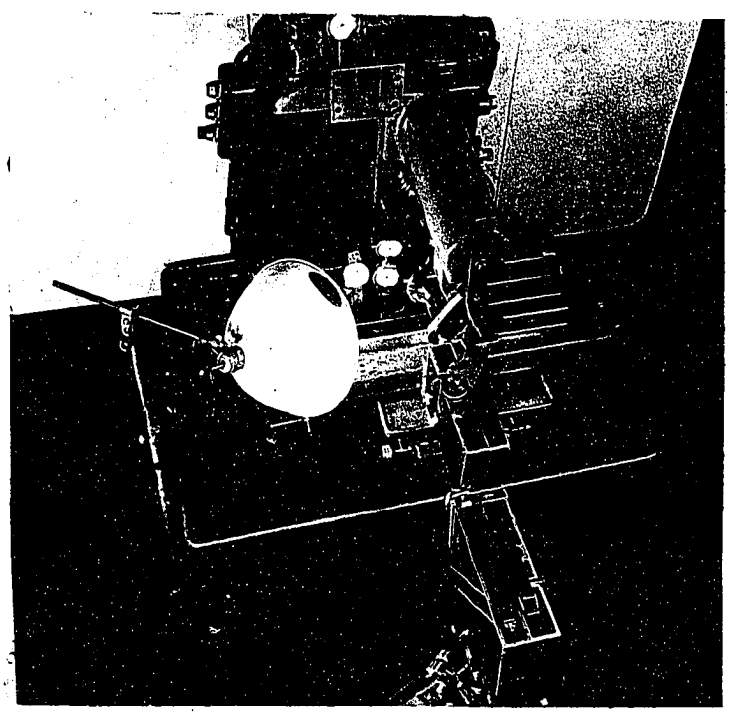

Figure 20b

Two "Cine Kodak Special" movie cameras, Fig. 20, were used to simultaneously record the cutting action through the microscope and the deflection of the tool and work indicators. The microscope camera was attached to the overarm by a bracket so that the axis of the microscope was in line with that of the camera shutter. The lens was removed from this movie camera. Focusing of the camera was accomplished by viewing the object through the regular ground glass provided with this camera.

The second movie camera was set up on a tripod (Fig. 20) and was focused on the two dial indicators as well as on a stop watch which was attached to the milling machine table. This camera had a f 1.9, 25 mm. lens. The illumination for this latter camera came from the same No. 2 photo flood lamp previously mentioned.

The syncronization of the force readings with their corresponding chip segments was accomplished as follows: The cut was first started and at the same time the stop watch was started and then both movie cameras were turned on. Next the entire illumination system was switched on from a single switch. After cutting for about one half minute the lights were switched off after which the movie cameras were stopped. The interval of illumination produced by the switching on and off of the lights was clearly visible on each of the movie films so that a definite position of starting and stopping of the cutting action could be accurately determined. About one to two seconds were required to form a single chip segment. The speed of the movie films was 24 frames per second so that

there were between 25 and 50 frames showing the formation of each segment.

The deflection readings corresponding to a given segment were determined by associating the deflection and the segment at the time that the lights were turned on. From then on the correspondence between force readings and segments was made by counting off force cycles and chip segments on the movie film. The stop watch gave the time interval during the cutting action so that the average film speed for each camera could be checked.

Selected frames from a scene showing the formation of a single chip segment are shown in Fig. 21. Here the depth of cut was .015" and the camera speed was 24 frames per second. Frame 1 shows the tool at the start of the segment with the previously ruptured segment still in view above the rupture plane. In frame 16 the tool had advanced a distance d = 0.0019" and shear is occurring to the inclined surface. The fact that shear is <u>not</u> occurring to the horizontal surface is indicated by the absence of deformation of the horizontal surface. In frame 20 where d = .0026" the shear has shifted to the horizontal surface as witnessed by the upward motion of the right hand portion of this surface. In successive frames the upward tilt of the horizontal surface becomes steeper and steeper. The intersection of this tilted surface and the horizontal surface is taken as the intersection of the shear plane with a horizontal surface. Frame 38 is the last frame prior to rupture. Rupture is observed to occur along a line

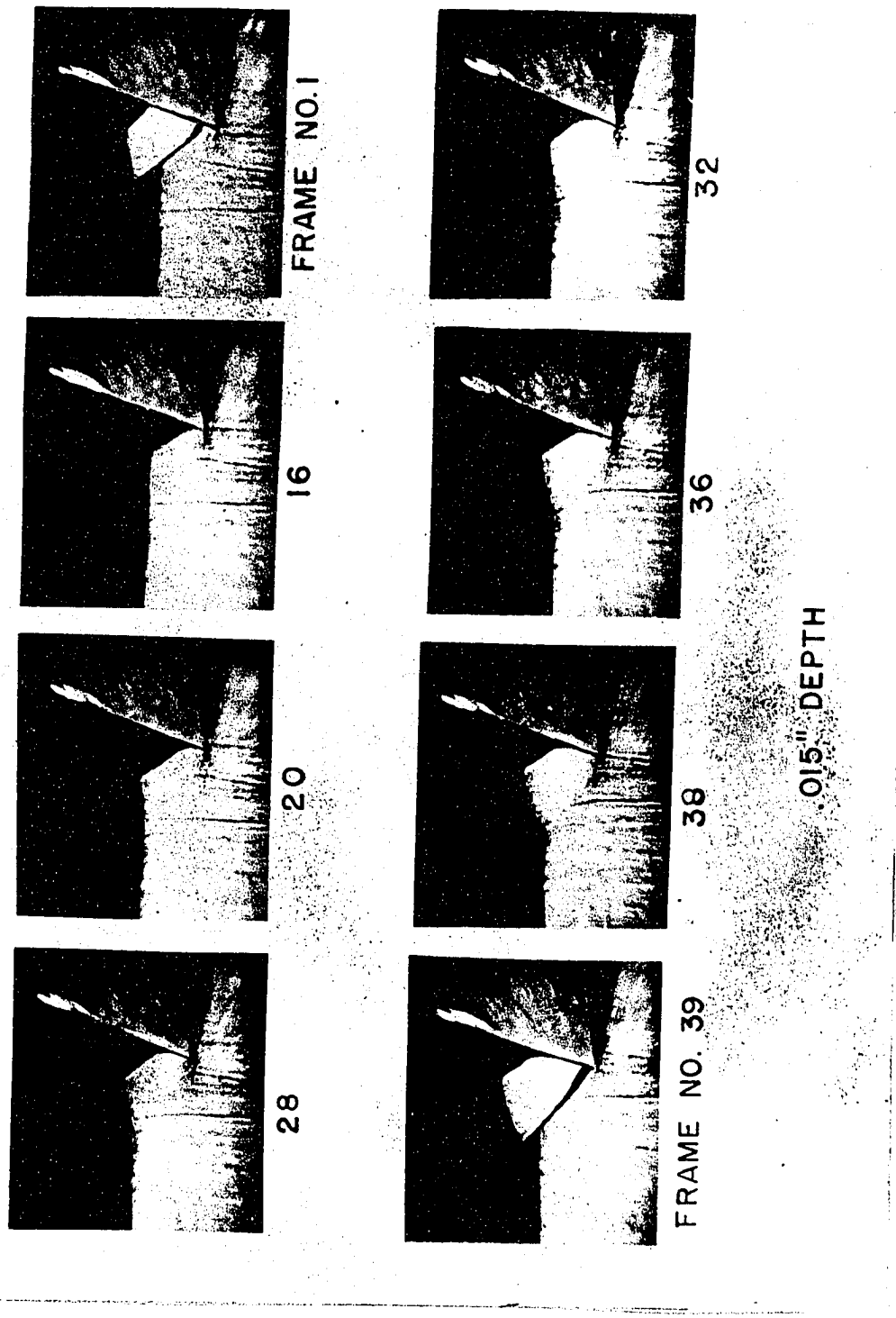

Figure 21

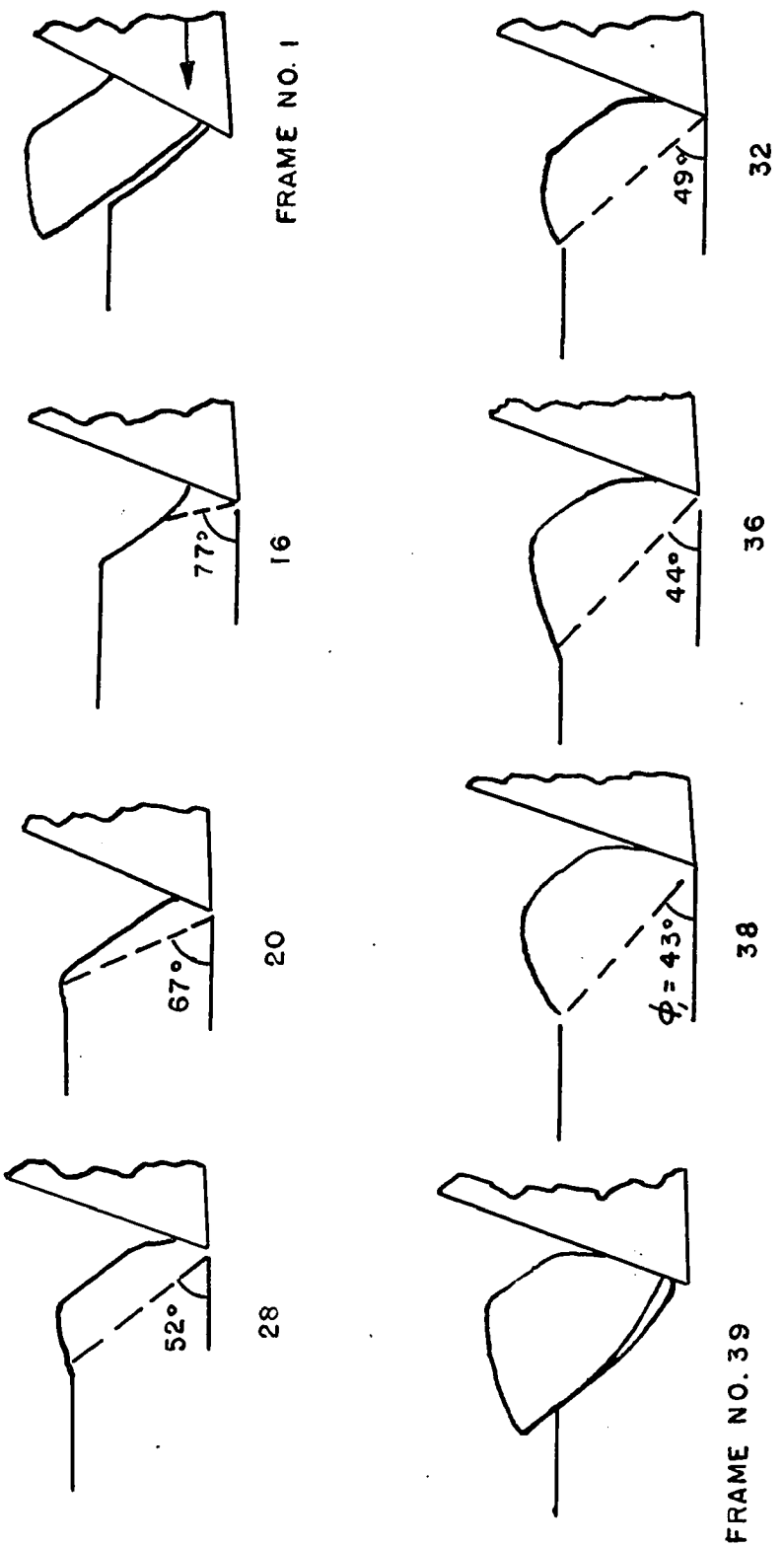

FIG. 22

TABLE I

Typical Data Sheet - Movie Scene "G", 7th Segment, t_1 = .015"

OBSERVED						CALCULATED					
Frame	Fc lbs.	Ft lbs.	d ins.	t ins.	ϕ, deg.	$\tau-\alpha$ deg.	τ deg.	μ	ϵ	S_s' psi	S_n psi
1	0	0	0	0	--	--	--	--	--	--	--
16	84.5	0.3	.0019	.008	77	0.2	14.2	.25	2.19	41300	182000
20	89.8	-0.9	.0026	.015	67	-0.5	13.5	.24	1.75	44000	101000
28	96.2	-4.0	.0047	.015	52	-2.4	11.6	.21	1.59	65500	76600
32	100.3	0.9	.0052	.015	49	-0.5	14.5	.26	1.58	65400	76500
38	100.3	1.7	.0076	.015	43	1.0	15.0	.27	1.63	65500	63200

extending from the tool point to the intersection of the horizontal and the tilted surface.

It should be noted that as the segment progresses the contact area between the chip and the tool face becomes larger and larger. As the chip slides across the tool face the coefficient of friction should increase due to the chip wiping off of all the contaminating agents from the tool face.

The photographs of Fig. 21 were enlarged from the movie frames and a good deal of the detail in the film was lost by reproduction. Thus the reflective surface on the deformed portion of the chip segment is hardly visible on these reproductions.

The actual study of the chip formation and the force readings was accomplished by placing both movie films side by side in a microfilm reader and lining up the frame of the force reading corresponding to that of the tool position. The image of the tool and chip segment was then traced onto drawing paper (the image was approximately 45 times larger than the original microscope scene). The chip segment shape and the shear and rupture planes were indicated on the sketch. The sketches corresponding to the photographs of the previous Fig. 21 are shown in Fig. 22.

A typical data sheet for this same segment is shown in Table I.

The behavior of the forces during the formation of a segment is shown in Fig. 23 where F_c and F_t are plotted

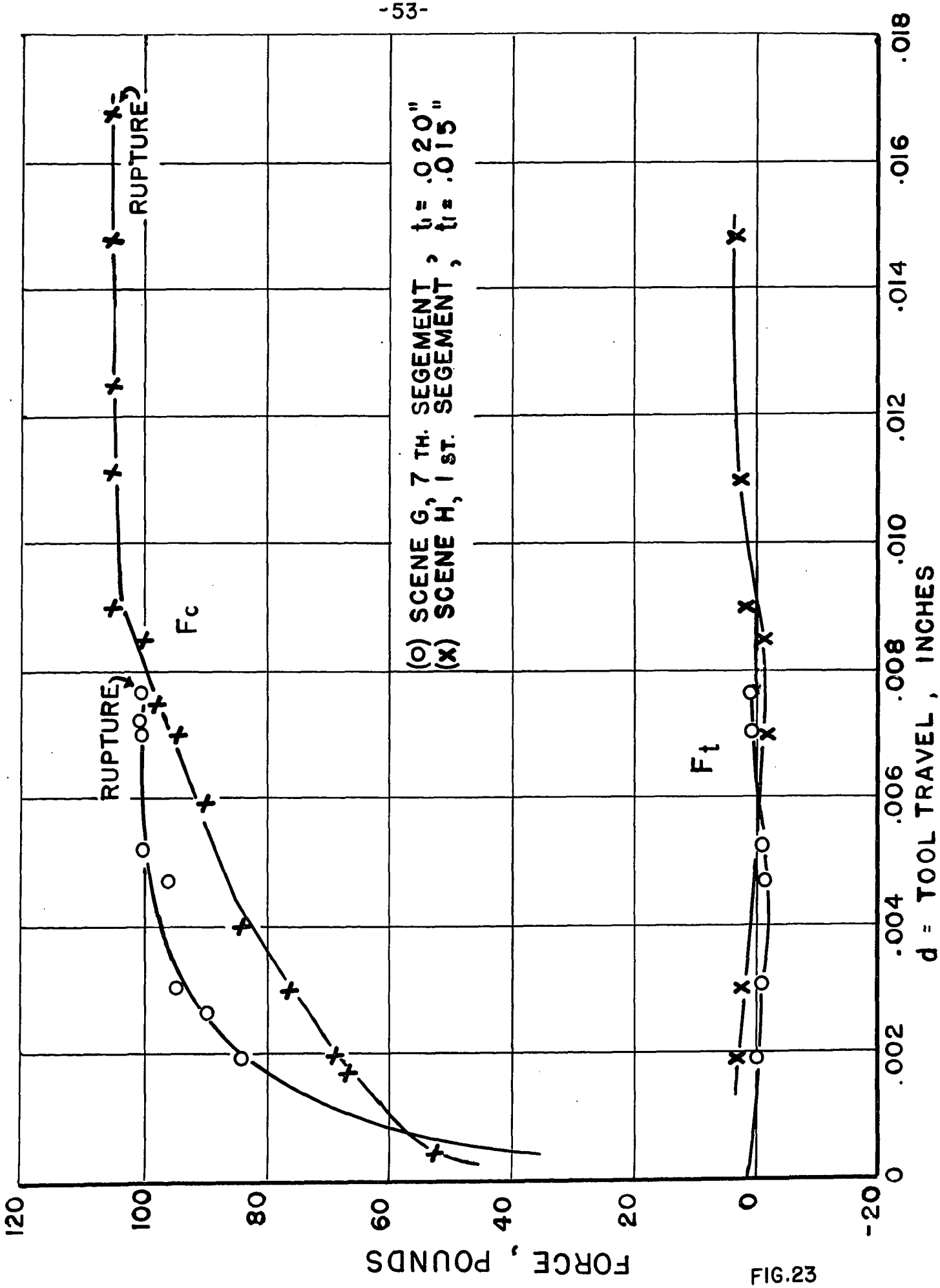

FIG.23

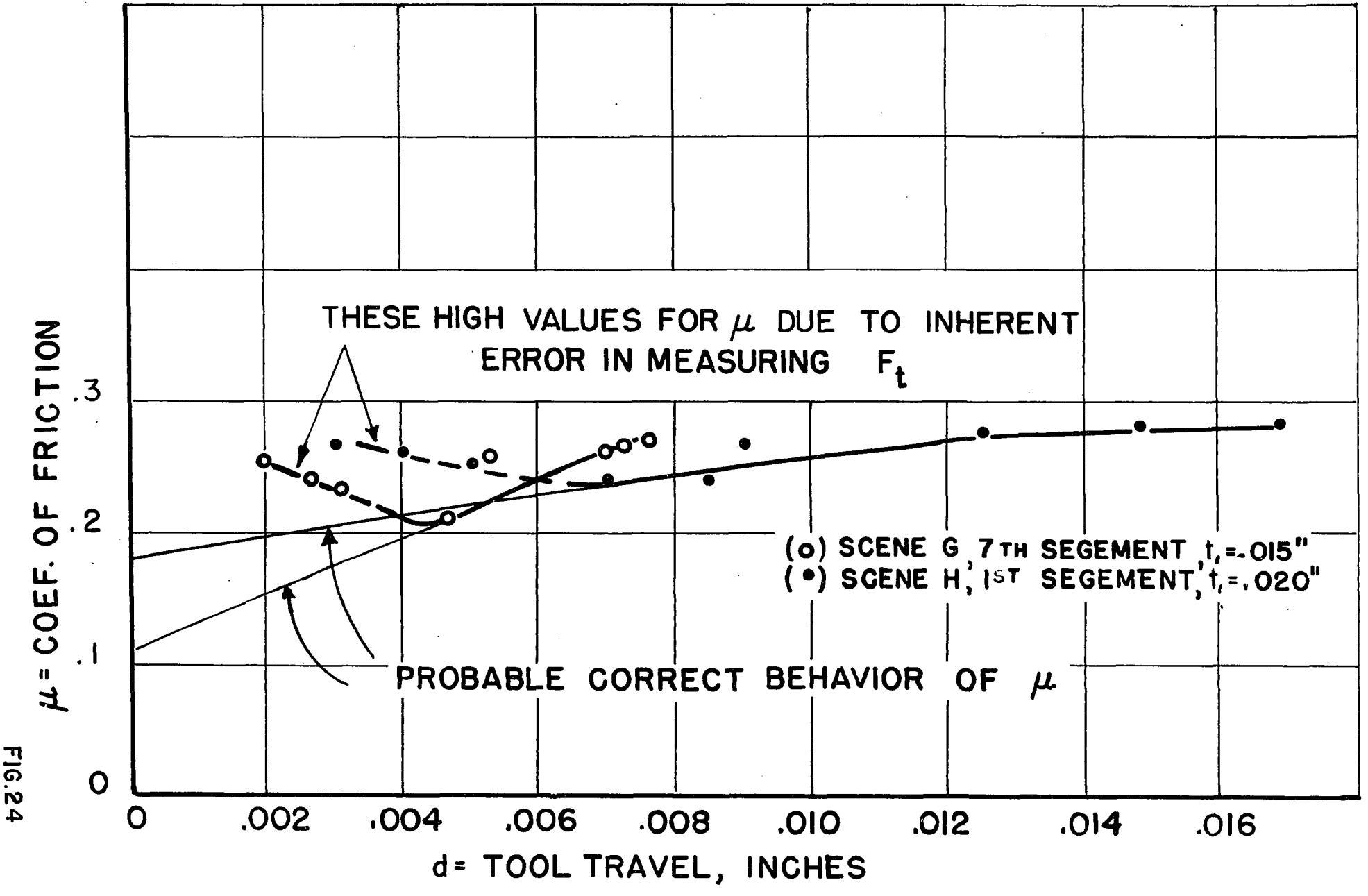

FIG.24

against the tool travel d for two depths of cut, .015" and .020". The cutting force F_c rises rapidly at the start of the cut but tapers off to a very slow rise at about half the total tool travel. The cutting force was never observed to decrease between the start of a chip segment and the time of rupture. This was true for every cut taken and is evidence of the condition that the minimum energy principle holds throughout the formation of a segment. The observed thrust force F_t had a positive value immediately after rupture. This value is due to the elastic deflection of the work and tool dynamometer and is an inherent characteristic of discontinuous chip formation. However, in this study the initial thrust value represented an error as far as the analysis is concerned. The thrust force assumes its correct value sometime after the tool enters the cut and for some distance prior to fracture the thrust force is the true value for that particular segment. The effect of the error was greatest on theevaluation of the correct friction angle β or the coefficient of friction μ especially during the first portion of the tool travel, Fig. 24. The actual values of the coefficient of friction can only be surmised in the region near the start of the segment.

The accuracy of the force readings is greatest prior to the time of rupture. This is fortunate since the rupture conditions are the most important, for herein lies the characteristic difference between the continuous and the discontinuous chip. The accuracy of the force readings at rupture are at their highest since the dynamometers have had time to steady themselves

TABLE II

MOVIE SCENE G. RUPTURE CONDITIONS, DEPTH CUT = .015"

OBSERVED				CALCULATED						
Segment	F_c lbs.	F_t lbs.	ϕ_1 deg.	$\tau-\alpha$ deg.	τ deg.	μ	ϵ	S_s' psi	S_n psi	$C=2\phi_1+\tau-\alpha$ deg.
1	84.7	2.27	42	1.5	15.5	.277	1.64	49600	47000	85.5
2	84.7	5.38	30	3.6	17.6	.317	2.02	42700	28300	63.6
3	84.7	8.22	42	5.6	19.6	.356	1.64	46500	46800	89.6
4.	95.2	2.83	41	1.7	15.7	.281	1.66	55500	51200	83.7
5	95.2	5.67	48	3.4	17.4	.313	1.58	53300	66800	99.4
6	100.5	2.27	52	1.3	15.3	.273	1.56	57200	76700	105.3
7	100.5	4.53	43	2.6	16.6	.298	163	58200	59200	88.6
8	105.7	8.78	39	4.7	18.7	.339	1.70	58200	55500	82.7
9	105.7	3.12	35	1.7	15.7	.281	1.57	58800	37700	71.7
10	105.7	3.12	45	1.7	15.7	.281	1.60	61700	65500	91.7

Average C= 86.2°

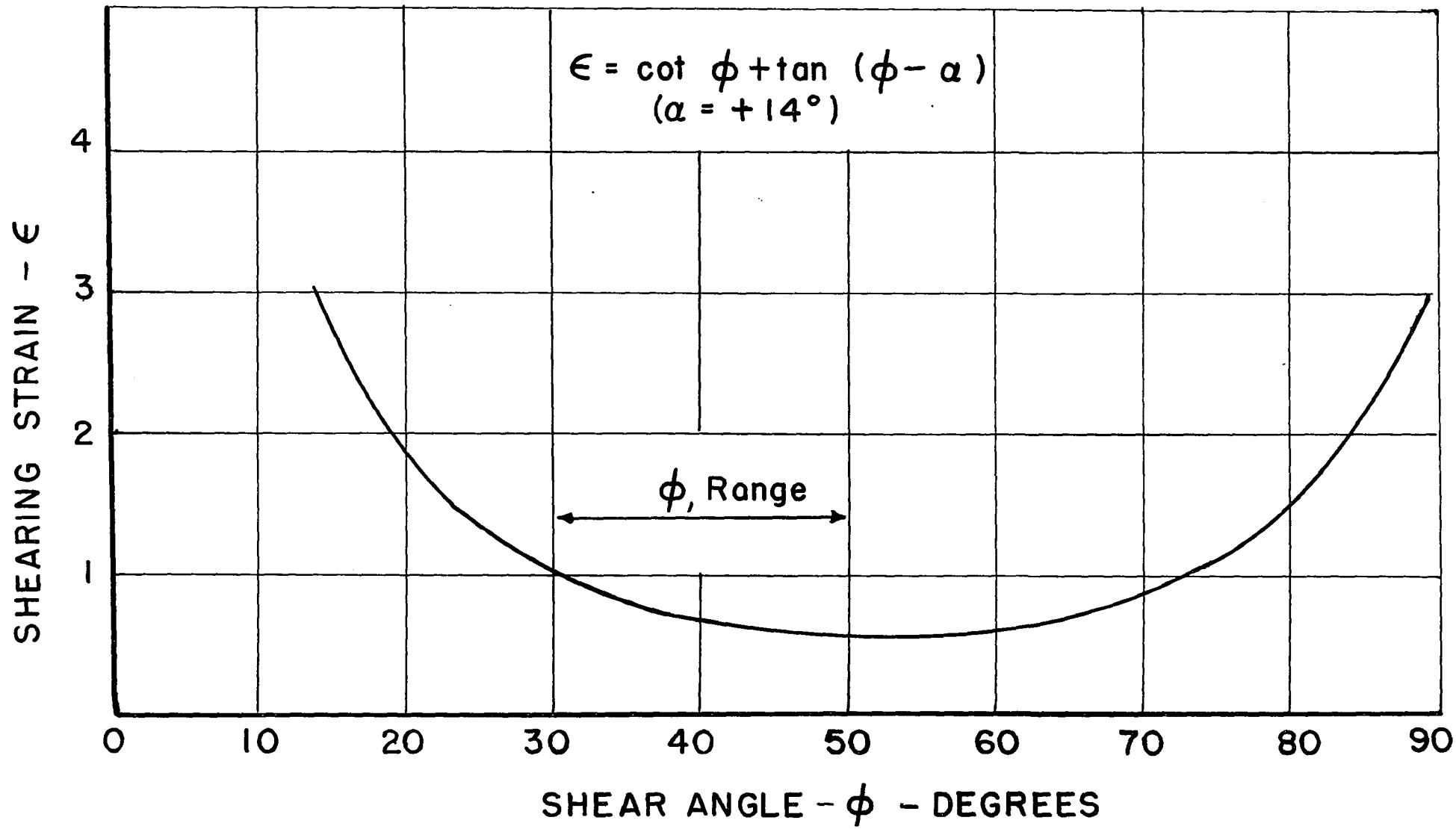

FIG.25

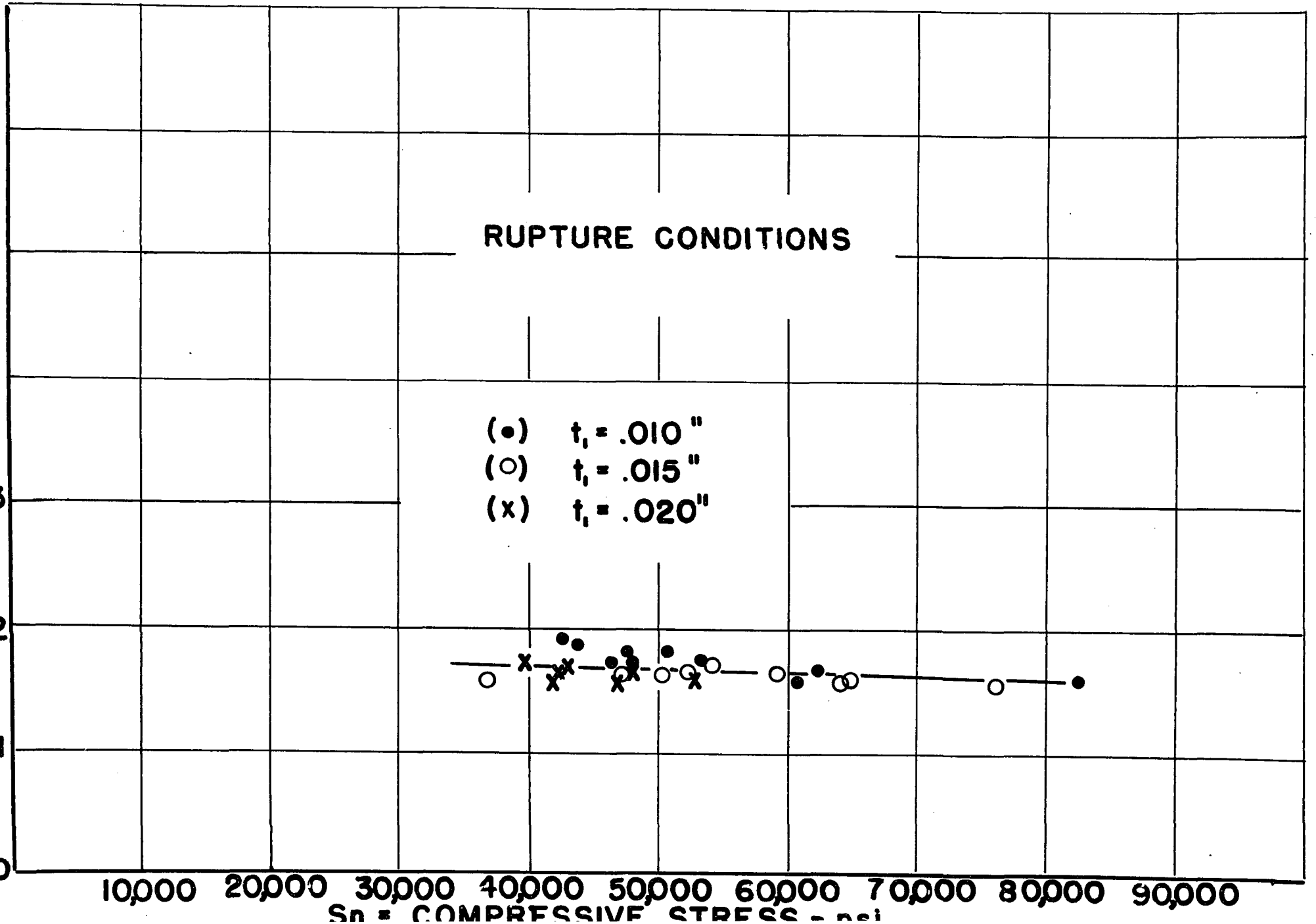

FIG. 26

from the shock of the previous rupture. Likewise the shear angle at rupture can be directly measured rather than inferred.

A typical data sheet for the rupture conditions for a .015" depth cut is shown in Table II. After examining such data immediate interest was aroused by the wide variation that was obtained for ϕ_1, the shear angle at rupture. The variation in ϕ_1 in this series of segments is seen to be between 30° and 52°. Similar wide variations were observed when taking the other cuts. These variations in ϕ_1 required a clear cut explanation if the developed theory was to have a meaning.

The shearing strain corresponding to the 14° rake angle tool is plotted in Fig. 25. For the most common rupture angles of 30° to 50° that were observed in the cutting tests, the shearing strain at rupture is seen to be between 1.6 and 2.1. It should be noted first of all that the large difference in shear angle at rupture produced a small difference in shearing strain because the ϵ vs. ϕ curve is fairly flat in the region in which rupture occurred.

If next the shearing strain vs. compressive stress relationship at rupture is examined, Fig. 26, it is seen that the shearing strain is practically constant over what appears to be a wide range in compressive stress (40,000 to 80,000 lbs. per square inch).

No further enlightenment is obtained by investigating the relationship existing between the shearing stress and the compressive stress at rupture, Fig. 27. A small increase in

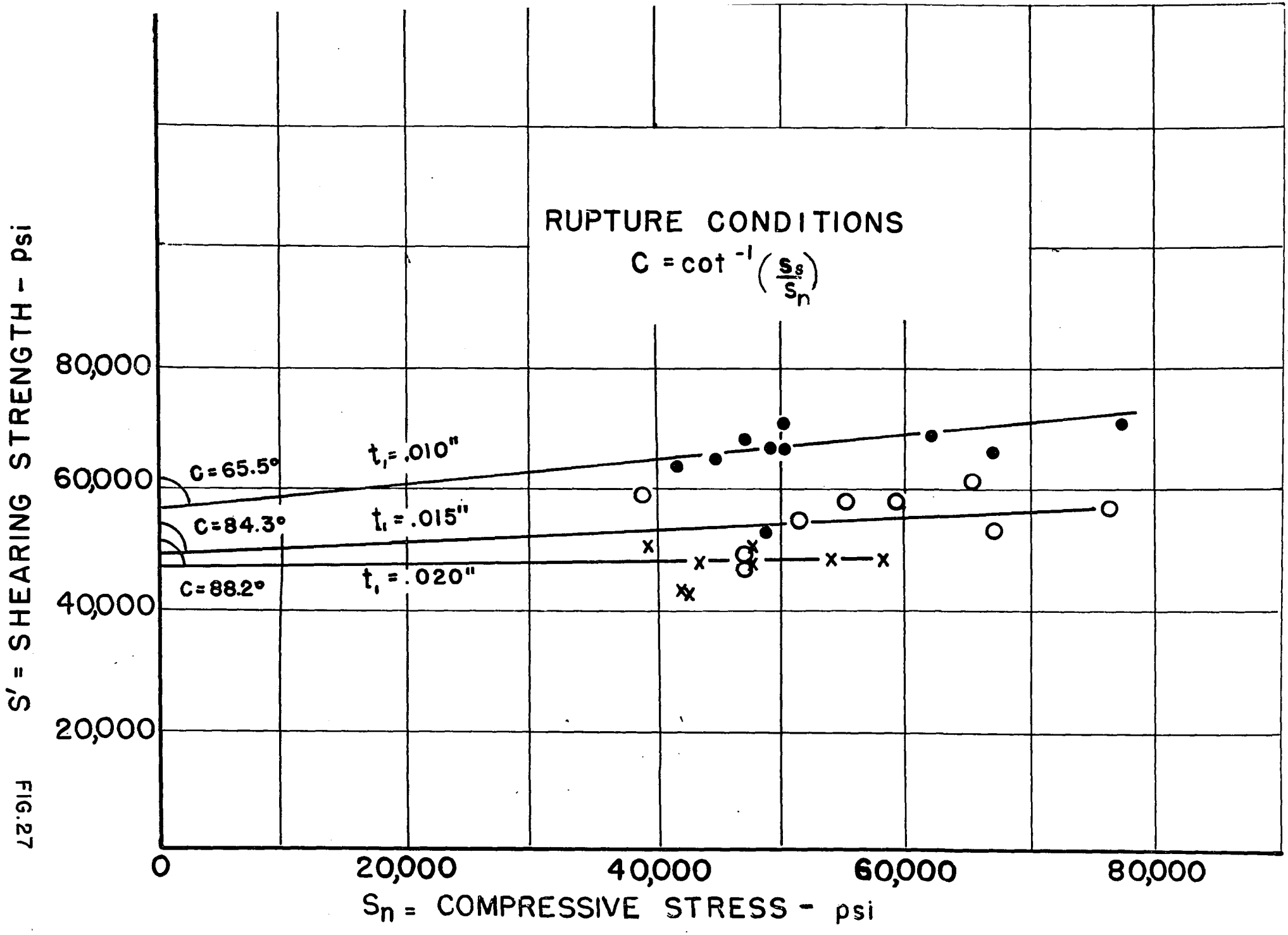

FIG. 27

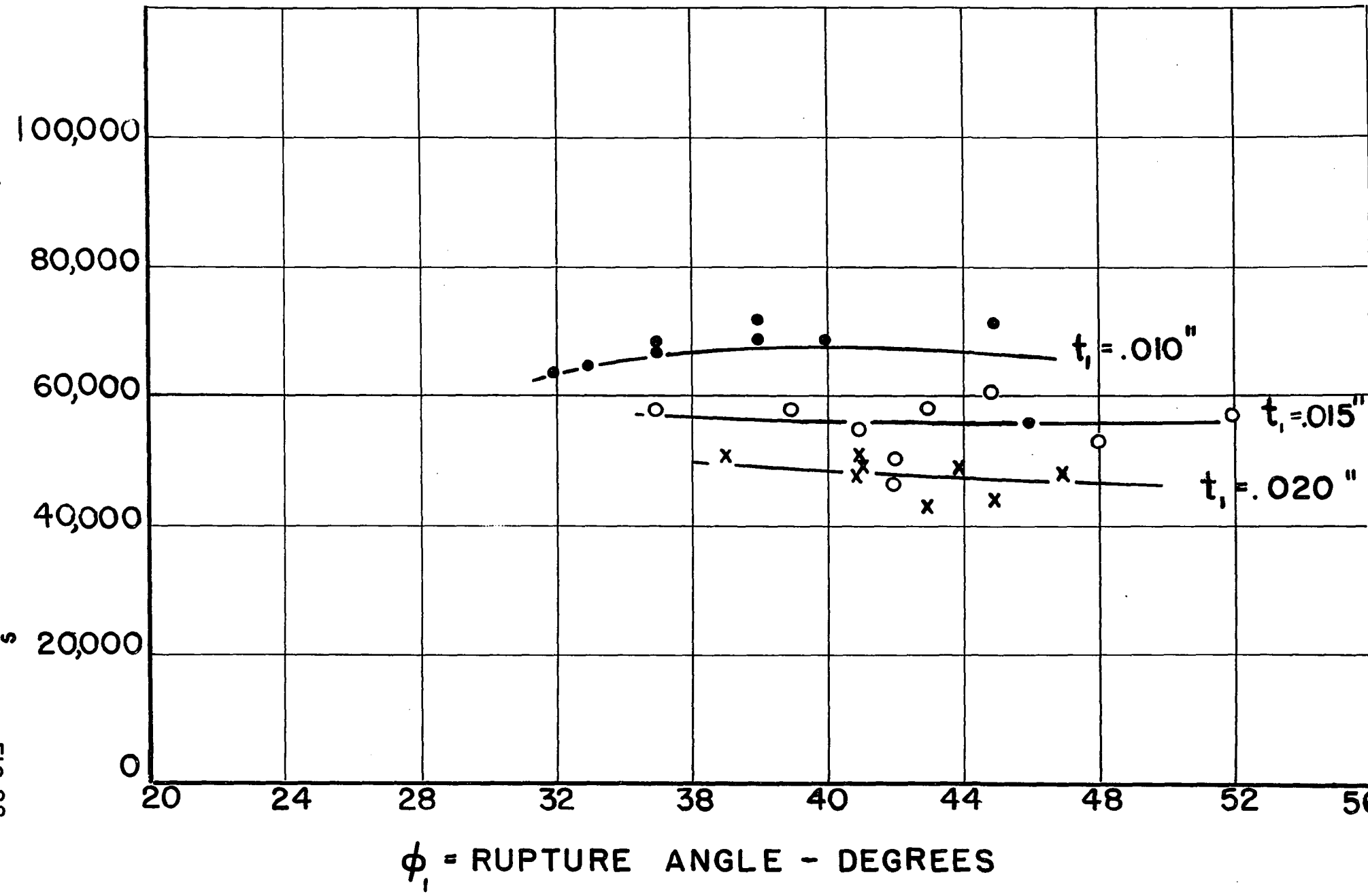

FIG. 28

shear stress was observed with the increase of compressive stress. The machining constant "C" for the bronze obtained from the slopes of these S_s' vs. S_n curves is seen to be 65.5° for .010" depth, 84.3° for the .015" depth and 88.2° for the .020" depth. This should be compared to the constants obtained from the relation $C = 2\phi_1 + \gamma - \alpha$. The average value of "C" calculated from this equation for all the chip segments was found to be 78.1° for .010" depth and 86.2° for the .015" and .020" depth. The correspondence between "C" as obtained from the S_s' vs. S_n curves and that calculated from $C = 2\phi_1 + \gamma - \alpha$ is considered to be a close correlation for the physical behavior of the metal at the instant of rupture.

Fig. 28 shows the shearing strength plotted against the shear angle at rupture. At a given depth of cut the shearing strength is observed to be fairly constant over the complete range of rupture angles. The shearing strength, however, was smaller at the greater depths of cut.

For an understanding as to the nature of rupture, the investigation has to go back to the happenings during the formation of the individual chip segment. Referring to the lower curve of Fig. 29 it is seen that in the early stages of the segment formation the compressive stress acting on a shear plane is very high (over 200,000 lbs. per square inch and as high as 400,000 lbs. per square inch). This high compressive stress is associated with the high shear angles that exist at the early part of the cut. Accompanying the high shear angle is a high

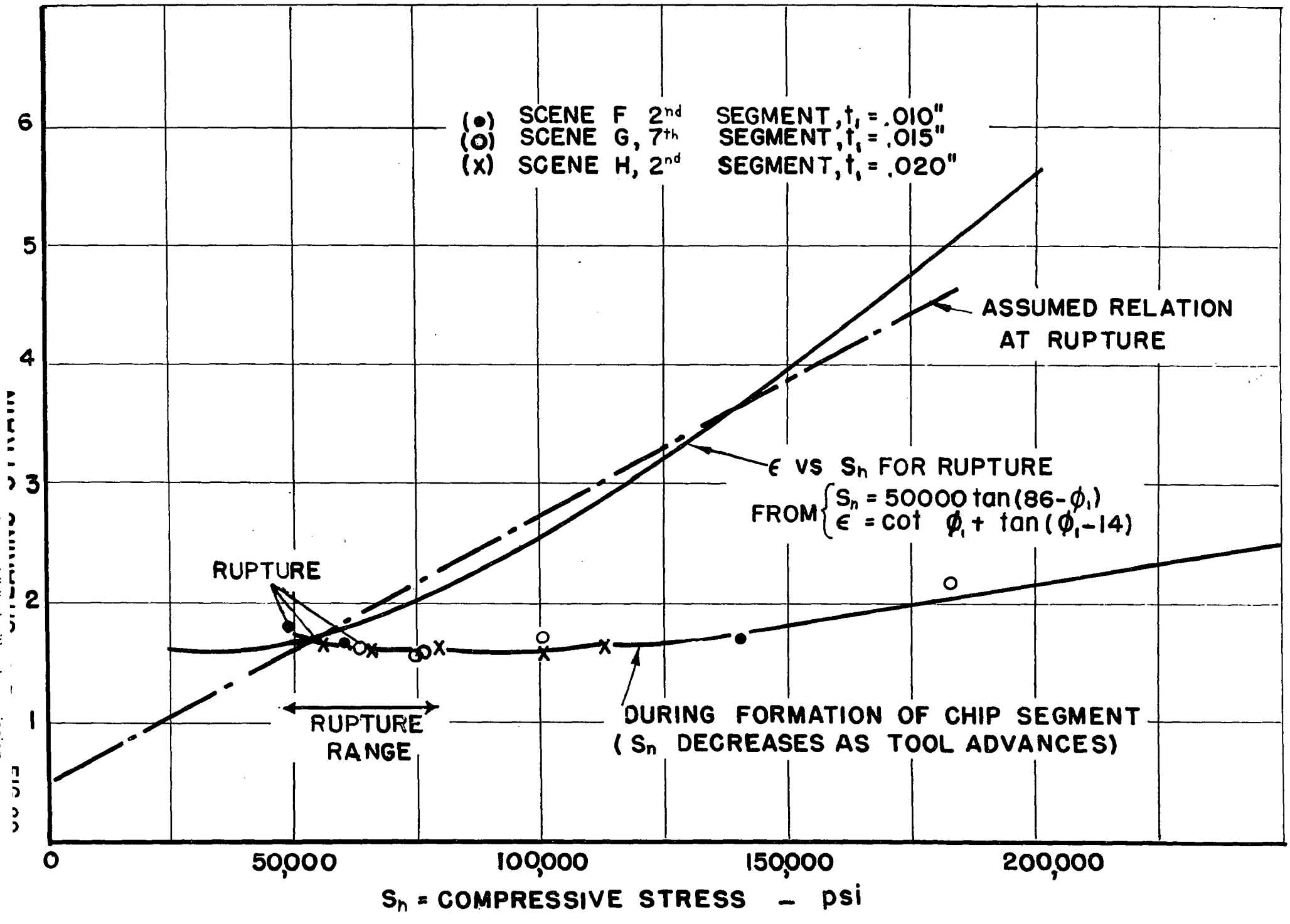

shearing strain. In fact the strain in the early stages of the cut are higher than the strain values at rupture. The metal does not rupture, however, because its ductility has been enormously increased by the presence of the aforementioned high compressive stresses acting on the shear plane. As the tool advances the shear angle decreases due to the shape of the work surface together with the continual increase in friction acting between the chip and tool face. This decrease in shear angle is accompanied by a rapid decrease in the compressive stress. When the shear angle reaches values of 50° down to about 30°, rupture occurs. Within this shear angle range the shearing strain remains fairly constant. However, rupture is caused by the rapid decrease in ductility that accompanies the decrease in compressive stress which in turn allows the work material to rupture at the same strain values.

The ϵ vs. S_n curve for rupture for our work material is not available and has to be obtained by a Bridgman[26] type test (such tests will get under way in our laboratory in the near future using an apparatus built by J. Kemeny[27]). However, the approximate behavior for the shearing strain with compressive stress for rupture was computed from the relations $S_n = S_s' \tan (C - \phi_1)$ and $\epsilon = \cot \phi_1 + \tan (\phi_1 - \alpha)$ by assuming a constant value of 50,000 for S_s' and a value of 86° for "C" which are the approximate values observed at rupture, see Fig. 27 and 28. The resulting ϵ vs. S_n curve necessary for rupture is also plotted in Fig. 29. It is seen that at the high compressive stresses existing at the start of the chip segment the shear-

ing strain within the chip is insufficient to produce rupture. However, as the compressive stress acting on the shear plane decreases the shearing strain in the chip becomes sufficient for rupture. Rupture occurs when the two curves intersect.

The apparent wide range in shear angles at rupture can be explained as follows: the range of compressive stress for the same ϕ_1 range (40,000 to 80,000 lbs. per square inch) is small compared to the compressive stress that existed at the beginning of the chip segment. The ϵ vs. S_n curve for rupture crosses the ϵ vs. S_n curve for the chip segment at a small angle. Any variation in the ϵ vs. S_n values for rupture will thus result in a wide variation for the compressive stress within the chip for rupture to occur. Such variations in the ϵ vs. S_n rupture conditions can be present in the work material due to inhomogenities from point to point within the work material.

It is interesting to see how closely the rupture conditions agree with the equation developed on the basis of shearing strain, equation (49a)

$$\epsilon = \epsilon_o + \frac{K S_o}{\cot (C - \phi_1) - \cot C} \qquad (49a)$$

By extending the straight line portion of the ϵ vs. S_n curve for rupture of Fig. 29, ϵ_o and K can be approximately determined as $\epsilon_o = 0.50$, $K = 2.27 \times 10^{-5}$ $\left[in^2\ lb^{-1}\right]$

Use S_o = 50,000 lbs./sq. in. from Fig. 28

$C = 86°$ (Average "C" for .015" and .020" depth cuts)

Substituting these values in (49a) gives the following relation between ϵ and ϕ_1 for our work material.

$$\epsilon = 0.50 + \frac{1.14}{\cot (86 - \phi_1) - 0.07} \qquad (51)$$

Table III shows the comparison between the shearing strain calculated from the actual strain values within the chip, (column 3) and the shearing strain calculated from equation (51) (column 2). A close correlation is obtained for the shear angles of 35° to 50° which include the region in which practically all the segments rupture.

TABLE III

COMPARISON OF CALCULATED FROM EQUATIONS (51) AND (3)

ϕ_1	ϵ from (51)	ϵ from (3)
25	2.9	2.3
30	2.4	2.0
35	2.0	1.8
40	1.8	1.7
45	1.6	1.6
50	1.4	1.6

Summary of Discontinuous Chip Formation

The geometry, mechanics and plasticity conditions for the discontinuous chip have been worked out.

After the rupture of a chip segment, the tool advances into the metal whose immediate upper surface is inclined at the rupture angle ϕ_1 with respect to the tool travel. As the tool advances the metal fails by a process of shear along a plane extending from the cutting edge to the inclined surface. During this time the depth of cut increases since the shear plane continually extends farther and farther up the inclined surface. All during this period the instantaneous shear angle ϕ_2, the friction angle β, and the rake angle α are related by the plasticity condition $2\phi_2 + \beta - \alpha - \phi_1 = C$ where "C" is a constant for the work material. As the tool moves along, the friction between the chip and tool increases and the shear angle thus decreases in accordance with this plasticity condition. When the tool reaches a certain distance the energy required for shear to occur to the horizontal surface becomes less than the energy required to shear to the inclined surface. From that point on the shear angle and the friction angle are related by the plasticity condition $2\phi + \beta - \alpha = C$ (which is the same condition that exists in continuous chip formation). Again as the tool advances the shear angle continues to decrease and eventually rupture occurs.

The shear angle at rupture is determined by the shearing strain and the compressive stress on the shear plane. Every

material has a characteristic shearing strain for rupture vs. compressive stress curve. The ductility of most materials is increased with increasing compressive stress, i.e., they will withstand a much higher shearing strain before rupturing if subjected to compressive stress. In the early stages of the chip segment formation the compressive stress on the shear plane is very high and may, in fact, reach values between 200,000 and 400,000 lbs. per square inch. This high compressive stress increases the ductility of the metal and hence inhibits rupture. As the chip formation continues the compressive stress decreases rapidly primarily because of the rapid decrease in shear angle. Eventually the compressive stress decreases sufficiently to allow the existing shearing strain in the metal to produce rupture.

"Brittle" materials such as cast iron will not withstand very high shearing strains at low values of compressive stress. Hence brittle materials invariably produce a discontinuous chip. "Ductile" materials such as steel may produce either a continuous or discontinuous chip depending upon the equilibrium value of the shear angle. Thus in steels the shear angle reaches an equilibrium value which is high enough so that the existing shearing strain is insufficient to produce rupture, and a continuous chip is hence formed. However, if the friction between the chip and tool is increased (e.g. by cutting dry with a high speed steel tool at low speeds) the shear angle tends to drop to a value so low that the resulting

shearing strain becomes great enough to produce rupture and a discontinuous chip is then formed.

PART II: X-RAY STUDY OF MACHINED SURFACES

Introduction

The object of any machining operation is to produce a surface having a specified contour, dimensional accuracy and surface finish. Previous studies have been directed toward the mechanism of the metal cutting process in which attention was focused on the region surrounding the shear plane. During the same process, however, a finished surface is produced and it is on the quality of this surface that this present study is directed.

It has been shown by Ernst and Merchant[16, 19] that the smoothness of the surface produced is a function of the "Built Up Edge" which forms in the cutting process. These particles of "Built Up Edge" are severely work hardened by the cutting process[8], increases in hardness of as much as 300 times having been observed by Zlatin and Merchant[28]. Fragments of this "Built Up Edge" are eventually sloughed off onto the workpiece and impart roughness to the finished surface[19].

During the metal cutting operation the work material is severely deformed and although the major portion of this deformed metal is removed in the cutting process, a considerable zone of work hardening is left on the machined surface.

Even the most superficial metal work operation, such as metallographic polishing, leaves a cold worked layer. H. Vacher[29] found that the ordinary mechanical metallographic polishing

procedures produced a cold worked region of 2 to 25 microns (0.00008" to 0.001") on steel, and 5 to 95 microns (0.0002" to .0037") on aluminum specimens.

Thomassen and McCutcheon[30] found depths of cold work up to 0.010" in milling brass and up to 0.020" in turning brass. In the milling tests a threefold increase of depth of cold work was observed on using a dull cutter instead of a sharp cutter. Zankl, Barkow and Schmidt[31] report depths of cold working of 0.003" to 0.005" in carbide milling Dowmetal surfaces and 0.002" in carbide milled SAE 1020 steel surfaces. In all of these studies x-ray diffraction back reflection technique was used to determine the depth of cold work.

J. Wulff[32] studied the depth and nature of the surfaces deformed by grinding, honing, and metallographic polishing. He employed the electron diffraction technique. For 18% Cr, 8% Ni stainless steel he found that dry grinding produced a deformation 11 microns deep, wet grinding 8 microns deep, honing and metallographic mechanically polishing about 1 1/2 microns deep. Originally the stainless steel had a coarse grained austenitic structure. In all of the surface finishing operations the worked region was composed of deformed austenite plus cold worked ferrite. (Austenite will transform to ferrite by cold working at temperatures under 200°C). Only in the case of dry grinding was a surface oxide film found. The film was approximately 0.3 microns thick and was caused by a flash surface temperature exceeding 500°C.

The working of any metal is accompanied by any one or

more of the following: 1) Reduction in grain size, 2) Deformation of the crystal, 3) Preferred orientation, 4) Phase change.

1) Reduction in grain size - During the working of a metal the grains are disbursed into crystallites of smaller size. W. Wood[33] has found that it is impossible, even after the most severe deformation, to break down the crystallite size below about 10^{-5} cm. Hence the crystallite must be regarded as a fundamental unit of the metallic grain. Wood found that the size of the fundamental crystallite was 0.7 X 10^{-4} mm. for copper, 1.2 X 10^{-4} mm. for nickel, 1 X 10^{-3} mm. for aluminum, and 3.2 X 10^{-4} mm. for iron.

2) Grain distortion - Working in metals produce "microstrains" or strains within the individual grains, and "macrostrains" which result from elastic distortion. Microstrains cause line broadening of the x-ray photograms while macrostrains result in line shifts.

The nature of the surface macrostresses can conveniently be determined by the x-ray method. Such studies are important on machine parts that are to be subjected to repeated stresses. Almen[34] has shown that residual compressive stresses at the surface increase the fatigue strength of a metal whereas residual tensile stresses seriously decrease the fatigue strength.

The x-ray stress measurement method is non-destructive and in addition can be used to determine the stress in very small areas (as little as 1/2 mm. diameter circle). Hence a stress

traverse can be made over various parts of a body. Such studies have been made of residual stresses produced in welded structures[35].

3) Preferred Orientation - Preferred orientation results from the tendency for the metal crystals to cleave and glide or slip along certain crystallographic planes[36]. Such planes of slip are usually among the most densely populated sets, i.e., sets of planes having more atoms per unit area than other crystallographic planes. The special direction of fragmentation and slip results in the fragments acquiring preferred orientation with respect to certain directions of the working process, e.g., with respect to the rolling axis in the case of rolling of metal. This preferred orientation may be beneficial or detrimental. Thus N. Goss[37] has found that the electrical properties of silicon sheet steel for transformer laminae are improved by allowing it to retain its preferential orientation. Such steel has a considerably higher magnetic permeability in the direction of roll. J. Snoek[38] has found that the resistance of nickel steel to corrosion improves when the orientation is preferential. In general, however, preferential orientation is objectionable because it weakens a metal and reduces its ability to withstand further deformation.

4) Phase changes - Usually result from temperature changes that accompany metal working, and in some cases phase changes may occur by the application of extreme pressures, for example, transofmration of austenite to ferrite.

In the machining of metals it was anticipated that any one

TABLE IV

Chemical and Physical Properties of Stainless Steels Used As Work Materials

AISI Type	C	M_n	P	S	S_i	C_r	N_i	S_e	UTS psi	Bhn	Stock Size Ins.
302	.06	.53	.02	.02	.52	18.11	8.55	--	85000	149	7/8x3
303Se	.06	.78	.13	.03	.42	17.69	9.58	.28	85000	153	7/8x2-1/2
303S	.06	.73	.03	.26	.57	17.99	9.27	--	85000	150	7/8x3-7/8

or all of the above four effects of metal working would be produced in the vicinity of the surface.

Machining Tests

Three types of austenitic stainless steels were chosen as the work material. All were of the 18 Cr, 8 Ni variety: A.I.S.I. 302, 303 Se and 303 S. The latter two were free machining types and contained selenium and sulphur additives. The complete chemical and physical properties of these materials are given in Table IV.

The stainless steel bar stock was hot rolled and annealed. Test pieces were cut off six inches long and the sides were milled to 1/2 X 2 1/2". These test pieces were clamped in a vise and face milled on a Cincinnati #3 Vertical Dial Type Milling Machine with a single tooth face milling cutter. The cutter radius was 2.1" and the cutter was positioned centrally with respect to the work. Fig. 30.

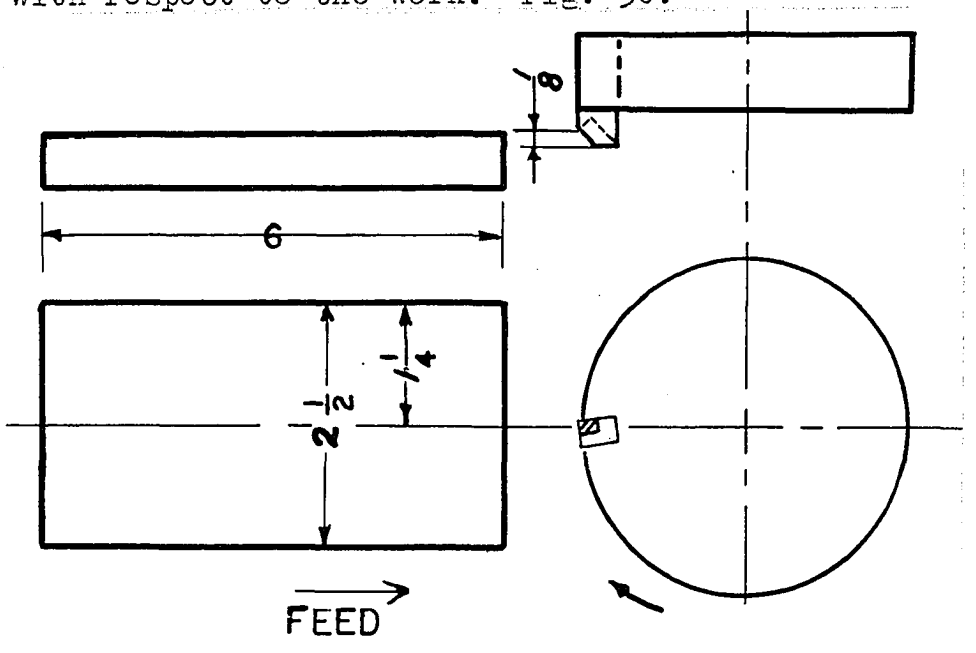

Figure 30

TABLE V

Cutting Data on Stainless Steels *

Run No.	AISI Type	True Rake Degrees	Cutting Speed Ft/Min.	Cutting Ratio	Surface Finish**	
					p	n
1	302	-30	300	.51	35	70
2	"	-30	1000	--	45	45
3	"	0	300	.55	18	30
4	"	0	1000	.54	16	20
5	303Se	-30	300	.49	45	65
6	"	-30	1000	--	40	55
7	"	0	300	.54	32	30
8	"	0	1000	.60	25	27
9	303S	-30	300	.51	40	45
10	"	-30	1000	--	32	43
11	"	0	300	.54	23	30
12	"	0	1000	.60	25	29

* Depth cut= .125"; Feed per tooth= .008"

** Surface finish in micro-inches, rms by Profilometer test; (p) is reading parallel to tool travel; (n) is reading normal to tool travel.

Carboloy 78 was used as the cutting material. Milling cuts were taken 0.125" deep, 2 1/2" wide, at a feed per tooth of .008". Two types of cutters and two cutting speeds were used on each work material. The first tool had a 22° negative axial and radial rake, a 45° corner angle and a true rake of -30 degrees[39]. The second tool had a zero degree axial and radial rake, a 45° corner angle and a zero degree true rake. With each cutter a cut speed of 300 and then 1,000 ft. per minute was used. The pertinent cutting data is given in Table V. The tool was sharpened with a diamond grinding wheel before each run.

After the test bars were milled, a cylindrical sample 5/8" diameter by 1/2" high was taken from the center of the test bar, Fig. 31, using a hollow mill for this purpose. The

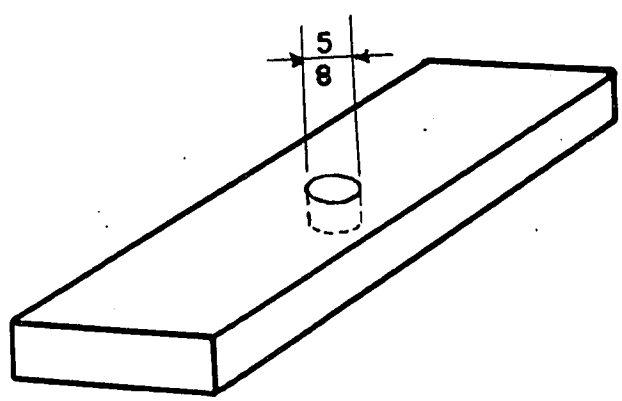

Figure 31

side of the specimen opposite the test cut was electrolytically polished using a solution consisting of 50% citric acid, 15% sulphuric acid and 35% water[40] with a current density of 1.8 amps per square inch. A total of .008" was polished off at a

rate of .006" per hour.

Instruments Available for X-Ray Studies

Two x-ray diffraction instruments were available for these studies. The first was a North American Phillips Co. type 12031 Diffraction Unit equipped with a precision back reflection camera, a powder camera, a flat transmission camera and a flat back reflection camera. The x-ray tubes were water cooled with non-removable targets. A copper, molybdenum and an iron tube were on hand.

The second instrument was a North American Phillips Geiger Counter X-Ray Spectrometer type 12021, equipped with a Brown Recorder. With this were two air-cooled x-ray tubes, copper and iron.

Lattice Constant for Stainless Steels

The unit cell dimension a_o was first obtained for each type of steel on a separate rectangular section 1/4 x 1/2 x 5/8". The 1/2 x 5/8" face was ground to a 5 cm. radius on a cutter grinder to conform with the periphery of the Phillips Precision Back Reflection Camera. The curved face of the specimen was electrolytically polished to remove .005". The following lattice constants were found using Fe-K_α radiation.

A.I.S.I.	Crystal System	a_o - Angstroms
302	F.C.C.	3.57
303 Se	F.C.C.	3.60
303 S	F.C.C.	3.62

General Considerations

Immediately after starting the x-ray study two important facts were realized.

1) Almost all studies would have to be by the reflection rather than the transmission method. This was not so much a matter of convenience as it was a necessity because of a) the thick samples; b) the worked region that was to be investigated was confined to within .005" of the surface; c) any attempt to remove a thin layer of the surface for transmission studies might introduce errors of greater magnitude than the disturbance that was being studied.

2) None of the x-ray tubes on hand was suitable for this work. The molybdenum target tube was unsuitable for back reflection work. The copper target tube produced fluorescence from the iron. The iron target tube was found to produce considerable fluorescence because of the high chromium content of the stainless steel. A chromium target tube seemed to have the necessary qualifications for back reflection study on the stainless steels. F. Gisen[41] had reported that chromium radiation produced sharp lines in heat treated steels. A chromium target tube was, therefore, ordered from North American Phillips Co. However, Phillips Co. has not been able to supply us with a chromium tube for they are experiencing difficulty in making such a tube. It was necessary, therefore, to use the iron target tube for the back reflection studies.

Residual Stresses in Machined Surfaces

Residual elastic stresses are measured in x-ray diffraction by a precise measurement of lattice dimensions. Back reflection is most sensitive for detecting small changes in atomic dimensions. This can be seen by differentiating Bragg's law: $n\lambda = 2d \sin\theta$

$$d\theta = -\frac{dd}{d} \tan\theta$$

but

$$\frac{dd}{d} = \epsilon = \text{strain}$$

$$d\theta = -\epsilon \tan\theta$$

For a given strain, $d\theta$ will be proportional to $\tan\theta$. Hence the largest values of $d\theta$ will occur as $\theta \rightarrow 90°$, for then $\tan\theta \rightarrow \infty$.

The sum of the principal stresses in the plane of the surface can be computed by placing the specimen face perpendicular to the x-ray beam at a predetermined distant, D, from the film, Fig. 32. If σ_1 and σ_2 are the principal stresses acting at a point in the specimen their sum can be determined from[42]:

$$\sigma_1 + \sigma_2 = -\frac{E}{\nu}\left(\frac{d_s - d_o}{d_o}\right)$$

where:

E = modulus of elasticity

ν = Poisson's ratio

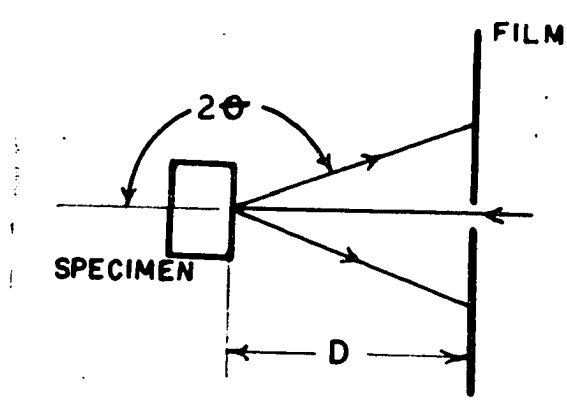

Figure 32

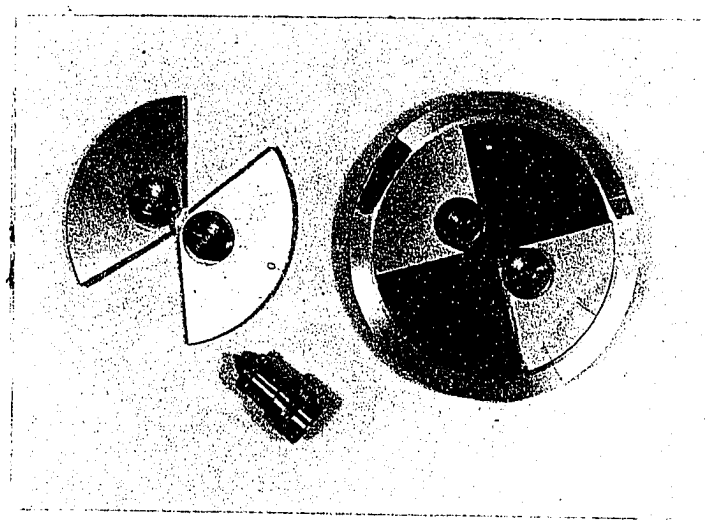

Figure 33

d_o = Spacing of atomic planes lying parallel to the surface for the unstressed metal

d_s = Spacing for stressed metal

In this relation $\frac{d_s - d_o}{d_o}$ is the strain normal to the surface produced by the surface stresses σ_1 and σ_2. (The stress σ_3 normal to the surface is zero.)

The accuracy of this method depends first on working with values of θ close to 90° so that the spacing between the planes perpendicular to the surface is measured, and second on the accuracy of determining d_s and d_o. This latter accuracy in turn is a function of the specimen to film distance, D, and the sharpness of the diffracted ring on the film. Various methods are available for determining D. The method finally used was one suggested by Thomas[43] in which D was set to within .001" by means of a gauge, Fig. 33. D can be accurately determined by placing an annealed powder such as gold or silver on the surface of the specimen and calculating the distance to the film corresponding to the ring diameter of the powder [43,44]. (It was found in our study using Fe radiation that a sharp calibrating ring could be obtained from molybdenum powder sprinkled on scotch tape which in turn was placed on the specimen face. However, this was not used in this stress determination.)

The sharpness of the diffracted ring in the photograph is dependent upon the grain size of the specimen and its

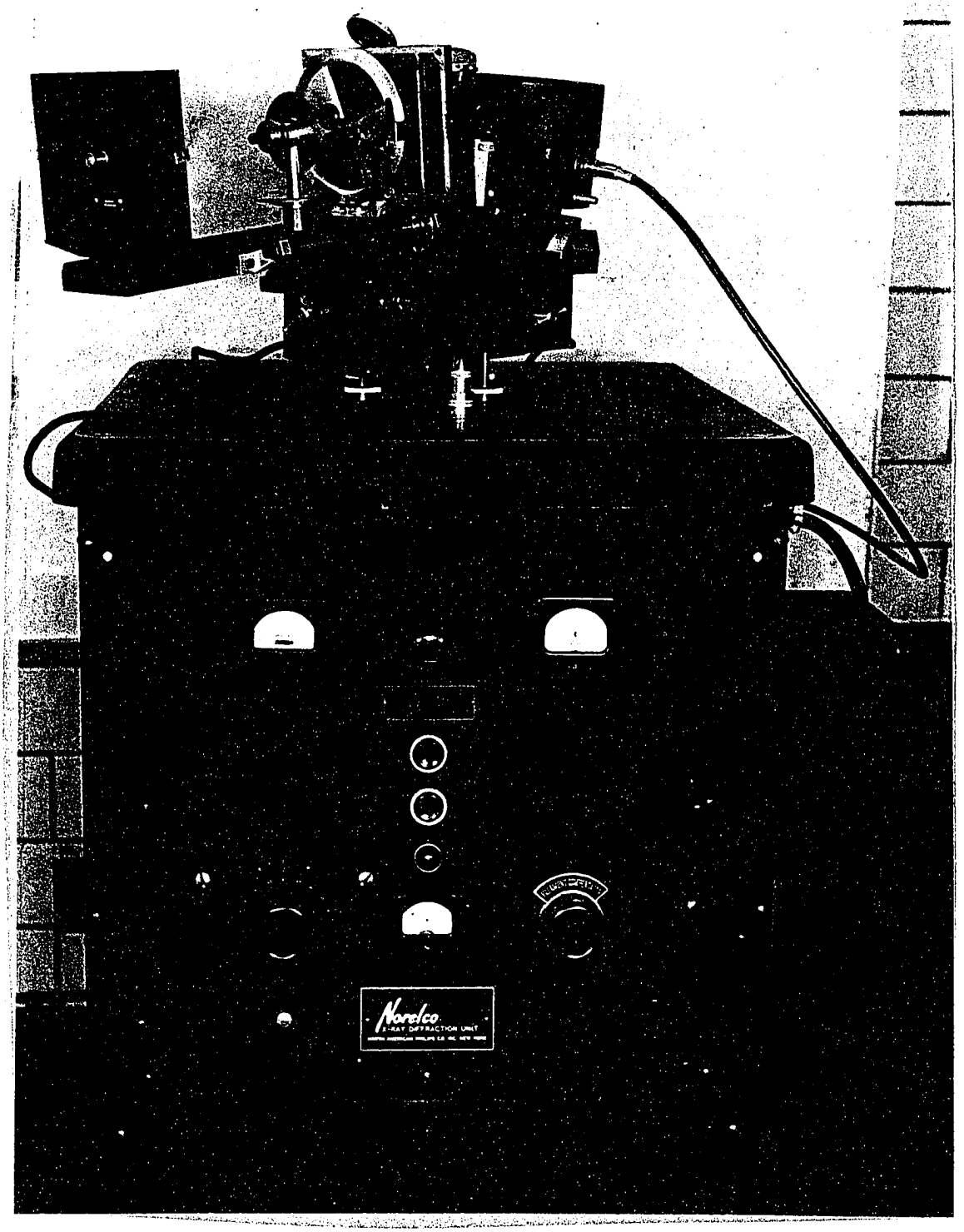

Figure 34

freedom from microscopic stress. Large grains produce a spotted ring which can be offset somewhat by oscillating the film. However, if the grain size is very small, or if microscopic stresses are present, the lines broaden and the $K_{\alpha 1}$ - $K_{\alpha 2}$ doublet merges into one broad line. This is just the condition that exists in cold worked metals or in machined surfaces. Under such conditions high accuracy in stress measurements is not feasible. Nevertheless, it is possible to determine the character of the stress, i.e., tensile or compressive and its general magnitude[45].

In our studies a circular cassette, Fig. 33, was used which could be oscillated $\pm$ 15° at a rate of one cycle per minute. The specimen was held in a goniometer and the specimen face was positioned parallel to the film. The film to specimen distance was set to 5 cm. by means of the gauge previously mentioned. A circular collimating tube 1 mm. in diameter was used. The general setup is shown in Fig. 34.

The unstressed side of this specimen which had previously been electrolytically polished to remove .008" was first presented to the x-ray beam. Only one-half of the film was exposed, the other half being covered by two segments, Fig. 33. The specimen was then turned end for end to bring the machined (or stressed) surface into position, at which time the two segments of Fig. 33 were shifted 90° so as to cover the previously exposed film. Thus the stressed and unstressed patterns were obtained on the same film, Fig. 35. The exposure time was 4 hours.

Figure 35

In all of the milled surfaces only tensile stresses were produced, the (approximate) values varying from 11000 to 45000 lbs. per square inch.

The tensile stresses that reside in the surface after milling may be explained as follows: In the milling process the surface of the metal is brought to a high temperature and is plastically deformed. The initial thermal stresses in this expanded metal are relieved by the working process and the

high temperature. This layer, in its stress relieved state, is then frozen by the quenching action of the base metal below the surface and so tries to contract. However, this contraction is prevented by the underlying metal and so the surface is left in a state of tension with respect to the base metal.

On the other hand if the surface were truly cold worked, i.e., if plastic deformation took place at room temperature (as in shot blasting) then the surface layer would try to expand but would be prevented from doing so by the base metal. Hence, in this case the surface would be held in a state of compression by the base metal.

Depth of Worked Layer

In the process of this investigation a new method[46] was devised for measuring the depth of the worked layer of a metal. This method utilized the Geiger Counter X-Ray Spectrometer[47] to measure the depth of cold work more rapidly than is possible with the x-ray diffraction camera technique.

A fixture, Fig. 36, was designed to position a flat specimen at the Bragg angle, and in addition to rotate the specimen about an axis normal to its flat surface (see insert, Fig. 36). By elevating the fixture so that the incident X-Ray beam struck the specimen below the axis of rotation, the rotation provided the effect of scanning the specimen surface.

Using this fixture it was found that if the specimen was positioned to one of the Bragg angles corresponding to the

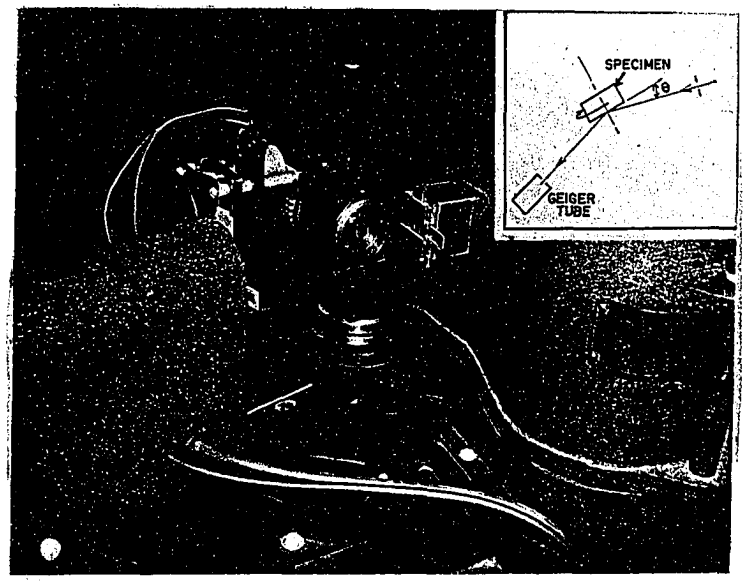

Figure 36

characteristic X-Ray radiation, then the output of the Geiger counter varied as the specimen was rotated slowly, i.e., as the specimen was scanned. It was also found that the amount of variation of the Geiger counter output, or of the intensity recorded by the potentiometer, was a function of the grain size of the specimen; small grain size produced a small variation in intensity and large grain size produced a large variation. Furthermore it was found that this method of detecting grain size by variation of intensity is most sensitive to grain size larger than 10^{-3} mm., i.e., to the size that produces a discontinuous ring in an x-ray diffraction photograph.

Thus far it has not been possible to correlate the variation in intensity with the actual grain size. However, the method has been found to provide a rapid means of determining the depth of cold work on a metal surface. The procedure is to record the intensity variation as the cold worked surface is slowly scanned. The surface is then etched to remove a known thickness of the cold worked layer, after which the intensity variation during scanning is again recorded. This process of alternately etching and scanning is repeated until the variation in intensity from the Geiger counter becomes a constant quantity.

An example of the method is shown in Fig. 37. Fig. 37a shows the intensity over one cycle of rotation of an S.A.E. 1020 steel specimen that had been sand blasted. The specimen was positioned at the Bragg angle, $\theta = 28.4°$, corresponding the the (110) planes for Fe - K_α radiation. The specimen was rotated at a speed of one revolution in fifteen minutes. (A somewhat faster rotation speed is equally practical. In fact the specimen can be rotated by hand and an observation made of the maximum and minimum intensity in less than one minute.) The variation in intensity is 6 micro-amps. Fig. 37c shows a forward reflection x-ray photograph taken of this same sand blasted specimen surface set at approximately the same Bragg angle to the x-ray beam. A continuous ring is obtained for the (110) plane using Fe - K_α radiation.

Figs. 37d and 37f show the spectrogram and the forward

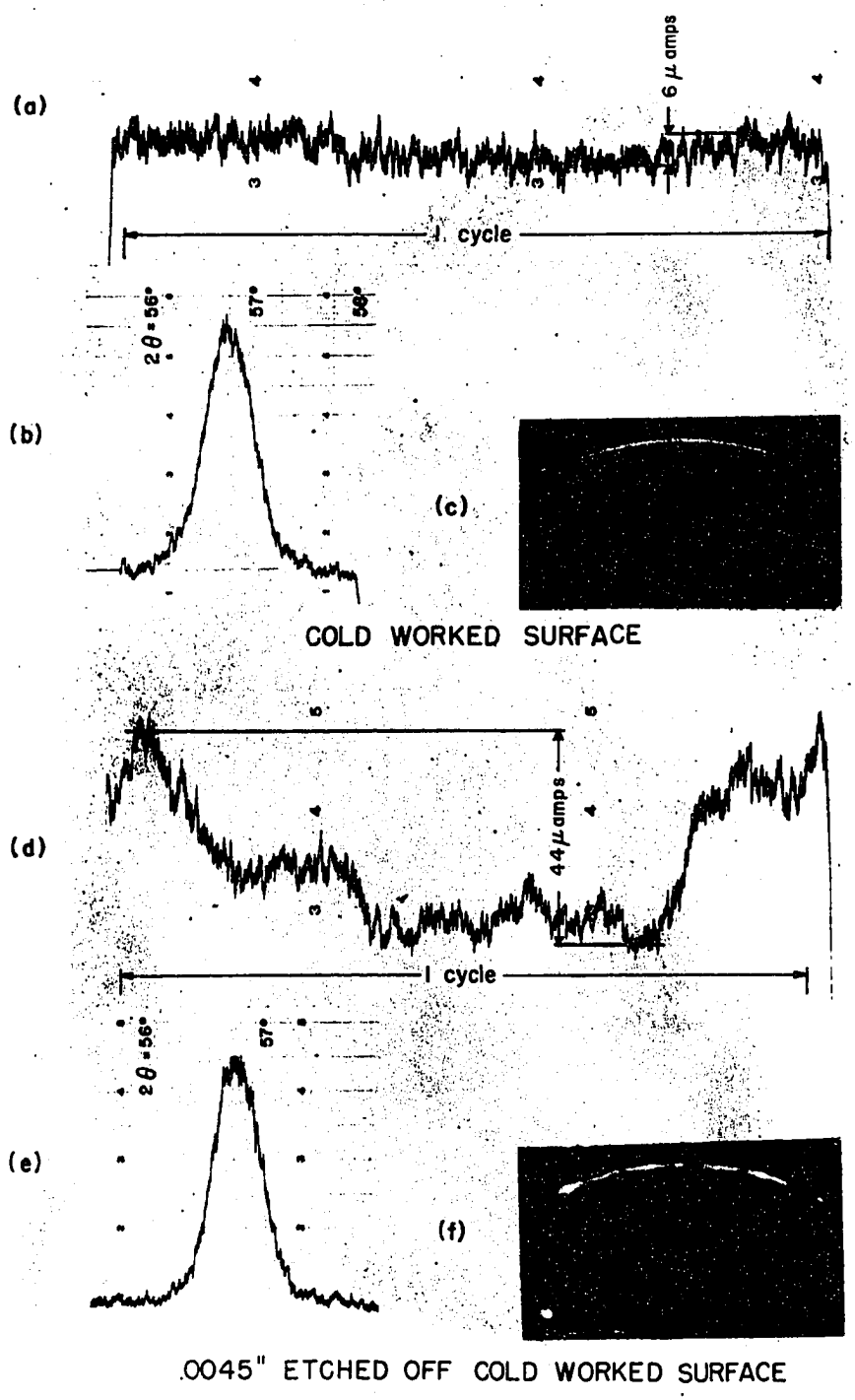

Figure 37

reflection photograph of the steel speciman after .0045" had been etched off the sand blasted surface. The variation in intensity in Fig. 37d corresponds to 44 micro-amps.

The ring in the photograph of Fig. 37f is now discontinuous indicating a large grain size. By similar investigations of intermediate steps, the depth of cold work due to sand blasting was found to be .002".

The major advantage of this method of measuring depth of cold work lies in the short time necessary to obtain the spectograms compared to the time required for the diffraction photographs. Thus 1 1/2 hours were required to determine the depth of cold work by etching 5 times and checking the sample on the x-ray Spectrometer 6 times, rotating the specimen by hand. A similar study by means of x-ray diffraction photographs would require about 10 hours.

The usual method of measuring changes in grain size by measuring the broadening of the line of the x-ray spectrometer is not expecially sensitive for the study of depth of cold work in a metal surface, since the grain size is seldom smaller than 10^{-4} mm. (the upper practical limit for line-broadening studies). Thus in this sand blasted steel specimen no appreciable line broadening was found with the spectrometer between the sand blasted and the deeply etched surface (compare Figs. 37b and 37e). To obtain these spectograms the specimen was rotated at a fast rate of 50 rpm. while the Geiger counter arm traversed along its sector arm at the rate of 1/4 degrees per minute in the normal manner.

It should be pointed out that a slow rotation of the specimen in a fixture of this types does not provide a method of determining preferred orientation (as might appear to be possible at first glance and as has sometimes been claimed.) This is because the only planes in the specimen which can diffract at a given θ are the planes which are parallel to the surface of the specimen, which itself is at the Bragg angle θ to the incident beam. Thus any of these planes oriented in a preferred manner at some particular angle with respect to the surface can never diffract. The intensity of reflection is merely a measure of the number of planes with a given set of Miller indices that lie parallel to the surface.

Preferred Orientation

The preferred orientation produced within the worked metal is perhaps the most intriguing of all the problems that were worked on. The usual method of making such a study has been to take a series of transmission photographs at different angles of the specimen in order to obtain sufficient information to construct a pole figure for the low order planes[48,49,50].

Such a procedure is long and tedious and is subject to various errors[51]. Thus J. Wood[52] took 112 photographs for plotting a single pole figure. If it is necessary to use a specimen in the form of a sheet then the density of the rings on the film must be corrected for the increased absorption as the inclination of the sample to the beam is increased[51]. Furthermore the relative intensities of the various portions

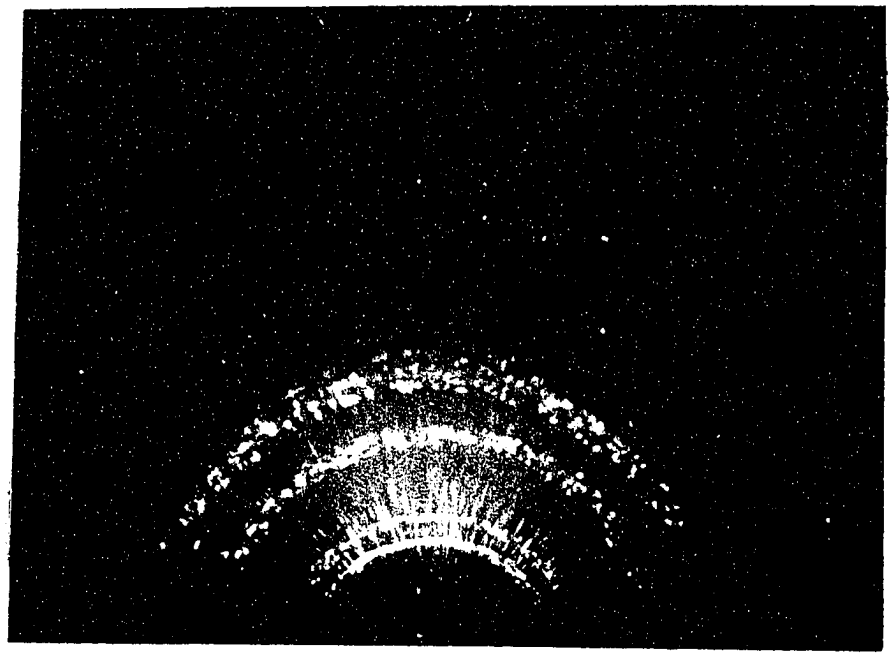

Figure 38a

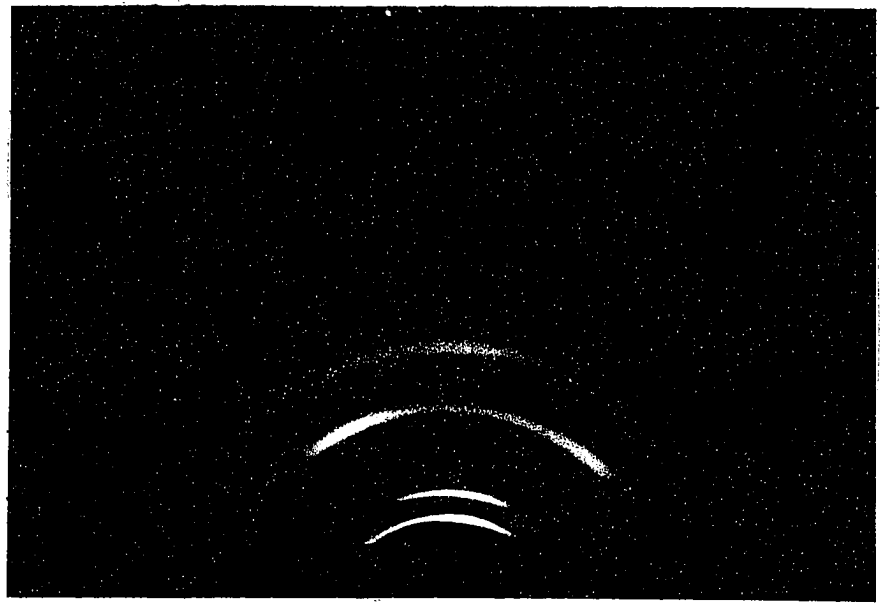

Figure 38b

of the diffracted ring are either estimated from visual examination or must be further analyzed by means of a photodensitometer.

The pole figure is a circle which is the stereographic projection of an imaginary spherical surface at the center of which a crystal is assumed to be placed. Each point on the sphere represents the orientation of the normal to one of the crystal planes. The relative number of planes in the sample is represented by the density of spots in the pole figure. For random orientation there is a uniform density over the entire pole figure. The pole figure of a single crystal contains regularly placed points of maximum density and the remainder of the figure would have zero density. In a cold worked metal the orientation is only partially preferred.

A preliminary examination for preferred orientation was made using the forward reflection camera with the specimen face inclined at 15° to the incident x-ray beam, using Mo - K_α radiation. Fig. 38a shows the unstressed surface of an A.I.S.I. 302 stainless steel sample and Fig. 38b shows the preferred orientation resulting after run No. 1. A major weakness of this method was the fact that the greater portion of the diffracted ring was cut off by the specimen face.

An attempt was next made to remove the thin worked layer from the machined surface of the specimen and to make a transmission study for preferred orientation. Although a procedure was carried out which enabled us to obtain a strip as thin as .003" to .005" it was felt that the deformation

produced by the specimen preparation would interfere with the original deformation produced in the milling process.

Attention was, therefore, turned toward divising a more suitable method for determining preferred orientation by using a reflection technique on the x-ray spectrometer.

Determination of Preferred Orientation on X-Ray Spectrometer

The specimen is positioned in the same fixture as shown in Fig. 36. However, the fixture was redesigned to allow the specimen face to protrude beyond the fixture body, Fig. 39.

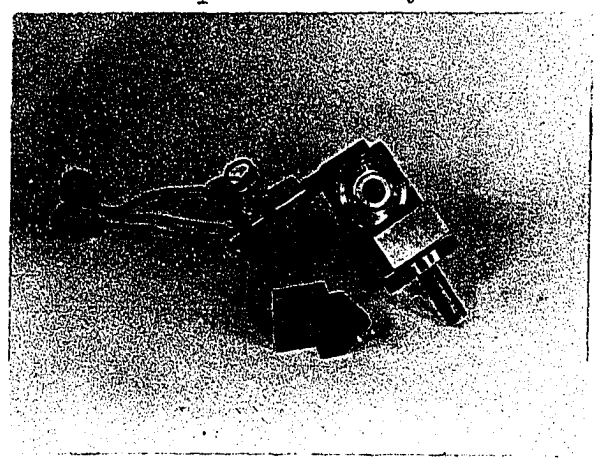

Figure 39

(The specimen, Fig. 40a is mounted so that its face is parallel

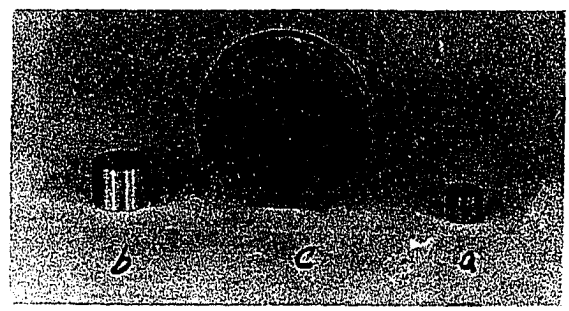

Figure 40

to the face of the bushing, Fig. 40b. The specimen is held

in the bushing by means of a material having a low melting point such as sulphur. The plate, Fig. 40c, is used to position the specimen in the bushing during the mounting process.) The fixture is so designed that the specimen can be rotated about an axis normal to the specimen face as indicated in the insert of Fig. 36. This axis of rotation is at the same height as the axis of the incident x-ray beam. The fixture can also be swiveled about a vertical axis, i.e., the face of the specimen can be positioned so as to depart from angle θ. An index plate is provided so that α, the angle of departure from θ, can be determined.

In making a preferred orientation study the fixture is first positioned so that the specimen face is at an angle θ with respect to the incident x-ray beam. At this time the Geiger Mueller tube is at 2θ. The θ, of course, corresponds to a definite (hkl) plane whose preferential orientation is being studied. The specimen is then rotated by means of the syncronous motor and gear reduction of Fig. 39 so that the specimen makes one revolution in 7 1/2 minutes. Meanwhile the intensity output of the Geiger tube is recorded on the Brown recorder. If the grain size is small (and it will be for a worked surface) a uniform intensity is recorded. The fixture is then swiveled away from θ by angle α but the Geiger tube is held at angle 2θ. The specimen is again rotated one revolution about its own axis. Any preferential orientation of the (hkl) planes at this angle α will result

in a variable intensity recorded by Brown recorder. The intensity is in fact a measure of the number of (hkl) planes in position to diffract. Since the Brown recorder record also travels at a syncronous speed it is possible to correlate the recorder record with respect to a reference position on the specimen surface. The specimen is then swiveled to a new angle α and the procedure repeated.

Now when passing from one angle of swivel α, to another there is a change of intensity even if there is no preferred orientation. This change is caused by several conditions:

1) the focusing effect of the spectrometer is altered;
2) the area of the specimen irradiated by the incident x-ray beam is changed;
3) the length of path that the x-ray beam must travel through the surface of the specimen is altered and hence there is a change of intensity due to absorption within the specimen.

It is, therefore, necessary to correct for the change in intensity cuased by swiveling the sample to the various α's. After this correction is made, the intensity recorded for any position of the specimen face can be related to the relative number of (hkl) planes at that same position. The position of the plane is represented by the position of N, the normal to the plane. N is specified by angles α and β where α is the angle of swivel, i.e., the departure of the specimen face from angle θ; and β is the angle of rotation of an arbitrary X axis on the specimen surface from the incident beam, see

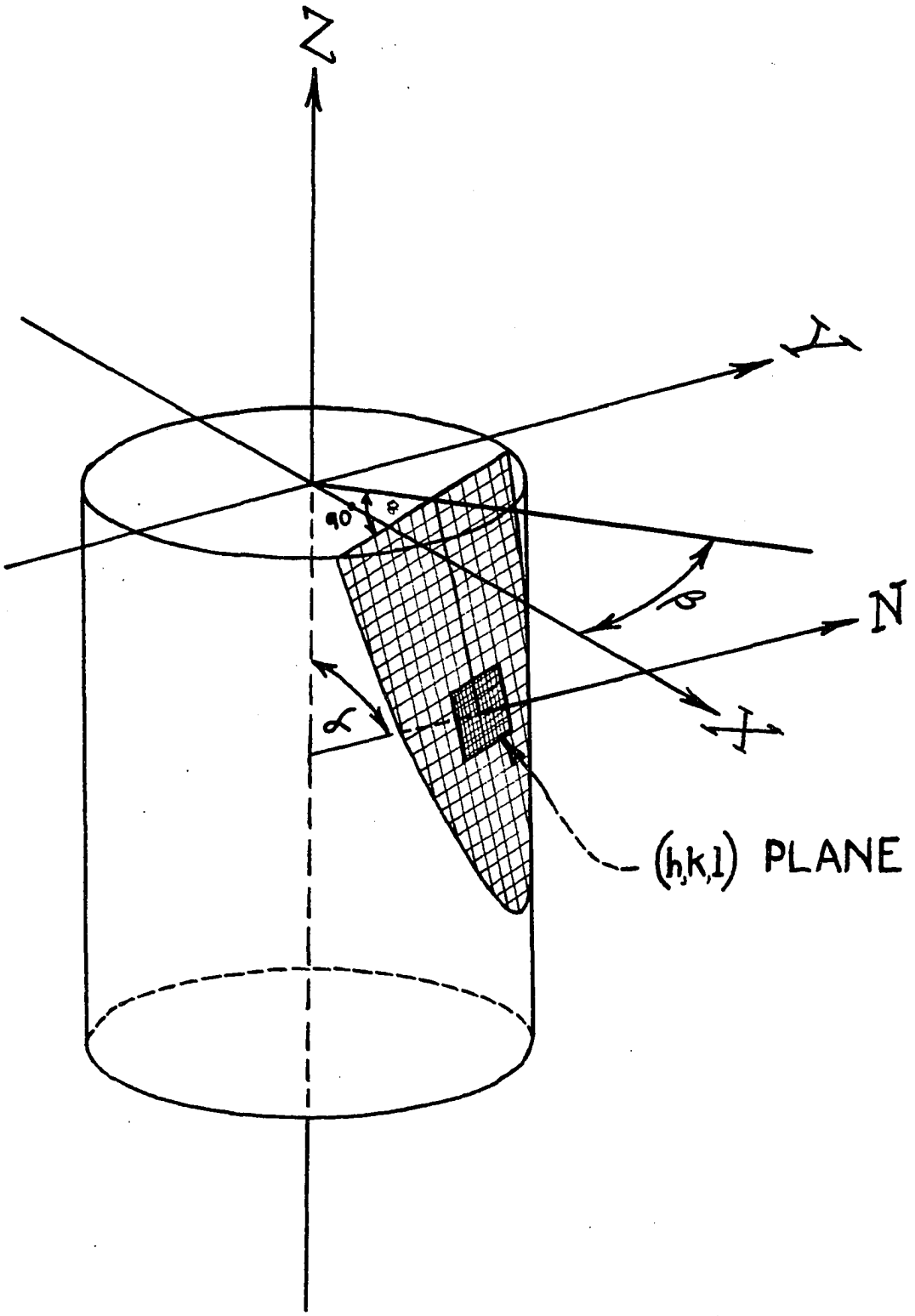

FIG. 41

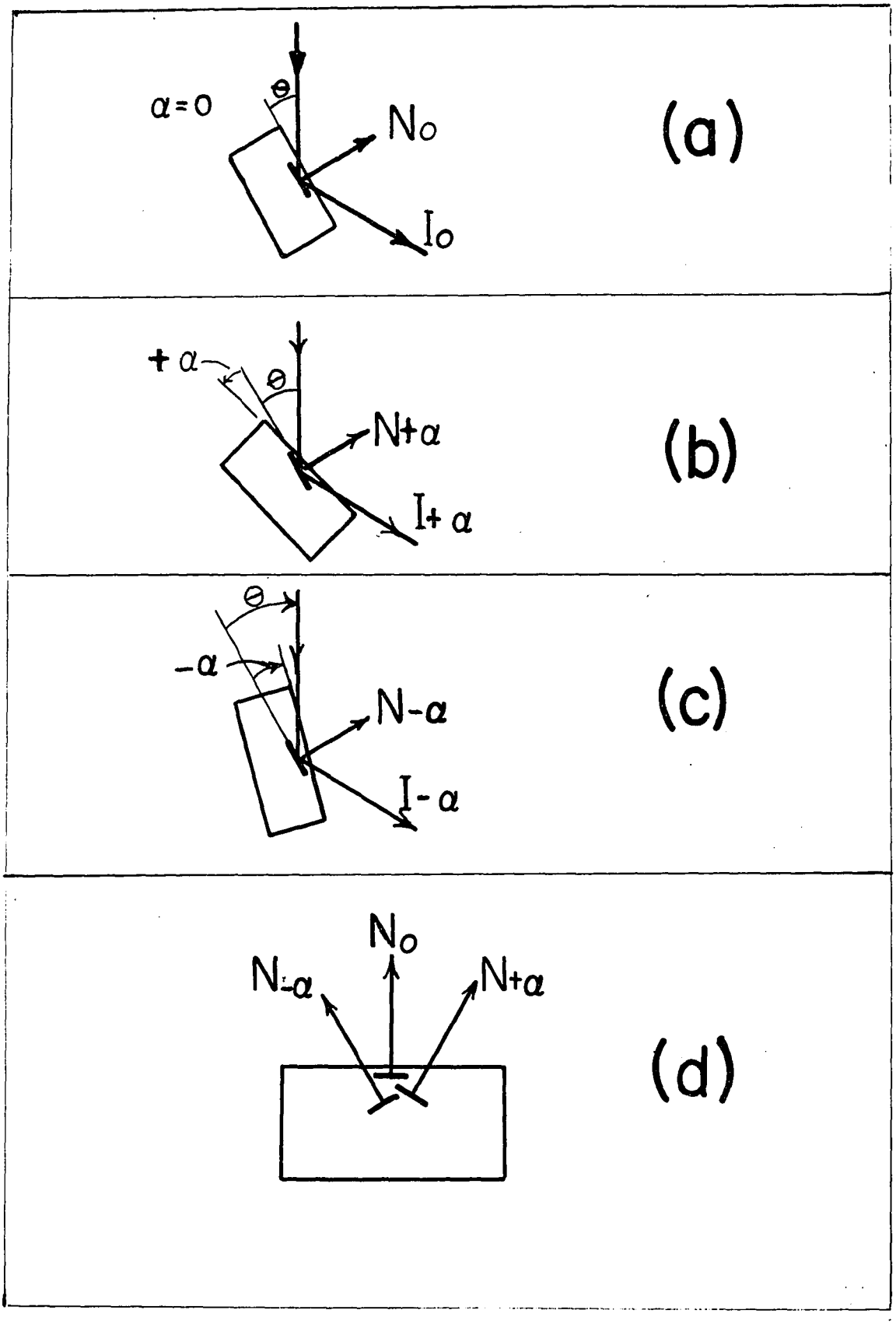

FIG.42

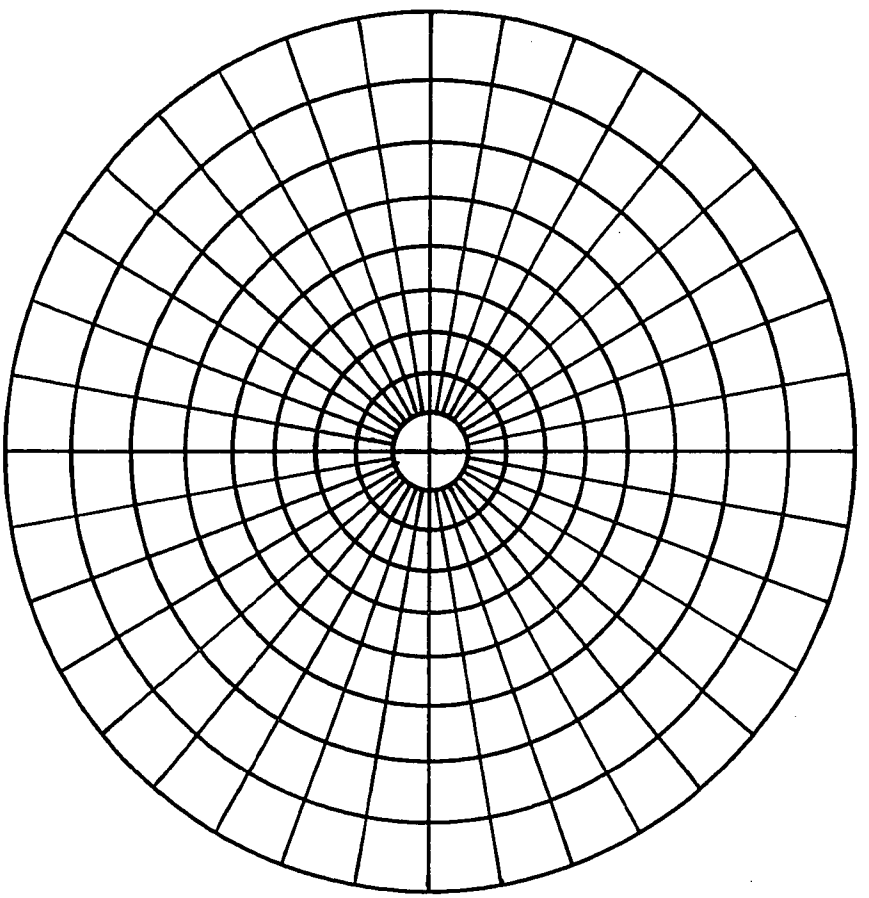

FIG. 43

Fig. 41. When the specimen is at angle θ with respect to the incident beam (i.e., $\alpha = 0$) then the diffracted intensity I_o corresponds to the planes whose normal N_o is perpendicular to the specimen face, Fig. 42A. When the specimen is swiveled to an angle $+\alpha$ then the diffracted intensity $I_{+\alpha}$ corresponds to the planes whose normal is represented by $N_{+\alpha}$, Fig. 42b. When the specimen is swiveled to an angle $-\alpha$ then the diffracted intensity $I_{-\alpha}$ corresponds to the planes whose normal is represented by $N_{-\alpha}$, Fig. 42c.

The location of these normals can be represented in stereographic projection by means of a polar net, Fig. 43, in which the north-south axis of the reference sphere is perpendicular to the projection plane[49]. The concentric circles on the net are the latitude circles and the radial lines are the meridians. Thus the intensity at $\alpha = 0$ would be represented at the very center of the polar net. Intensity at $\alpha = +10°$ would be represented on the latitude circle ten degrees from the North Pole. The intensity at $\alpha = 10°$ and $\beta = 40°$ would be represented on the 10° latitude circle and at a meridian 40° away from the zero meridian. (The zero meridian is made to correspond to a given direction on the specimen face, for example, the direction of tool travel).

It should be noted that the intensity at a given α and β is repeated at $-\alpha$ and $(\beta + 180°)$. This means (Fig. 42d) that at a given α the plane represented by $N_{+\alpha}$ is again picked up as $N_{-\alpha}$ when the specimen is rotated 180° about its own axis. It is, therefore, necessary to use either $+\alpha$ or $-\alpha$ but

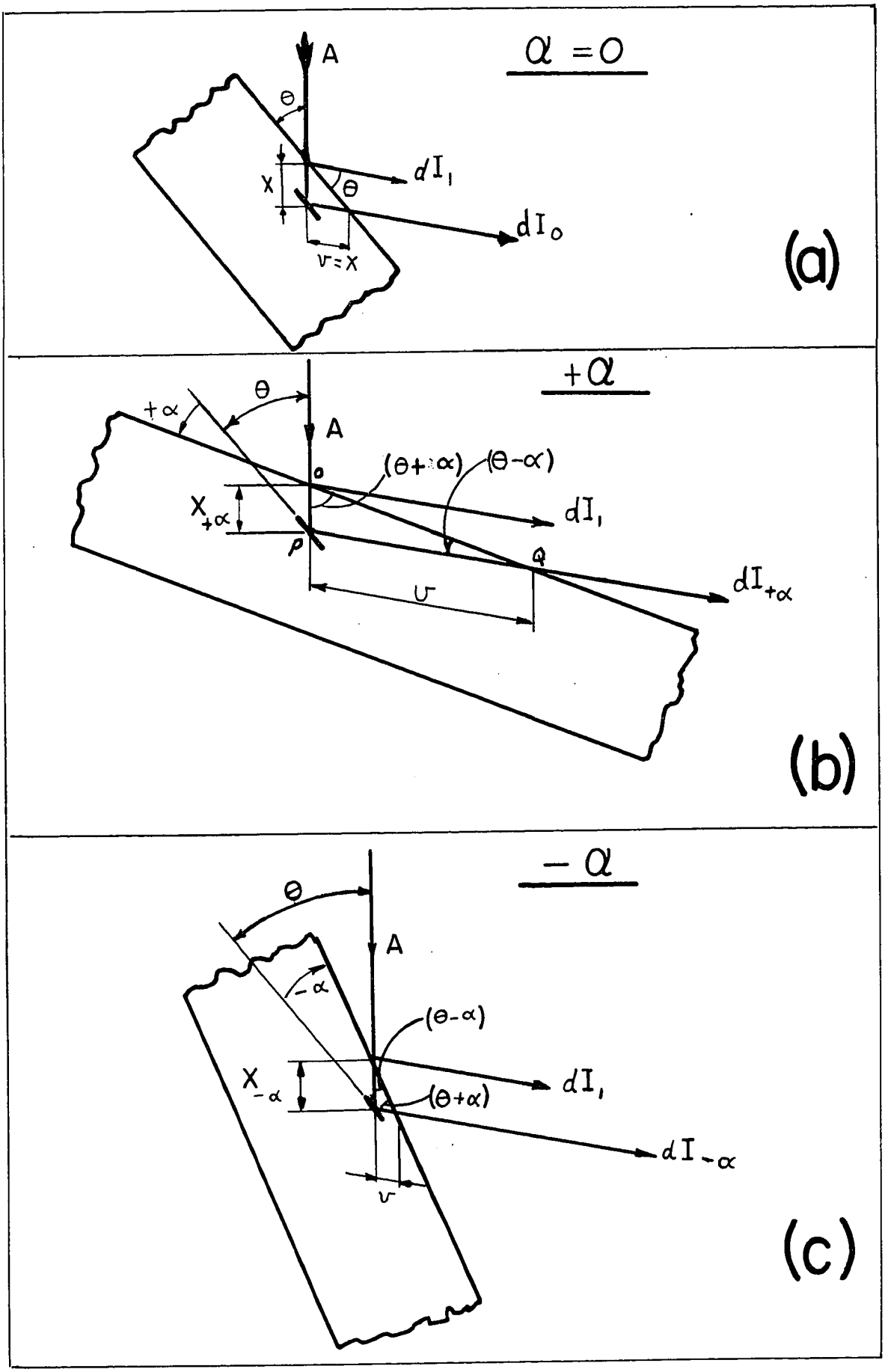

FIG. 44

not both swivel positions to complete a preferred orientation study.

The correction for change in intensity with α (the departure of the specimen face from θ) is determined as follows: Consider the case where the specimen face is at the angle θ to the incident x-ray beam, i.e., $\alpha = 0$, Fig. 44a.

Let

A = Incident intensity

dI_o = Incident intensity diffracted from an element of thickness dx.

x = Path length within sample before diffraction occurs.

μ = Coefficient of absorption of material.

The incident diffracting intensity after penetration into specimen a distance, x, is: $Ae^{-\mu x}$.

Let D be the fraction of the incident intensity per unit thickness at any point in the sample. "D" is a constant for random orientation. Then for a diffracting element dx, the diffracting intensity transmitted is

$$dI_o = Ae^{-\mu x} Ddx e^{-\mu x} \qquad (1)$$

$$= ADe^{-2\mu x}\, dx$$

and

$$I_o = AD \int_o^x e^{-2\mu x}\, dx$$

$$= \frac{AD}{-2\mu}\left[e^{-2\mu x}\right]_o^x \qquad (2)$$

Let dI_1 = intensity due to diffraction from element at surface of specimen

$$dI_1 = ADdx \tag{3}$$

Assume that the x-ray beam penetrates into the specimen until

I_o = P% of I_1

or

$$dI_o = PdI_1 \tag{4}$$

substitute (1) and (3) into (4)

$$ADe^{-2\mu x}\, dx = PAD\, dx$$

$$e^{-2\mu x} = P$$

$$x = -\frac{\ln P}{2\mu} \tag{5}$$

substitute (5) as the upper limit into (2) and get

$$I_o = \frac{AD}{-2\mu}\left[e^{\ln P} - 1\right]$$

or

$$I_o = \frac{AD}{-2\mu}(P - 1) \tag{6}$$

If the specimen is swiveled so that its face departs from θ by an angle $+\alpha$, Fig. 44b, then from triangle OPQ,

$$v = x\,\frac{\sin(\theta + \alpha)}{\sin(\theta - \alpha)} \tag{7}$$

By similar reasoning that led to equation (1) it is found that

$$dI_{+\alpha} = Ae^{-\mu x}\, Ddx e^{-\mu x}\,\frac{\sin(\theta + \alpha)}{\sin(\theta - \alpha)}$$

or $$dI_{+\alpha} = ADdx\, e^{-\mu x}\left[1 + \frac{\sin(\theta + \alpha)}{\sin(\theta - \alpha)}\right] \qquad (8)$$

let $$N = \left[1 + \frac{\sin(\theta + \alpha)}{\sin(\theta - \alpha)}\right]$$

then (8) becomes

$$dI_{+\alpha} = AD e^{-\mu N x}\, dx \qquad (8a)$$

and $$I_{+\alpha} = \frac{AD}{-\mu N}\left[e^{-\mu N x}\right]_0^{x+\alpha} \qquad (9)$$

Again let dI_1 = intensity due to diffraction from element at surface

$$dI_1 = AD\, dx \qquad (3)$$

Assume $$dI_{+\alpha} = P dI_1 \qquad (10)$$

substitute (8a) and (10) into (3)

$$AD e^{-\mu N x}\, dx = PAD\, dx$$

$$x = -\frac{\ln P}{\mu N} \qquad (11)$$

Substitute (11) as the upper limit into (9) and get

$$I_{+\alpha} = \frac{AD}{-\mu N}(P - 1) \qquad (12)$$

Divide (12) by (6)

$$\frac{I_{+\alpha}}{I_o} = \frac{2}{N} = \frac{2}{1 + \frac{\sin(\theta + \alpha)}{\sin(\theta - \alpha)}} \qquad (13)$$

Equation (13) is the ratio of the diffracted intensity

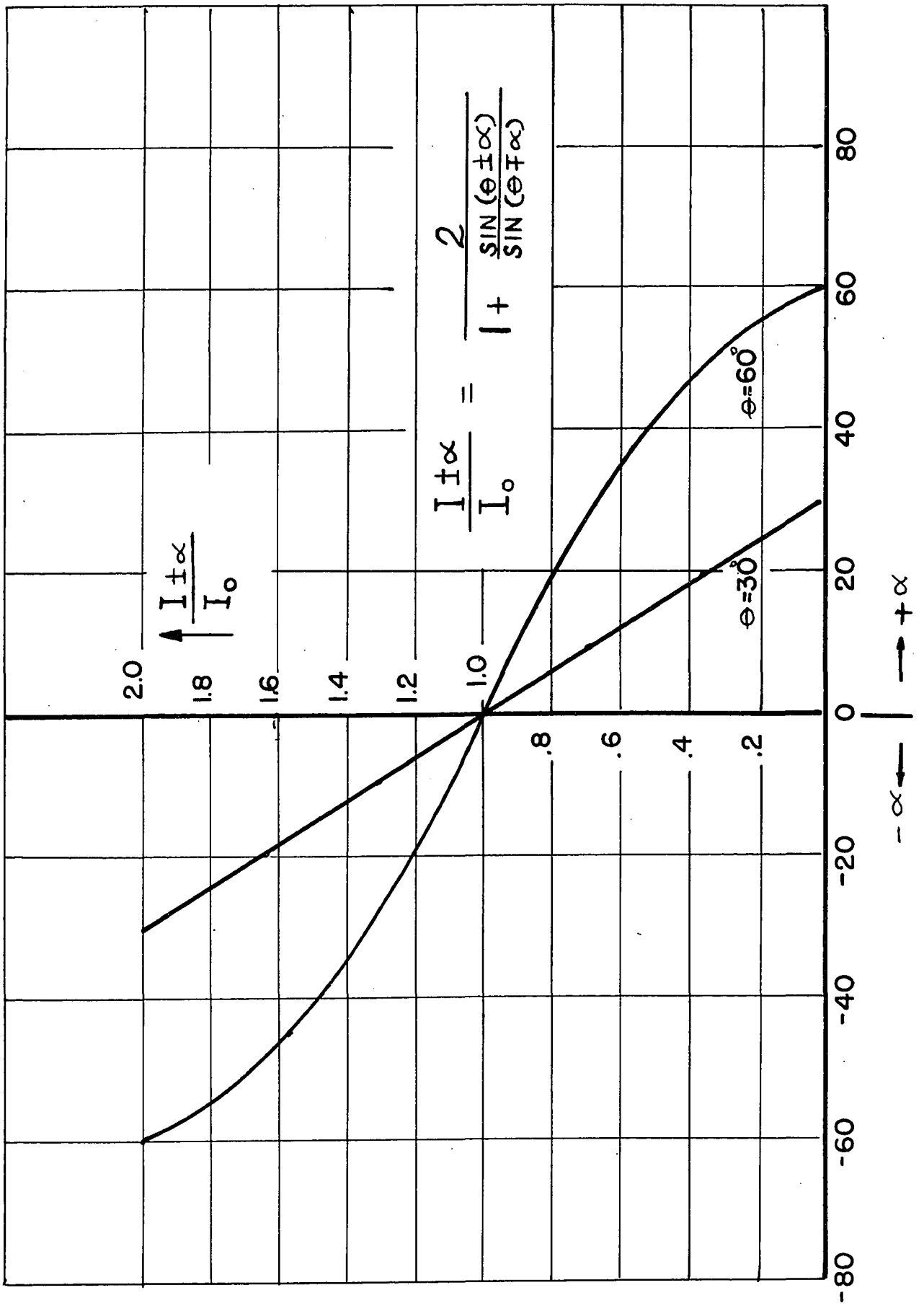

FIG. 45

when the specimen face is at angle α, to the diffracted intensity when the specimen is at angle $\alpha = 0$.

If the specimen is swiveled so that its face departs from θ by an angle $-\alpha$, Fig. 44c, then by similar reasoning

$$\frac{I_{-\alpha}}{I_o} = \frac{2}{1 + \frac{\sin(\theta - \alpha)}{\sin(\theta + \alpha)}} \qquad (14)$$

Equations (13) and (14) can be combined to give

$$\frac{I_{\pm\alpha}}{I_o} = \frac{2}{1 + \frac{\sin(\theta \pm \alpha)}{\sin(\theta \mp \alpha)}} \qquad (15)$$

Equation (15) is plotted in Fig. 45 for $\theta = 30°$ and $\theta = 60°$. It is interesting to note that for negative values of α, $\frac{I_{-\alpha}}{I_o} > 1$ or the intensity $I_{-\alpha}$ increases with respect to I_o. The maximum possible value of $I_{-\alpha}$ is seen to be 2 when the magnitude of $-\alpha$ equals θ. Other facts relating to equation (15) should be noted: 1) the ratio of intensities is independent of the mass absorption coefficient; 2) when $\alpha = 0$ the ratio becomes unity; 3) when $\theta = 90°$ then $\frac{I_{\pm\alpha}}{I_o} = 1$ for <u>all</u> values of α including $\alpha = \pm 90°$. 4) the magnitude of the swivel angle α can never be greater than θ. Physically this means that when the specimen is swivelled to an angle $+\alpha = \theta$ the specimen face cuts off the reflected beam $I_{+\alpha}$. When the specimen is swivelled to angle $|-\alpha| = \theta$ then the specimen face cuts off the incident x-ray beam A.

Now in order to make a complete preferred orientation study by reflection methods the specimen must be swivelled through angles α = 0 to 90°. This means that θ must also reach 90°. However, the Geiger Counter Spectrometer in our Laboratory has a range of angles up to θ = 45°. Hence this spectrometer placed a limitation on the extent of the preferred orientation that could be investigated. However, North American Phillips Co. has recently announced a "High Intensity Geiger Counter Spectrometer with Extended Angular Range" which will increase the usefulness of this method.

Comparison Between Equation 15 and Experimental Results

A specimen of A.I.S.I. 302 stainless steel was mounted in the fixture of Fig. 39 with its annealed and electropolished surface exposed to the x-ray beam. Fe - K_α radiation was employed and the Geiger tube was set at 2θ = 55.25° corresponding to the (111) plane. The specimen was rotated at 40 revolutions per minute about its own axis so as to minimize the effects of the large grain size. The slit in front of the x-ray tube was adjusted to 3/4 mm. width and 2.5 mm. height. The slit height in front of the Geiger tube was maintained at a height of 2.5 mm. but the width was varied from a minimum of 1 mm. to the maximum possible width of 10 mm. The results are shown in Fig. 46 where $I_{\pm\alpha}/I_o$ is plotted against positive and negative values of α. In the region of

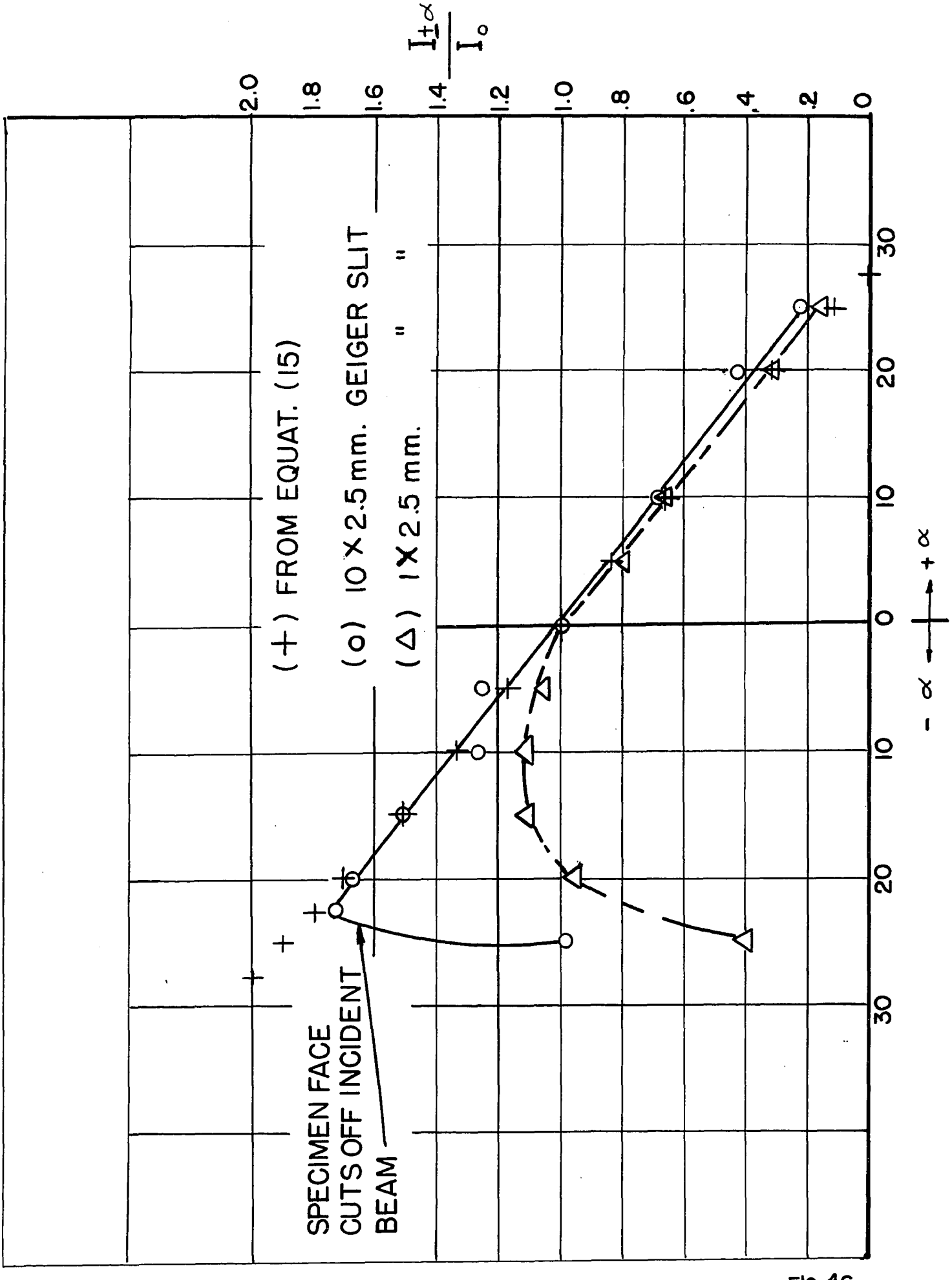

FIG. 46

positive α, a close correspondence was found between the intensity ratio based on equation (15) and the experimental results for the 1 mm. wide Geiger slit. The correspondence was poorer in the $+\alpha$ region while using the wide Geiger slit, probably because of the background effects. In the region of negative α there was a poor correspondence between equation (15) and the experimental results while employing the 1 mm. Geiger slit, because as the specimen is swivelled in the direction of $-\alpha$, the diffracted beam widens and only a small portion of the beam is received through the narrow slit at the Geiger tube. However, if the 10 mm. slit at the Geiger tube is employed then a close correspondence is obtained in the region of $-\alpha$ until this angle becomes so great that the specimen face cuts off the incident x-ray beam.

The most accurate combination was thus found to be the 3/4 mm. wide x-ray slit and the 1 mm. wide Geiger slit and $+\alpha$; this combination was used in the preferred orientation studies of the machined surfaces. As previously mentioned it was not necessary to use negative values of α for this region could be explored by setting the sample at $+\alpha$ and rotating to $(\beta + 180°)$.

Preferred Orientation in Milled Surfaces

Preferred orientation studies were made on all of the specimens of Table V using Fe - K_α radiation. Two planes were investigated: the (111) plane for which $\theta = 26.6°$ and the (200) plane for which $\theta = 32.4°$. The orientation was

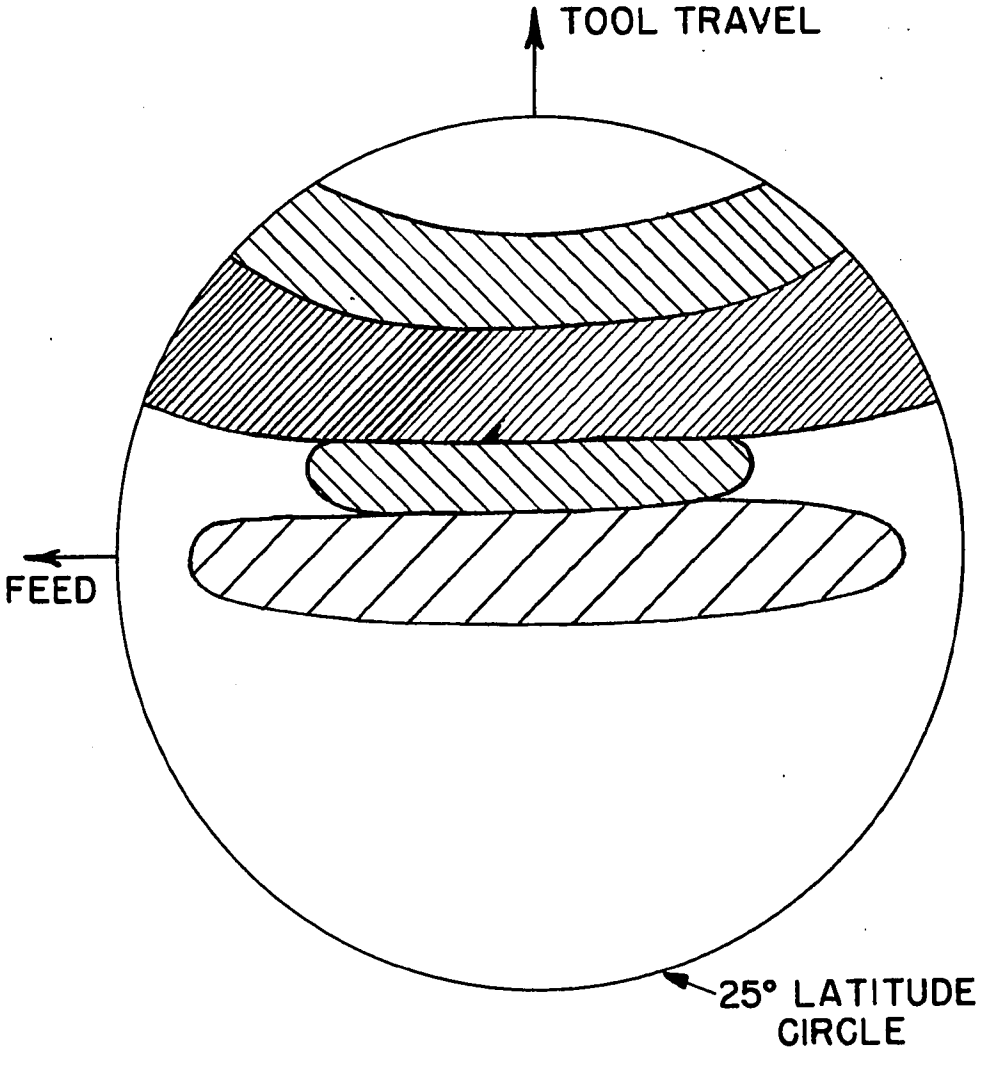

(III) PLANES

FIG. 47

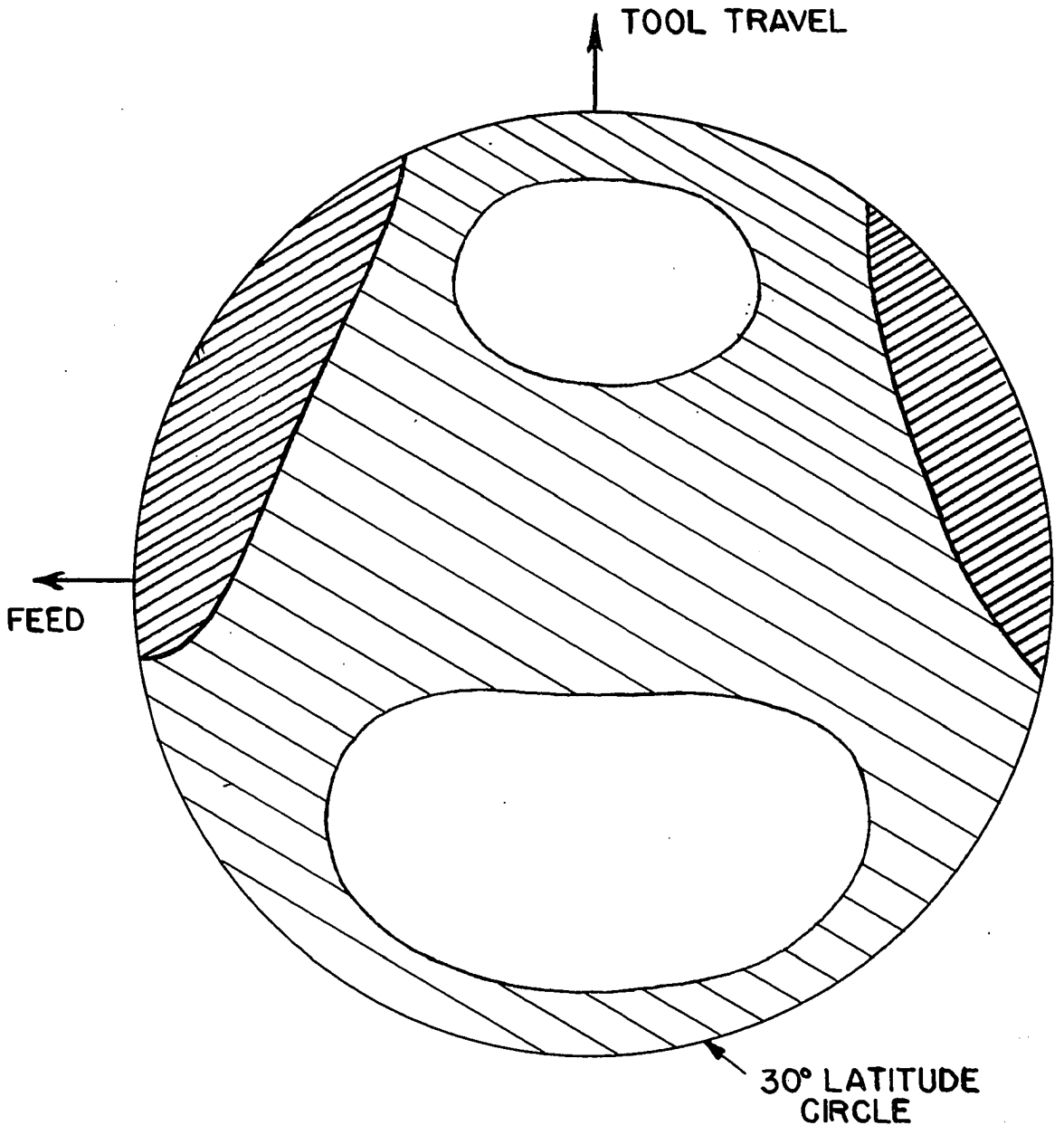

(200) PLANES

FIG. 48

determined from $\alpha = 0$ to $\alpha = 25°$ for the (111) planes, and from $\alpha = 0$ to $\alpha = 30°$ for the (200) planes. The pole figures for these respective planes are illustrated in Figs. 47 and 48 for run No. 5, Table V. The (111) planes, Fig. 47 were found to be inclined at an angle of 15 to 20° to the milled surface in the direction of the tool travel. Their orientation was symetrical with the direction of tool travel. The (200) plane orientation, Fig. 48, is in accord with the restrictions set up by the (111) orientation of Fig. 47.

The pole figures of the other runs of Table V were similar to that shown in Figs. 47 and 48.

While the writer was engaged in divising a method for determining preferred orientation by reflection methods on the x-ray spectrometer, two other groups worked out a transmission method for determining prererred orientation on the same instrument. They were J. T. Norton at M.I.T.; and Decker, Asp and Harker at General Electric. The General Electric group presented a paper at the Summer, 1947 Meeting of the American Society for X-Ray and Electron Diffraction[53] (as yet unpublished) describing their transmission methods. Their procedure likewise affords a simple and accurate means for determining pole figures. They present a correction formula which takes into account absorption change and change in diffracting volume as the sample changes position with respect to the x-ray beam.

Summary of X-Ray Study of Machined Surfaces

Stainless steels of the 18% Cr, 8% Ni class were machined with carbide milling cutters at various cutting speeds. The milling process produces a deformed layer of metal .003" to .005" deep. The effect of this deformation is to produce line broadening when back reflection photographs are made on the x-ray diffraction unit. The line broadening is caused by a reduction in grain size combined with the setting up of microstresses within the austenitic grains of the stainless steel. The line broadening furthermore produces a merging of the $K_{\alpha 1}$ - $K_{\alpha 2}$ doublet. The determination of the residual stresses in the machined surface cannot be accurately accomplished because of the impossibility of obtaining a precise measurement of the diffracted ring diameters. However, the study revealed that residual tensile stresses are set up in the machined surface of the order of magnitude of 10,000 to 45,000 lbs. per square inch.

A distinct preferred orientation was observed within the deformed surface layer. It was mandatory that reflection rather than transmission methods be employed to investigate the nature of this preferred orientation, since any attempt to isolate a strip of the thin surface layer might alter the preferred orientation produced by the original machining operation.

A new method was hence devised for determining preferred orientation by reflection technique on the Geiger Counter

Spectrometer. This method was found to be faster and more accurate than that possible by means of the photographic procedure with the diffraction unit.

By employing the new preferred orientation method it was found that the (111) planes are aligned at an angle of 15 to 20 degrees to the milled surface in the direction of tool travel. The orientation of the (111) planes was found to be symetrical with respect to the direction of the tool travel.

In the course of this investigation another new method was devised for determining the depth of the worked surface layer of metal by means of the x-ray spectrometer. This new method is far more rapid than the previous procedure in which the back reflection diffraction photographic technique was employed. This new technique further offers a possibility for the determination of grain size in the region of grain size greater than 10^{-3} cm.

PART III: EFFECT OF MICROSTRUCTURE ON THE MACHINABILITY OF CAST IRON

Introduction

This study is one of a series conducted at the University of Cincinnati to determine the basic factors affecting the machining properties of cast iron. A discontinuous chip is characteristic to the milling of cast iron and the theory of Part I was concurrently developed to aid in the understanding of the overall machining problem.

At the time that this study was begun there were no available methods for evaluating the expected tool life, surface finish or power requirements in milling cast iron. This investigation revealed the fact that the microstructure of cast iron is a reliable criterion for predicting the above mentioned machinability factors. As a further consequence of these findings various industrial consumers have begun to demand controlled cast iron structures which have suitable machining characteristics.

The two papers which follow are reprints from Transactions A.S.M.E., August, 1947, and contain a detailed account of the entire investigation. This research was conducted in conjunction with Dr. E. E. Stansbury, former Assistant Professor of Metallurgical Engineering at the University of Cincinnati, who is now at the University of Tennessee.

Effect of Microstructure on Machinability of Cast Irons—I

By MICHAEL FIELD[1] and E. E. STANSBURY,[2] CINCINNATI, OHIO

Test bars were prepared to study the effect of the following structures in the milling of cast iron: Graphite-pearlite of various gradations of coarseness; graphite-pearlite plus about 5 per cent of free-carbide segregation; graphite-ferrite. Quantitative results of the relative machinability of these structures are presented in terms of (1) tool life, (2) power requirements, (3) surface finish. Tool life was found to increase as much as 2:1 as the graphite-pearlite structure was varied from fine to coarse. For the same graphite-pearlite size, the presence of free carbides had no effect on tool life at a cutting speed of 200 fpm but seriously reduced tool life between 250 and 1000 fpm. The increase in tool life for the graphite-ferrite structure as compared to all other structures was outstanding, e.g., at 1150 fpm the increase was of the order of 8:1, compared to the pearlite structure, while at 300 fpm the increase was of the order of 50:1. All of the graphite-pearlite structures required the same amount of power to mill at a constant rate of metal removal for the same feed per tooth. The graphite-ferrite required approximately 1/2 to 2/3 the power per cubic inch for the same feed per tooth compared to graphite-pearlite structures. The sharpness of the cutter played an important role in power requirements. A "dull" cutter required as high as 3 times the power as that for a sharp cutter at 0.002 in. feed per tooth, and 1.3 times as much power at 0.020 in. feed per tooth. Surface finish improved as the cutting speed increased and as the graphite distribution became finer.

Introduction

In previous investigations[3,4] forming a part of the carbide-milling project at the University of Cincinnati, it was observed that cast irons having similar physical properties often differed in their machining characteristics. For example, it was noticed in certain cases that appreciable differences in tool life occurred with cast irons having only slight differences in Brinell hardness. Therefore Brinell hardness, as such, was found to be an unreliable index of relative machinability, although, as a general trend, tool life was observed to increase as the hardness decreased. It seemed logical, then, to continue the research on the fundamental factors controlling the milling of cast irons by investigating a possible direct correlation of machinability with their microstructures.

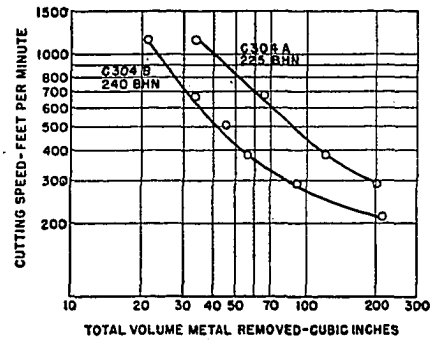

Fig. 1 Cutting Speed Versus Total Volume Metal Removed Between Grinds for 0.030-In. Wear Land

[Cutter: Single tooth; 6-in. radius; +3-deg axial rake, +3-deg radial rake, 30-deg corner angle, +4-deg resultant rake; (+3, +3, 30, +4). Cut dimensions: 3/16 in. depth, 6 in. width, 0.015 in. feed per tooth].

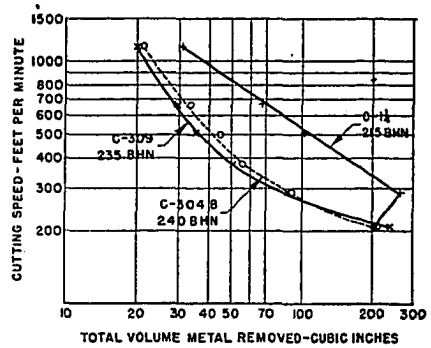

Fig. 2 Cutting Speed Versus Total Volume Metal Removed Between Grinds for 0.030-In. Wear Land

[Cutter: Single tooth; 6 in. radius; (+3, +3, 30, +4). Cut dimensions: 3/16 in. depth, 6 in. width, 0.015 in. feed per tooth.]

Two experiences in the milling project accelerated interest in this investigation. At one phase of this work it was observed that two different groups of alloy cast-iron test blocks with virtually identical chemical analyses and physical properties gave widely different values of tool life. An examination of the microstructure of the two groups revealed that the set of blocks which had inferior machining characteristics (designated as C-304B in Fig. 1), contained free-carbide segregations, while that of the superior group, designated as C-304A, contained only small traces of free carbides. It appeared therefore that the presence of the large hard free-carbide formations seriously reduced the tool life.

At another phase of the earlier investigation it was observed that an alloy cast iron of analysis C-309 (see Table 1) had the same tool-life curve as that of the C-304B (see Fig. 2). A check on the microstructure revealed a marked similarity in spite of the fact that the two materials were of different chemical compositions and had been cast in different section sizes.

These indications of a dependence of tool life upon microstructure therefore spurred the separate investigation of the effect of microstructure on the machinability of cast iron, the speci-

---

[1] Cincinnati Milling Machine Company; Research Fellow, University of Cincinnati. Jun. A.S.M.E.

[2] Assistant Professor of Metallurgical Engineering, University of Cincinnati.

[3] "Milling Cast Iron With Carbides," by Michael Field and W. E. Bullock, *Mechanical Engineering*, vol. 67, 1945, pp. 647–658.

[4] "Speed and Feed Selection in Carbide Milling With Respect to Production, Cost, and Accuracy," by Hans Ernst and Michael Field, Trans. A.S.M.E., vol. 68, 1946, pp. 207–215.

Contributed by the Research Committee on Metal Cutting Data and Bibliography and presented at the Semi-Annual Meeting, Detroit, Mich., June 17–20, 1946, of The American Society of Mechanical Engineers.

TABLE 1 CHEMICAL ANALYSIS AND PHYSICAL PROPERTIES OF CAST IRONS USED IN MILLING TESTS

Analysis	Per cent									Ult. tensile strength, psi[a]	Bhn[b]
	Total carbon,	Si	S	P	Mn	Mo	Ni	Cr	Cu		
A	3.22	1.37	0.126	0.14	0.85	0.10	...	0.07	...	50000	190
C-304A	3.15	2.62	0.083	0.20	0.89	0.49	...	0.60	...	45000	225
C-304B	3.17	2.58	0.088	0.20	0.87	0.51	...	0.70	...	45000	240
C-309	3.15	1.97	0.105	0.18	1.02	0.05	...	0.65	2.77	40000	235
C-3 1/4	3.17	1.82	0.162	0.13	0.92	...	...	...	...	40000	195
C-1 1/4	3.10	1.80	0.160	0.15	0.96	...	...	...	...	42500	215
C-3/4	3.10	1.76	0.156	0.18	0.92	...	...	...	...	41000	218
C-3 1/4 annealed	2.98	1.73	0.149	0.14	0.90	...	...	...	...	23300	121

[a] Average values from 1.2 in. arbitration bar.
[b] Average Brinell hardness values from machinability test blocks.

fic object of which was to determine quantitative relationships between microstructure and machinability, thereby obtaining a reliable index for the relative machinability of cast iron.

Preparation of Test Blocks

The metallurgical phase of this investigation involved the production of a number of sets of machinability test blocks of cast irons having different microstructures. The blocks in each set were required to have the same microstructure, and the microstructure throughout each block had to be as uniform as possible. To meet these requirements the inherent metallurgical characteristics of cast iron were used as guides to the production of the test blocks.

Cast irons are characterized by their relatively great sensitivity to changes in microstructure with slight changes in chemical composition, melting practice, and rate of cooling. In general, the basic structure of a gray cast iron may be considered as one having a pearlite matrix in which graphite flakes are embedded. In addition to these two major microconstituents, the following ones may also be present: Ferrite, carbides, steadite (iron-phosphide eutectic), martensite, manganese sulphide, and various inclusions. In the "as-cast" state, conditions may be varied in some cases so as to allow the presence and distribution of these microconstituents to be regulated as desired. For example, increasing the phosphorus content of the iron will increase the amount of steadite present. On the other hand, the remaining microconstituents are so related to the same casting variables that they may be separately varied only over narrow limits. Particular reference is made to the simultaneous appearance of fine graphite with fine pearlite, and coarse graphite with coarse pearlite.

The microstructures produced in a cast iron of a given analysis depend upon the rate of cooling of the material through two temperature ranges. The rate of cooling from the melt down to about 1600 F controls the graphite-carbide relationships, and the rate of cooling from 1600 F down to room temperature controls the matrix structure. Since the machinability tests covered in the present investigation were confined to the gray cast irons, it was not necessary to consider the formation of white cast iron resulting from the casting of iron low in carbon and silicon.

Very slow cooling of a cast iron of normal composition will produce a structure of graphite and ferrite. Under these conditions the graphite forms partially on solidification, then by precipitation from austenite on cooling from the freezing temperature down to the lower critical temperature, and the balance by decomposition of austenite into graphite and ferrite on cooling through the critical-temperature range. As the rate of cooling is increased, the separation of graphite is first prevented at the utectoid, producing a structure of graphite and pearlite. With still greater rates of cooling, the separation of graphite from austenite (on cooling from the melting temperature to the lower critical temperature) will be suppressed, resulting in a structure of graphite, carbide, and pearlite.

In general, an appreciable increase in cooling rate is required to go from the condition of graphite-pearlite to graphite-pearlite-free carbide. As rates of cooling are increased within a range extending from a rate which just prevents ferrite formation, to a rate which just allows carbide formation, the pearlite-graphite distribution becomes finer. Increasing the carbon and silicon contents have the same effect as reducing the cooling rate. By decreasing the carbon and silicon content, and by adding carbide-forming alloying elements, the microstructure will be changed in the same manner as if the cooling rate had been increased. Since the fineness of the pearlite depends mostly upon the rate of cooling as such, the addition of carbide-forming alloying elements allows the production of cast irons with structures of varying graphite-pearlite distributions together with varying amounts of free carbides.

The size of the graphite flakes and their distribution may be controlled further by adding inoculating agents to the melt just before casting. These additions produce a finer graphite distribution and hence a higher-strength cast iron. Furthermore, the melt so treated is less affected by differences in cooling rates as exist between the outside and center of a given section and so will produce a casting of more uniform structure throughout. All of the cast-iron test blocks used in this investigation were cast by the Meehanite process in which inoculations of calcium silicide are used. These blocks were cast in the foundry of the Cincinnati Milling Machine Company.

The initial milling tests were carried out on $6\frac{1}{2} \times 6\frac{1}{2} \times 20\frac{1}{2}$ in. castings of analysis A and C-309 which had been poured into green-sand molds. The chemical analysis and physical properties of these materials are given in Table 1. With the exception of the hardnesses, the physical properties refer to those shown by the arbitration bar and represent comparative properties of the various materials tested rather than the properties of the actual test blocks. The hardness values given refer to averages taken from the actual test blocks. The graphite distributions of these two materials are shown in Fig. 3, and the microstructures in Fig. 4. Both materials had average graphite-flake sizes corresponding to AFA No. 4.

The microstructure of the analysis A cast iron was essentially graphite and normal pearlite with very little phosphide eutectic or free carbide present. The analysis C-309 material had about the same matrix structure as the analysis A but in addition an appreciable amount of free carbide was distributed throughout the structure.

Subsequently, in an attempt to produce a harder cast iron with a correspondingly finer structure, analysis C-304 was cast into skin-dried molds to produce test blocks $3\frac{1}{2} \times 6\frac{1}{2} \times 20\frac{1}{2}$ in. The analysis of this material is given in Table 1. In two separate pourings of the C-304 great differences in tool life were found, Fig. 1. These two pourings were made from two separate heats, both within specifications; however, slightly different foundry conditions resulted in materials with different machining characteristics. The microstructures of the test blocks produced by each heat are shown in Fig. 4.

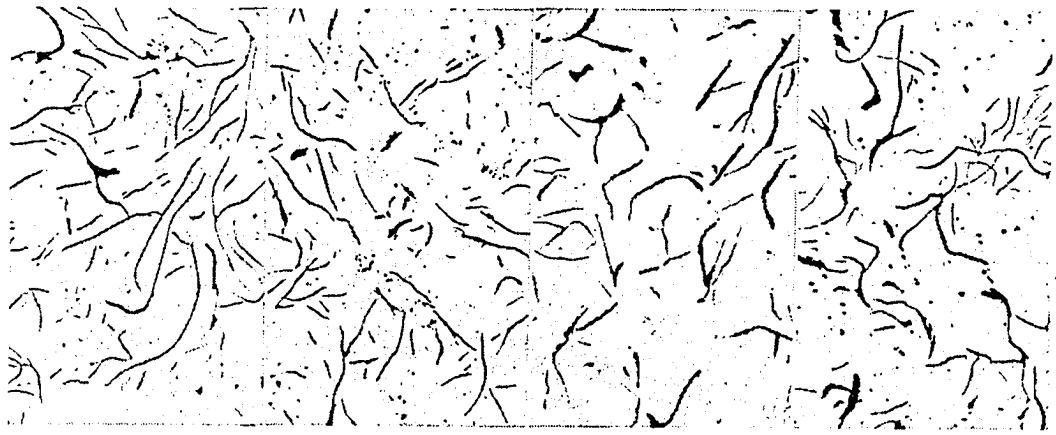

(*a*) (*b*) (*c*) (*d*)

FIG. 3 PHOTOMICROGRAPHS OF GRAPHITE DISTRIBUTION

(*a*, Analysis C-304A, 225 Bhn. *b*, Analysis C-304B, 240 Bhn. *c*, Analysis C-309, 235 Bhn. *d*, Analysis A, 190 Bhn. Unetched; ×50.

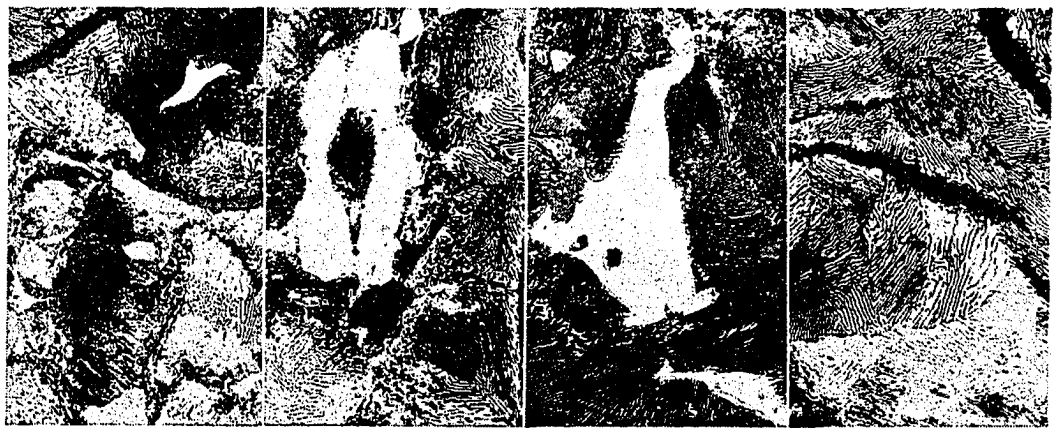

(*a*) (*b*) (*c*) (*d*)

FIG. 4 PHOTOMICROGRAPHS OF MICROSTRUCTURE

(*a*, Analysis C-304A, 225 Bhn. *b*, Analysis C-304B, 240 Bhn. *c*, Analysis C-309, 235 Bhn. *d*, Analysis A, 190 Bhn. Nital etch; ×375.)

FIG. 5 SKIN-DRIED MOLD ASSEMBLY

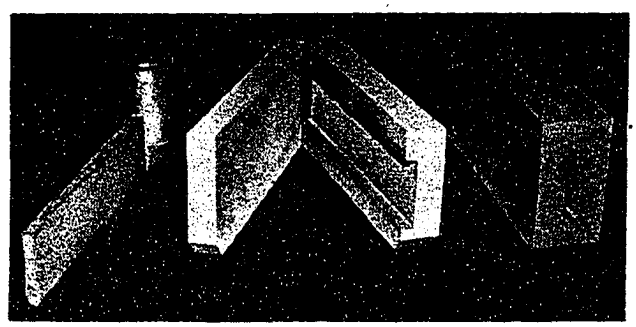

FIG. 6 CORE-SAND-MOLD INSERT

As shown in Fig. 3, the graphite distribution was about the same in both sets of blocks. A relatively small amount of free carbide was found in blocks produced by one heat, as shown in Fig. 4. This material will be referred to as analysis C-304A to differentiate it from the material of the second heat, which showed a greater amount of free carbide, Fig. 4. This latter material will be referred to as analysis C-304B.

The results obtained on the analysis C-304 blocks emphasized the need for close control in the preparation of test blocks if definite structures were to be produced. Therefore subsequent test blocks were cast into a different type of mold which consisted of baked core sand inserts in a skin-dried mold. The final mold assembly is shown in Fig. 5, and the core-sand insert in Fig. 6. The metal was poured through a baked strainer core (shown at

FIG. 7 TRANSFERRING METAL FROM MIXING RESERVOIR TO LADLE

center right in Fig. 5), and then gated to five or six mold cavities from a common runner.

In order to obtain sufficient castings for a complete machinability test, it was necessary to pour two ladles of metal. Close control of chemical composition from ladle to ladle was obtained by drawing the metal from a continuously fed mixing reservoir, as shown in Fig. 7. Since the amount of metal withdrawn from the mixing reservoirs into successive ladles was small relative to the amount of metal added from the cupolas, a satisfactory degree of uniformity of chemical composition was obtained. The castings were then cleaned and machined to a depth of 1/8 in. on all surfaces to produce the final test blocks.

The large section sizes used for the blocks of analyses A, C-309, and C-304 would not permit the range of cooling rates desired. The limitations, imposed by the use of large test blocks necessary for the milling tests, forced consideration of the use of smaller sections which would allow the production of blocks of more uniform structure from surface to center due to a more uniform casting rate, and would allow a greater range of structures to be produced. These thinner sections were stacked together to form a laminated test block of the desired section.

In order to establish the range of structures which could be expected due to changes in the rate of cooling, these blocks were cast 20 1/4 in. long, 4 1/2 in. wide, and in the following thicknesses: 3 1/4 in., 2 1/4 in., 1 1/4 in., 1 in. and 3/4 in. Of these, the 3 1/4 in., 1 1/4 in. and 3/4 in. sections were found to give a representative range of structures, and sets of bars were subsequently cast in these sections to produce bars for the cutting tests. The uniformity of any set of test blocks was checked by taking Brinell hardness readings across each block and by microexamination of a sample from the same position of each block for graphite distribution and microstructure. In addition, the uniformity of graphite distribution throughout a given block was checked by taking samples at four points on the block. This was done on several blocks chosen arbitrarily from each set. Approximately 650 specimens were prepared for microexamination in this investigation. Any gross deviations of either hardness or microstructure were thus detected, and the bars in which they were found were rejected.

Castings of analysis C, Table 1, were made in these three sections thus producing three sets of bars, each set being of uniform structure but producing different graphite-pearlite distributions in each of three sets.

Fig. 8 shows the graphite distributions produced in the 3 1/4-in., 1 1/4-in., and 3/4-in. sections of this material which correspond to AFA graphite size numbers 4, 5, and 6, respectively. These structures not only represent the average graphite distributions found in the respective test blocks but are representative of the graphite size and distribution found throughout most of a given section. Deviation in graphite distribution occurred along the edges and on the corners of the blocks, but these were small compared to the differences found from one section size to another.

Representative etched microstructures for these three sections are shown in Fig. 9. There is a definite gradation of pearlite lamellar spacing in going from the thick to thin section. Most of the pearlite in the 3/4-in. section was too fine to be resolved at 375 magnification.

A duplicate set of 3 1/4-in. blocks of analysis C were annealed to break down the pearlite completely into ferrite and graphite. The annealing cycle consisted of heating to 1600 F, holding at this temperature for 8 hr, followed by a furnace cool. The increased amount of graphite produced in this manner may be seen by comparing the annealed set with the as-cast set in Fig. 8. The etched structure is shown in Fig. 9 for comparison with the etched microstructures of the other materials used in this investigation.

EQUIPMENT USED AND METHOD OF CONDUCTING TESTS

The cutting tests were run on a Cincinnati 5-60 hydromatic

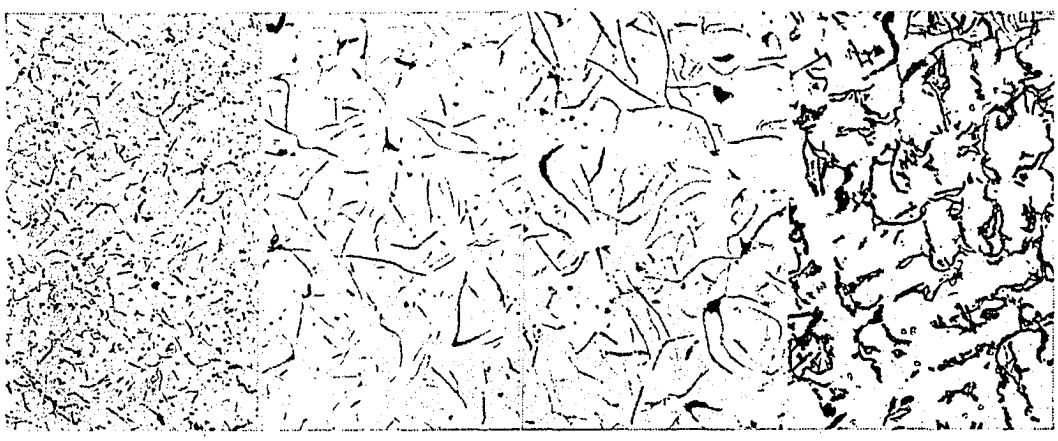

(a) (b) (c) (d)

FIG. 8 PHOTOMICROGRAPHS OF GRAPHITE DISTRIBUTION

(a, Analysis C-3/4, 218 Bhn. b, Analysis C-1 1/4, 215 Bhn. c, Analysis C-3 1/4, 195 Bhn. d, Analysis C-3 1/4 annealed, 121 Bhn. Unetched; ×50.)

(*a*) (*b*) (*c*) (*d*)

FIG. 9 PHOTOMICROGRAPHS OF MICROSTRUCTURE

(*a*, Analysis C-3/4, 218 Bhn. *b*, Analysis C-1 1/4, 215 Bhn. *c* Analysis C-3 1/4, 195 Bhn. *d*, Analysis C-3 1/4 annealed, 121 Bhn. Nital etch; ×375.)

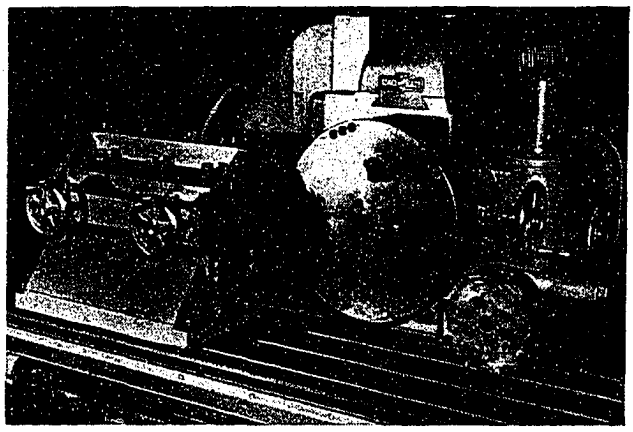

FIG. 10 MILLING MACHINE, CUTTERS, AND FIXTURE USED FOR MACHINABILITY TESTS

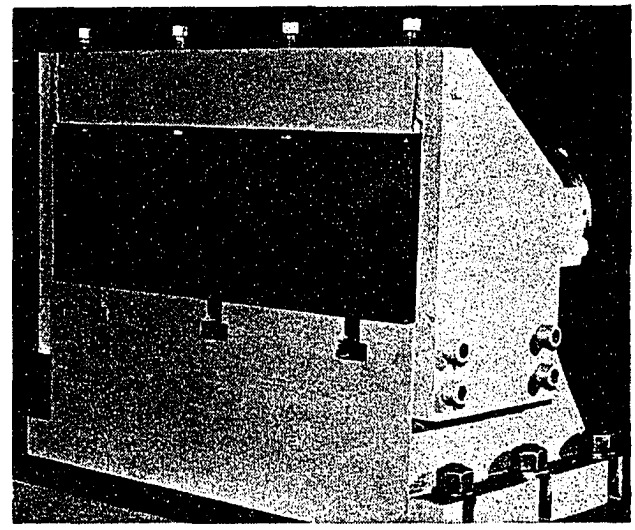

FIG. 11 FIXTURE FOR TEST BLOCKS

milling machine. A 6-in-radius single-tooth cutter held in a 500-lb flywheel was used for the tool-life and surface-finish tests, Fig. 10. The tooth had a +3-deg axial and radial rake, a 30-deg corner angle, and a +4-deg resultant rake. In all tests a cut was taken 3/16 in. deep, 6 in. wide, and 20 in. long with the cutter positioned centrally, relative to the work. The feed per tooth was held constant at 0.015 in. Carboloy 44A was employed as the carbide and was induction-brazed to the shank, using a silver-solder brazing alloy. The carbide was ground with a diamond grinding wheel.

All defects plus 0.010 in. were ground off the tool face as well as all the clearance lands in resharpening. A 7-deg clearance angle was ground behind all the cutting edges. All milling was done dry.

Fixture for Test Blocks. The C-309 A and C-304 test blocks were individually bolted to a massive fixture for their respective milling tests. The C-3/4, C-1 1/4, and C-3 1/4 test bars, which had to be built up into a composite test block, were stacked into a special fixture to form the test block 4 1/4 in. wide, 20 in. long, and 6 in. high. Thus twelve 1/2-in. slabs, six 1-in. slabs, or two 3-in. slabs were stacked to form the 6-in. high block. Fig. 11 shows the six 1-in. blocks in position. The slabs were securely clamped by a series of screws along the front of the fixture and by a long clamp at the rear of the fixture. The resultant test block was positioned to overhang the fixture by only 1/4 in. so that when the 3/16-in. depth of cut was taken, the cutter cleared the front of the fixture by 1/16 in. Means were provided to relocate the test block to the same position after each pass.

Tool-Life Measurement. The width of the wear land on the clearance of the carbides was measured with a calibrated eyepiece microscope after each pass. When the width of the uniform wear became 0.030 in., the tool-life test was stopped. In general, a uniform wear over the whole carbide clearance land was obtained at cutting speeds of 290 fpm and higher. However, at 210 fpm, localized breakdowns occurred at one or more positions along the clearance land. These localized breakdowns developed into grooves which eventually exceeded the length of the uniform wear. These grooves were permitted to develop to 0.040–0.050 in., depending upon the width of the grooves, provided the uniform wear remained under 0.030 in.

MACHINABILITY RESULTS

There are three important elements of machinability, namely, tool life, power requirements, and surface finish. Knowledge of these three elements is necessary to appraise completely any milling operation and to calculate the most economical combination of feed and speed.

Tool Life. The effect of the graphite-pearlite size on tool life of the "C" analyses is shown in Fig. 12 where cutting speed is

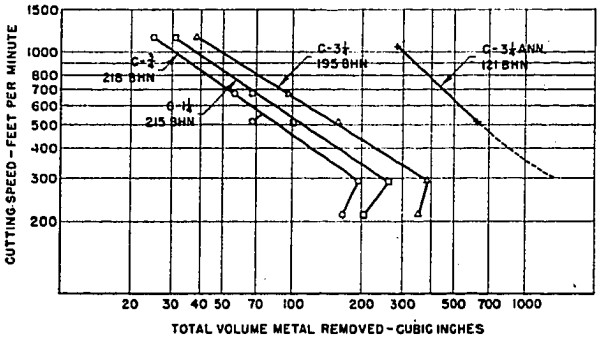

FIG. 12 CUTTING SPEED VERSUS TOTAL VOLUME METAL REMOVED BETWEEN GRINDS FOR 0.030-IN. WEAR LAND

[Cutter: Single tooth, 6 in. radius; (+3, +3, 30, +4). Cut dimensions: 3/16 in. depth, 6 in. width, 0.015 in. feed per tooth.]

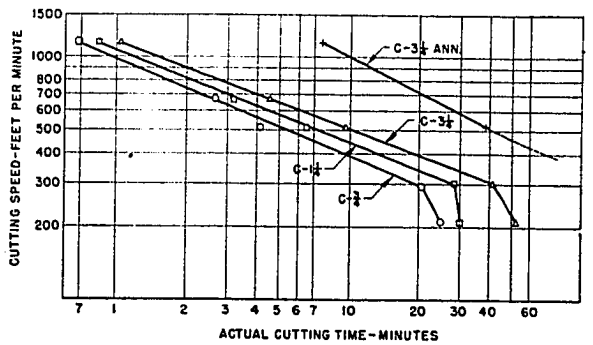

FIG. 14 CUTTING SPEED VERSUS ACTUAL CUTTING TIME FOR 0.030-IN. WEAR LAND

[Cutter: Single tooth, 6 in. radius; (+3, +3, 30, +4). Cut dimensions: 3/16 in. depth, 6 in. width, 0.015 in. feed per tooth.]

plotted against volume of metal removed to produce a 0.030 in. dulling of the tooth. This log-log chart shows that the tool life increased as the graphite-pearlite size became larger. At 290 fpm, the life for C-3¼ was twice as much as for C-¾. At 1150 fpm, the life for C-3¼ was 1.5 times that of the C-¾. The curves are straight lines on log-log co-ordinate paper from 1150 down to 290 fpm. Within this speed interval the wear on the carbide was uniform over the whole edge. However, at 210 fpm, the tool failed by a localized breakdown; the effect of this is indicated by the turning back of the curve. This same break in the speed-life curve has been reported in previous papers.[3,4]

The curve on the extreme right is that of C-3¼ annealed. The enormous increase in tool life produced by the transformation of pearlite to ferrite is obvious. For example, at 1150 fpm, the life for the C-3¼ annealed was 7.5 times as much as the C-3¼ and 11.5 times as much as the C-¾. The tool-life curve for the annealed material is only drawn down to 500 fpm because at lower speeds the tool life was so great that sufficient test blocks were not on hand to obtain a 0.030-in. wear. A test was made at 290 fpm, and all the available test blocks were cut up to produce a mere 0.005 in. of wear on the carbide tooth.

A truer representation of the relative tool life of the four cast irons under discussion is brought out by replotting the cutting speed versus volume of metal removed, on rectangular co-ordinate paper, Fig. 13. It is evident here that the change in tool life is small for large speed differences at high cutting speeds, whereas it is very much greater for the same speed difference at low cutting speeds. The actual tool life at high speeds for all the graphite-pearlite structures was very small so that the percentage difference in tool life between them is of slight significance. However, at low speeds, e.g., 300 fpm, the tool life is of practical significance, so that a 2-to-1 difference in life is very important.

The actual increase in tool life produced by annealing to a graphite-ferrite structure is also emphasized in its true proportions by Fig. 13. It is interesting to note that the tool life for this structure at 1150 fpm was the same as the C-3¼ analysis at a speed of 360 fpm.

Tool life is plotted against the actual cutting time in minutes for the same four materials in Fig. 14. Within the cutting-speed range of 1150 down to 290 fpm, the curves are represented by the following equations:

Analysis	Equation
C-¾	$VT^{0.403} = 980$
C-1¼	$VT^{0.377} = 1060$
C-3¼	$VT^{0.365} = 1160$
C-3¼ annealed	$VT^{0.483} = 3000$

As mentioned in a previous paper,[3] 0.030 in. wear was taken as a limit for tool life, and the choice of this magnitude permitted comparison of results with those of other investigators. However, in actual shop applications it frequently happens that carbide milling cutters must be removed from service before a wear land of 0.030 in. has been reached. On some jobs, for example, where the thermal distortion caused by an excessive wear land would produce dimensional inaccuracy, the wear land cannot exceed 0.015 in. It is therefore desirable to know relative tool

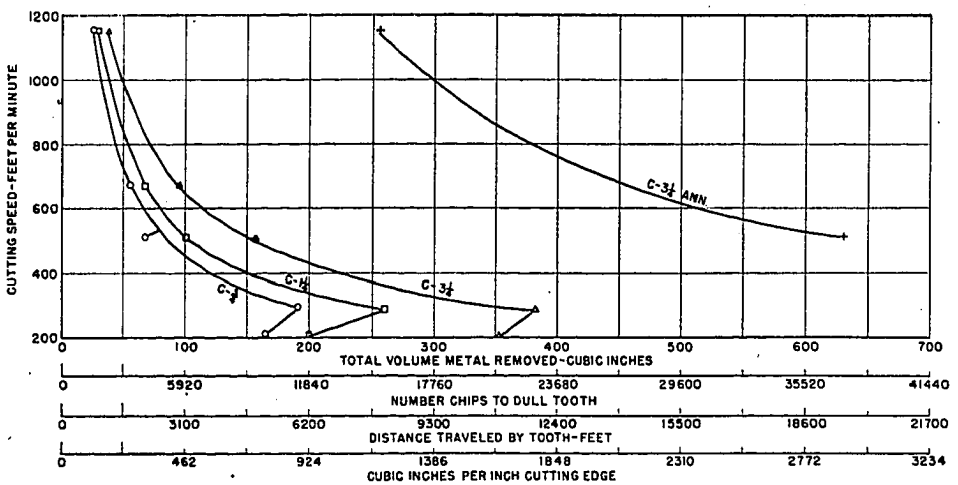

FIG. 13 CUTTING SPEED VERSUS VARIOUS TOOL-LIFE CRITERIA FOR 0.030-IN. WEAR LAND; RECTANGULAR CO-ORDINATES

[Cutter: Single tooth, 6 in. radius; (+3, +3, 30, +4). Cut dimensions: 3/16 in. depth, 6 in. width, 0.015 in. feed per tooth.]

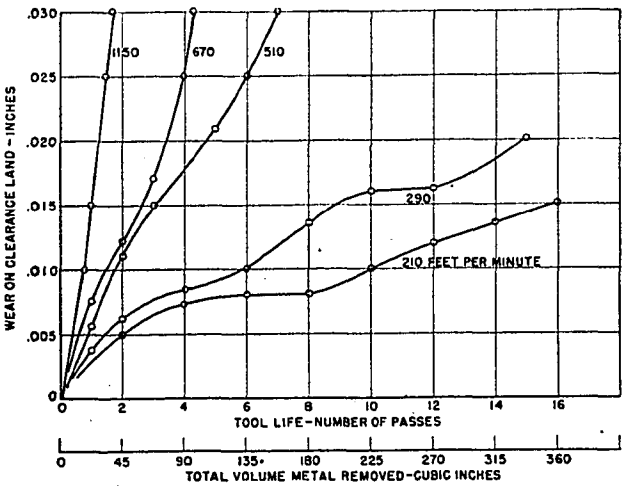

FIG. 15 WEAR ON CLEARANCE LAND OF CARBIDE TOOTH VERSUS TOOL LIFE AT VARIOUS CUTTING SPEEDS

[Material: Analysis C-3¼. Cutter: Single tooth, 6 in. radius; (+3, +3, 30, +4). Cut dimensions: 3/16 in. depth, 6 in. width, 0.015 in. feed per tooth; length of one pass = 20 in.]

life for the various structures at any and all wear lands. This was achieved by keeping a record of the progress of tool wear with tool life.

A typical set of tool-wear versus tool-life curves is shown in Fig. 15 for the C-3¼ analysis. At high cutting speeds the tool wear progressed at practically a constant rate, but at low cutting speeds the rate of tool wear was not steady, as exemplified by the irregularity of the curves. By means of such curves it is possible to plot cutting speed versus tool life for any constant wear land.

Thus in Fig. 16 is shown a set of curves for 0.015-in. uniform wear land, again for the four previously mentioned structures. The relative tool life at 0.015-in. wear is similar to that of the 0.030-in. wear except that no break in the curves appears at the low speed. The break in the curves is absent because these curves represent only the uniform wear and not the localized breakdown, which usually determines the end point at low speed for the 0.030-in. wear test. Localized breakdowns were present in some cases, also at the 0.015-in. wear point, but their magnitudes were not much more than 0.015 in., and in no case were they sufficiently large to justify a withdrawal of the tool from service.

Cutting speed - tool life curves for 0.005-in. wear land are presented in Fig. 17. In these cases localized breakdowns had not started so that the wear was uniform over the entire edge. The curves are thus continuous throughout the speed range of 1150 down to 210 fpm. It is only in this set of curves that the tool life of the ferritic structure can be compared with that of the pearlitic structures at 290 fpm. At this speed 1550 cu in. of the C-3¼ annealed material was removed with one tooth, with a wear of only 0.005 in. This phenomenal tool life was 50 times as much as

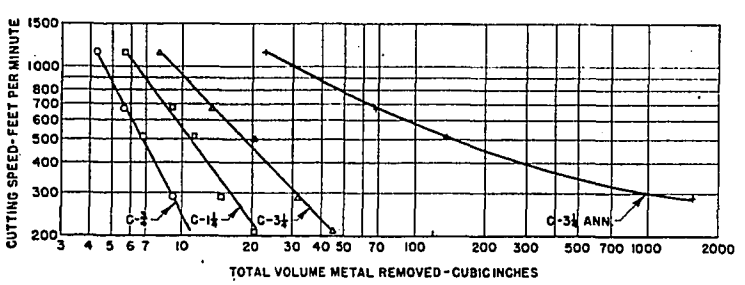

FIG. 17 CUTTING SPEED VERSUS TOTAL VOLUME METAL REMOVED BETWEEN GRINDS FOR 0.005-IN. UNIFORM WEAR LAND

[Cutter: Single tooth, 6 in. radius; (+3, +3, 30, +4). Cut dimensions: 3/16 in. depth, 6 in. width, 0.015 in. feed per tooth.]

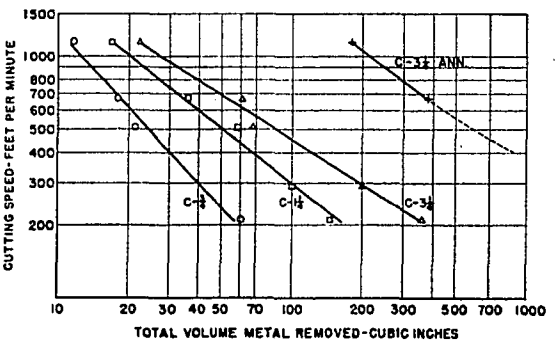

FIG. 16 CUTTING SPEED VERSUS TOTAL VOLUME METAL REMOVED BETWEEN GRINDS FOR 0.015-IN. UNIFORM WEAR LAND

[Cutter: Single tooth, 6 in. radius; (+3, +3, 30, +4). Cut dimensions: 3/16 in. depth, 6 in. width, 0.015 in. feed per tooth.]

that of the C-3¼ analysis. The tremendous improvement in tool life produced by annealing should certainly find applications on many machine or structural parts where the lower physical properties of the graphite-ferrite structure can satisfactorily be employed.

The effect of free-carbide segregations on tool life is shown in Fig. 2 where the cutting speed - tool life curves for 0.030-in. tool wear are presented for the C-309 and C-304B materials. While these analyses are considerably different, as shown in Table 1, their microstructures are much alike and, as previously mentioned, their tool-life curves are remarkably similar. As shown by their photomicrographs, Fig. 4, both structures contain relatively large carbide segregations which may account for the appreciably lower tool life in the normal speed range between 250 and 1000 fpm, as compared with the C-1¼ analysis. These carbides have a Knoop hardness of the order of 1000, while pearlite has a Knoop hardness of only 300 to 400. It is also significant that the cutting speed - tool life characteristics no longer give a straight-line relationship on log-log co-ordinate paper.

The tool life for both the C-309 and the C-304B at 210 fpm was about the same as that of the C-1¼ analysis. An examination of the microstructure revealed that the lamellar spacing and grain size of the pearlite in the C-309, the C-304B, and the C-1¼ analyses were all of the same order of magnitude, Figs. 4 and 9. The presence of free-carbide segregations embedded in a given graphite-pearlite structure does not appreciably alter tool life at 210 fpm, but seriously reduces tool life in the neighborhood of 250

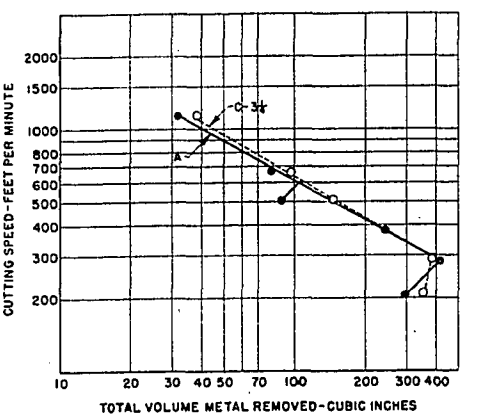

FIG. 18 CUTTING SPEED VERSUS TOTAL VOLUME METAL REMOVED BETWEEN GRINDS FOR 0.030-IN. WEAR LAND

[Casting size: 6½ × 6½ × 20½ for analysis A, 3¼ × 4½ × 20¼ for analysis C-3¼. Cutter: Single tooth, 6 in. radius; (+3, +3, 30, +4). Cut dimensions: 3/16 in. depth, 6 in. width, 0.015 in. feed per tooth.]

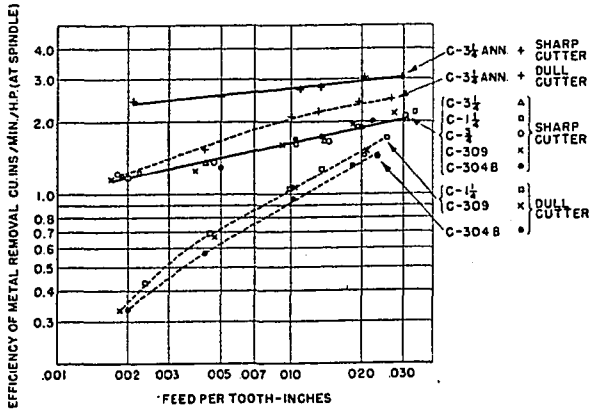

FIG. 19 EFFICIENCY OF METAL REMOVAL VERSUS FEED PER TOOTH
(Cutter: 8 teeth, 9¹/₁₆ in. diam, +3-deg axial rake, +3-deg radial rake, 30-deg corner angle, +4-deg resultant rake; carbide = 44A. Cut dimensions: ³/₁₆ in. depth, 6 in. width; cutting speed = 220 fpm; dull cutter had 0.030-in. wear land on carbide teeth.)

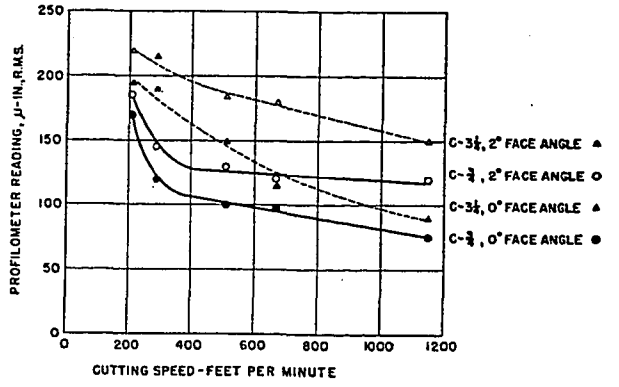

FIG. 20 PROFILOMETER READING VERSUS CUTTING SPEED
[Cutter: Single tooth, 6 in. radius; (+3, +3, 30, +4). Cut dimensions: ³/₁₆ in. depth, 6 in. width, 0.015 in. feed per tooth.]

to 1000 fpm. Furthermore, it appears that the tool life would be the same in the vicinity of 1700 fpm.

An additional confirmation of the dependence of tool life on microstructure can be seen in Fig. 18 where the cutting speed-tool life curves of the C-3¹/₄ and the A analysis are shown. These materials also had almost identical tool-life curves and quite similar microstructures, in spite of their differences in chemical composition and section sizes.

Power Requirements. The power required for milling the various cast irons was determined, using an 8-tooth, 9¹/₁₆-in-diam carbide-tipped solid-body face mill, Fig. 10. The tool angles on the multitooth cutters were the same as that of the single-tooth cutter, i.e., +3 deg axial and radial rake and 30-deg corner angle, giving a +4-deg resultant (or "true") rake. The power at the cutter was measured in terms of the kilowatt input to the motor, the milling machine having been calibrated by means of a Prony-brake test. Cuts were taken 6 in. wide, 0.187 in. deep at a constant cutting speed of 220 fpm, and at feeds per tooth of 0.002 to 0.030 in. The results are shown in Fig. 19 where the "efficiency of metal removal" (in cubic inches per minute per horsepower at the spindle) is plotted against feed per tooth for both sharp and dull cutters. For the sharp-cutter test, the cutter was ground immediately before each run. The dull-cutter tests were made with a cutter in which the carbide teeth had previously been worn to 0.030-in. wear land. All the sharp-cutter curves were straight lines on the log-log co-ordinate paper. The efficiency of metal removal for the C-3¹/₄ annealed test bars varied from 2.4 cu in. per min per hp at 0.002 in. feed per tooth to 3.0 at 0.030 in. feed per tooth. The entire group of the graphite-pearlite analysis, including the C-309 and the C-304B which contained the free carbides, had about the same "efficiency" curves when milled with the sharp cutter, the values increasing from 1.2 at 0.002 in. feed per tooth to 2.1 at 0.030 in. feed per tooth.

The sharpness of the cutter was observed to exert a very great effect on the power requirements. At 0.002 in. feed per tooth, the efficiency for the C-3¹/₄ annealed bars dropped from 2.4 to 1.4 owing to the dulling of the cutter, while at 0.020 in. feed per tooth, the efficiency dropped from 3.0 to 2.3. This means that the dull cutter required 1.8 times as much power per cu in. per minute at 0.002 in. feed per tooth, and 1.3 times as much power at 0.020 in. feed per tooth while milling the ferritic structure.

The drop in efficiency, or the increase in power consumption, due to dulling of the cutter, was even greater with the pearlitic cast irons. Thus at 0.002 in. feed per tooth, the power per cubic inch per minute increased 3 times with the dull cutter.

Two important conclusions can be stated on the subject of power requirements:

(*a*) Graphite-pearlitic cast irons differ little in power consumption for a given cutter under given cutting conditions.

(*b*) The increase in power consumption due to dulling of the cutter may be as much as 3 times at small feeds per tooth, but the increase is much less at high feeds per tooth.

Surface Finish. The surface finish produced on the work was measured with a profilometer at the start and end of each run. In addition, a Faxfilm repliea was made of the surface finish after the first run. In general, the surface finish did not change appreciably as the run progressed. The method of grinding the face-cutting edge had an important bearing on the finish obtained, and in fact, was found to be as influential as the microstructure. All tests were made first with a 2-deg face angle and then with a 0-deg face angle, or flat land 0.040 in. long. In general, the surface finish was better for the fine graphite-pearlite structures. In Fig. 20 is shown the combined effects on profilometer reading of cutting speed, face angle, and microstructure. For all materials the finish improved as the speed was increased. For the C-3¹/₄

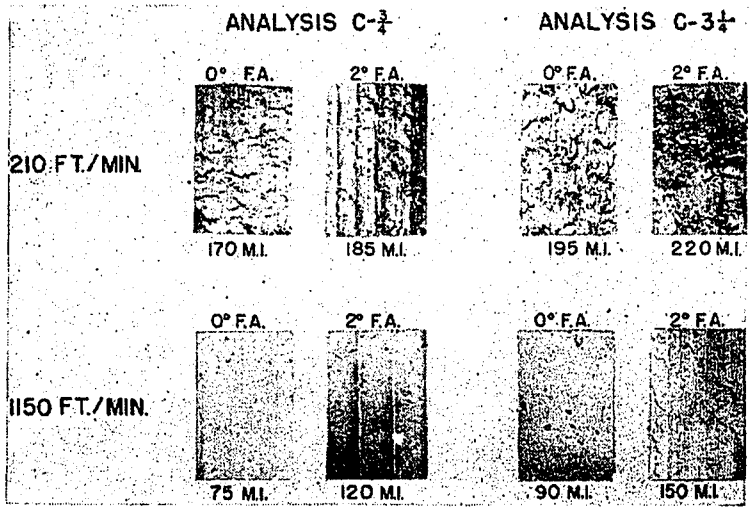

FIG. 21 SURFACE FINISH REPRODUCED FROM FAXFILM REPLICAS
[Cutter: Single tooth, 6 in. radius; (+3, +3, 30, +4). Cut dimensions: ³/₁₆ in. depth, 6 in. width, 0.015 in. feed per tooth; ×23.]

bars milled with a 0-deg-face-angle cutter, the profilometer reading decreased from 195 microinches at 210 fpm to 90 microinches at 1150 fpm. By using the 0-deg face angle, it was possible to obtain almost as good a finish on the C-3¼ bars as on the C-¾ test bars.

Photomicrographs of the Faxfilm replicas are shown in Fig. 21 for the C-¾ and the C-3¼ test bars at 210 and 1150 fpm. These photomicrographs are good reproductions of the actual appearance of the surface finish on the test bars. The similarity in finish on the C-¾ and C-3¼ test blocks for the same cutting speed and face angle is readily observed.

Conclusions

The results of this investigation show that microstructure rather than chemical analysis or physical properties of a cast iron is the major factor governing the tool life in carbide-milling. For each microstructure there exists a characteristic cutting speed versus tool life curve. These curves must be known in order to predict the relative tool life in milling the various cast irons employed commercially. The results thus far have shown that for cast irons containing graphite and pearlite only, the tool life was doubled in going from a fine to a coarse distribution of these microconstituents. The complete graphitization of these structures by annealing resulted in a material containing ferrite and graphite only, which had a tool life as great as 50 times that of the graphite-pearlite structure.

The presence of free carbides in an otherwise normal pearlite-graphite cast iron was shown to have relatively no effect on tool life at a cutting speed of 210 fpm, but seriously reduced the tool life in the range of 250 to 1000 fpm.

The power required for milling at a given rate was found to be the same for all the graphite-pearlite structures, including the ones with the free carbides. The power per cubic inch per minute required for all structures decreased as the feed per tooth increased. The graphite-ferrite structure required one half to two thirds the power per cubic inch for the same feed per tooth. The sharpness of the cutter was found to play an exceedingly important role in power consumption. At small feeds per tooth, for example, 0.002 in., dull cutters required 3 times as much power as sharp cutters, whereas at high feeds per tooth the increase in power was of the order of 1.3.

The surface finish on the work was better for cast irons having the finer graphite distribution. The surface finish improved as the cutting speed increased for all structures. In addition, the surface finish was found to be improved by grinding a flat land in the face-cutting edge of the cutter.

In order to extend the knowledge of the effect of microstructure of cast irons on their machinability, additional work is in progress on irons containing varying amounts of steadite or phosphide eutectic, and martensitic segregation. In addition, various malleable cast irons are to be investigated. The relative machinability of these structures have been correlated into those already studied and the results are presented elsewhere in this issue.[5]

Acknowledgments

The authors wish to express their appreciation for the experimental work done by Messrs. James Solsman, Robert Rizick, Robert Fleming, and Robert Valvano, co-operative students in the Engineering College of the University of Cincinnati. The authors also acknowledge the valuable co-operation of Messrs. Hans Ernst, research director; Herman Ewig, foundry superintendent; William Rengering, assistant foundry superintendent; H. S. Binns, chief metallurgist; M. E. Merchant, research physicist; Norman Zlatin, research engineer; and Miss Jane Alexander, research technician, all of the Cincinnati Milling Machine Company.

[5] See Part II, pp. 675–682.

Discussion

A. O. Schmidt.[6] These careful and well-evaluated tests of the milling of cast iron invite a thorough study. They will provide an answer to many cases of unexplained production troubles in machining castings. The authors have made an especially fine presentation in plotting their data, showing not only the general tool life - cutting speed charts but bringing out the interrelationship of number of passes, volume of metal removed, and other pertinent factors. The graphs can be read with understanding without looking at the text, which in itself is a worthwhile achievement.

The metallurgical analysis of the test pieces should be a guide to many foundrymen, engineers and foremen, who are engaged in the production and subsequent working of cast iron.

Concerning feed per tooth, the authors' findings of a high increase in tool wear with thin chips, accompanied by a subsequent increase in power consumption of as much as 300 per cent, agree with the observations of the writer. In many cases the small feed per tooth used in early experiments with negative rake angles in milling at high speeds often led to erroneous conclusions.

The fact that free-carbide segregations in a graphite-pearlite structure do not appreciably alter tool life at 210 fpm cutting speed but do have a pronounced influence in reducing tool life at cutting speeds above 250 fpm might be attributed to the increased temperature the tool tip will have at the higher cutting speed.

The writer believes that an investigation of tool temperatures would shed further light on the interdependent factors of machinability.

Authors' Closure

The kind remarks of Dr. Schmidt are appreciated. The reduction in tool life due to the presence of free-carbide segregations in cast iron is undoubtedly caused by the inherent abrasiveness of the hard free-carbide constituents within the cast iron. These free-carbide segregations have a Knoop hardness ranging from 1000 to 1300 while the pearlite matrix has a Knoop hardness of the order of 400. The prevention of the extremely hard carbide segregations in cast irons is of course desirable in order to prolong tool life. This can generally be done by the proper selection of analysis for the section size of the casting.

[6] Research Engineer, charge Metal Cutting, Kearney & Trecker Corporation, Milwaukee, Wis.. Mem. A.S.M.E.

Effect of Microstructure on Machinability of Cast Irons—II

By MICHAEL FIELD[1] AND E. E. STANSBURY,[2] CINCINNATI, OHIO

The general investigation of the effect of microstructure on the machinability of cast iron reported in Part I[3] was continued on structures of varying pearlite and graphite size but with the addition of about five per cent of free steadite, the iron-iron phosphide eutectic. Finally, straight malleable iron and one type of pearlitic malleable iron were studied. The straight malleable iron had a structure consisting of ferrite and nodular graphite while the pearlitic malleable structure consisted of recombined carbon, ferrite, and nodular graphite. The tool life, power requirements, and surface finish were determined for these structures, and comparisons are shown with the structures of Part I. By means of these data the expected machinability of a cast iron can be determined by comparing its microstructure with those presented in this and the previous paper.[3]

Introduction

IN THE first report of the present investigation, a general summary of cast-iron metallurgy was given. It was pointed out that the microstructure and the mechanical properties of cast irons could be varied over wide ranges by changes in chemical analysis, melting practice, rate of cooling, and by heat-treatment. Utilizing these characteristics of cast iron, sets of test blocks were prepared each having a different microstructure. The machinability was reported for cast irons of the following microstructures: (1) Alloyed cast irons having different amounts of free carbides. (2) Cast irons of the same chemical analysis, in which the graphite distribution and pearlite fineness were controlled by varying the cooling rate through the use of castings of different section sizes. (There were no free microconstituents in these cast irons other than graphite and pearlite.) (3) Cast iron having a structure of ferrite and graphite in flake form. This was produced by annealing a straight cast iron until all of the pearlite had broken down into graphite and ferrite.

Preparation of Test Blocks

In continuing the general investigation into the machinability of cast irons, it was thought desirable to produce structures of varying pearlite fineness and graphite size as in item (2), but in addition to have a dispersion of steadite, the iron-iron phosphide eutectic, throughout each structure. Accordingly, melts having a base analysis similar to that of the "C" cast iron used previously were prepared using a higher percentage of Southern pig iron in the cupola charge, which increased the amount of phosphorus, thus producing the desired amount of steadite. The melts were treated with calcium silicide as the inoculating agent by the Meehanite process.

TABLE 1 CHEMICAL ANALYSIS AND PHYSICAL PROPERTIES OF CAST IRONS USED IN MILLING TESTS

	Per cent					Ultimate tensile strength,	
Analysis	Total carbon	Si	S	P	Mn	psi	Bhn
E-3¼	3.40	1.85	0.185	0.34	0.74	36000	176
E-1¼	3.36	1.82	0.20	0.31	0.70	36000	197
E-¾	3.38	1.74	0.19	0.35	0.72	36000	197
M	2.50	0.90	0.09	0.12	0.37	54000	113
PM	2.23	0.98	0.100	0.18	0.27	75000	172

Three sets of test blocks of this material were prepared, each set consisting of a sufficient number of bars to allow complete machinability tests to be run. The graphite and pearlite distributions were varied by casting the bars in the three thicknesses that had been previously used, i.e., ¾ in., 1¼ in., and 3¼ in., each bar being 20¼ in. long and 4½ in. wide. The bars were cast into a skin-dried mold with the test-bar cavities lined with a baked-core-sand insert. Previous experience had shown that such an assembly produced the most uniform castings. The metal was poured through a baked strainer core and then grated to five or six mold cavities from a common runner. The castings were then cleaned and machined to a depth of ⅛ in. on all surfaces to produce the final test blocks.

The chemical analysis and physical properties of these three sets of bars are given in Table 1. With the exception of the hardness values, the physical properties refer to those shown by the arbitration bar and represent comparative properties of the materials tested rather than the properties of the actual test blocks. The uniformity of any set of test blocks was checked by taking Brinell hardness readings across each block. Blocks whose average hardness or hardness distribution deviated unduly from the average for the lot were rejected. The hardness values given in Table 1 refer to these averages on the actual test blocks.

Sections were cut from each bar for microexamination as a check on the uniformity of structure from bar to bar in the same lot, and as a means of getting the best average structure for each set of test blocks. Several blocks from each lot were sectioned at the corners, along the edge, on the face, and in the center, to ascertain the degree of uniformity that was being obtained in the various section sizes. The graphite-flake sizes and distributions for the analysis E iron in the three section sizes is shown in Fig. 1. Since the carbon content of the analysis E material was slightly higher than that of the analysis C material, the graphite was coarser for the same section size, being AFA graphite size numbers 3, 4, and 5 for the 3¼-in., 1¼-in., and ¾-in. sections, respectively. Representative etched microstructures for these three section sizes are shown in Fig. 2.

It is to be noted that the interlamellar spacing of the pearlite increases as the section size increases. A comparison of these structures with those in Fig. 9 of part I indicates that the interlamellar spacing of the analysis E cast iron is greater for a given section-size casting than the analysis C material. Thus the pearlite-graphite size in the analysis E-¾-in. bars is comparable to the analysis C-1¼ in., the analysis E-1¼ in. to the analysis C-3¼ in., while the analysis E-3¼-in. bars had a coarser structure than any other material studied. All of the analysis E bars con-

[1] Cincinnati Milling Machine Company, Research Fellow, University of Cincinnati. Jun. A.S.M.E.

[2] Assistant Professor of Metallurgical Engineering, University of Cincinnati.

[3] Part I, pp. 665-674.

Contributed by the Special Research Committee on Metal Cutting and Bibliography and presented at the Annual Meeting, New York, N. Y., December 2-6, 1946, of The American Society of Mechanical Engineers.

E-3/4 E-1 1/4 E-3 1/4

FIG. 1 PHOTOMICROGRAPHS OF GRAPHITE DISTRIBUTION
(Unetched; ×50.)

E-3/4 E-1 1/4 E-3 1/4

FIG. 2 PHOTOMICROGRAPHS OF MICROSTRUCTURE
(Nital etch; ×375.)

tained particles of steadite as a discontinuous network around the grain boundaries. Such a distribution is quite common in iron of this analysis, since the steadite which is the iron-iron phosphide eutectic is the last material to solidify and hence of necessity must be at the grain boundaries. Based upon the analysis of the material and from microstructural examination, it is estimated that 3–5 per cent of steadite was present in these structures.

In part I of this investigation, the results of milling tests on annealed C-3 1/4 analysis were reported. The microstructure of this material consisted of ferrite and graphite in flake form. Since such a structure may be considered a simulated malleable iron, it was thought that additional milling studies on several grades of commercial malleable cast iron would be valuable for comparison. Accordingly, a sufficient number of test blocks of standard malleable iron were procured to allow complete milling tests to be made upon them. These bars were 1 1/4 in. thick, 20 1/4 in. long, and 4 1/2 in. wide. The iron was melted in and cast from a conventional type, pulverized-coal-fired air furnace, and the resulting castings were heat-treated by packing in tightly sealed pots in a pulverized-coal-fired pot oven using a 7-day anneal cycle.

The unetched and etched structures of the standard malleable iron (designated by "M") are shown in Figs. 3 and 4. These photomicrographs show the ferrite grain structure, and the temper carbon (nodular graphite) particles resulting from the decomposition of iron carbide during the annealing cycle. The chemical analysis and physical properties of this material are given in Table 1. Figs. 3 and 4 also show the photomicrographs of the etched and unetched structures of the C-3 1/4 annealed material so that comparisons can be made with the malleable-iron structure.

In order to continue the studies on the milling of all types of cast iron, test blocks of a heat-treated malleable iron were procured. Since the object of this investigation was to correlate the microstructure of the various cast irons with their machinability, the study of a heat-treated malleable iron introduced a material having a different type of graphite distribution and a different matrix. The structure of the material was obtained by reheating the malleabilized iron above the critical temperature, quenching and then drawing to the desired structure and physical properties. This treatment causes recombination of carbon (mostly at the grain boundaries) such that a high-strength tempered structure surrounds and partially fills the grains. The material was supplied in bars 20 1/4 in. long, 4 1/2 in. wide, and 3/4 in. thick; 1/8 in. was machined from all surfaces in order to produce test blocks which could be built up into a composite for the machinability tests. The unetched structure of this material is shown in Fig. 3 (designated "PM"), in which it is to be noted that there is less free

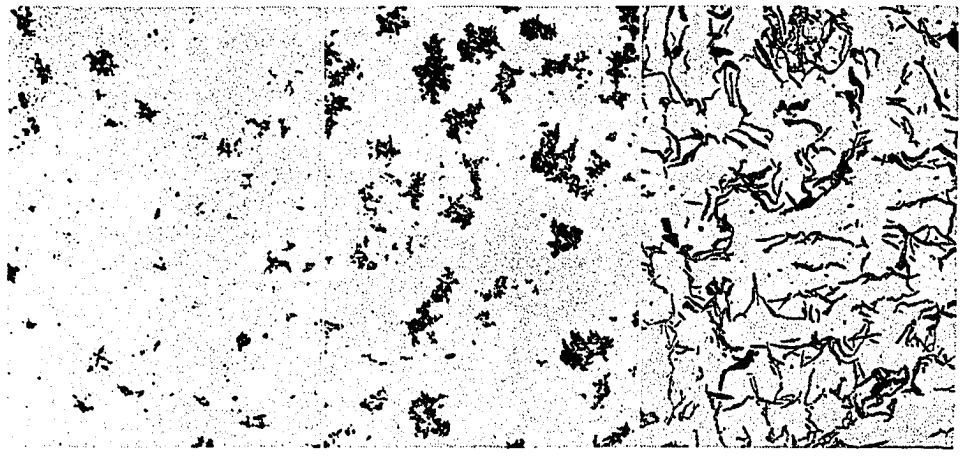

PM M C-3¼ANN

FIG. 3 PHOTOMICROGRAPHS OF GRAPHITE DISTRIBUTION
(Unetched; ×50.)

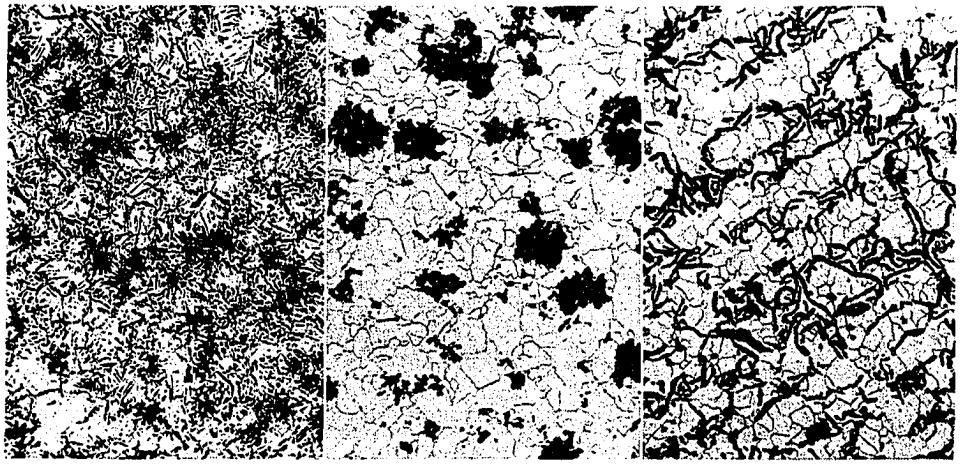

PM M C-3¼ANN

FIG. 4 PHOTOMICROGRAPHS OF MICROSTRUCTURE
(Nital etch; ×50.)

FIG. 5 PHOTOMICROGRAPH OF MICROSTRUCTURE OF PM
(Nital etch; ×375.)

graphite than in any other of the cast irons considered in this investigation. The etched structure at the same magnification is shown in Fig. 4. The dark areas other than the nodular graphite are recombined carbon and the white areas ferrite. The structural details of the etched material may be more clearly seen in Fig. 5, at 375 diam. The chemical analysis and physical properties of the pearlitic malleable are given in Table 1.

Since the cutting process involves the flow of the chip across the face of the tool and the abrasion of the clearance land by the cut surface, it was thought that the hardness values of the individual microconstituents might correlate to some degree with the tool-life results. Accordingly, the hardness of the individual microconstituents were measured with a Tukon microhardness tester. Several hundred readings were taken on the samples and averaged to give the following Knoop hardness values for the indicated microconstituents:

Pearlite	350
Ferrite	200
Graphite	20
Carbide	1000 to 1300
Steadite	880
Recombined carbon areas of pearlitic malleable	425

These values represent the hardness of these constituents at room temperature. Their relative hardness may change considerably at the elevated temperatures present in the cutting process.

TEST CONDITIONS

The cutting tests were conducted under the same conditions

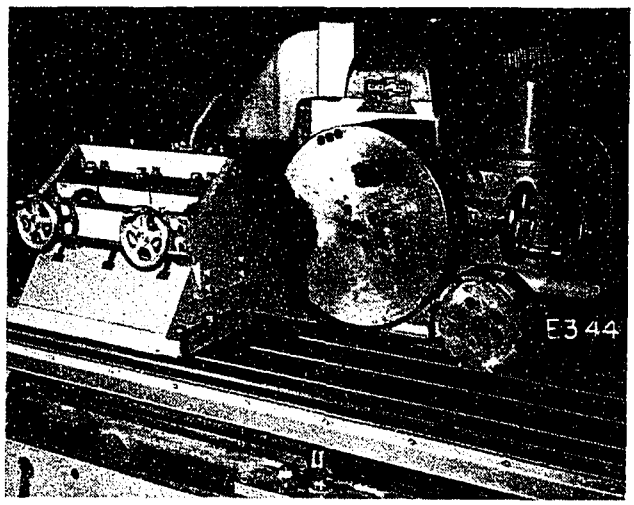

FIG. 6 CINCINNATI 5-60 HYDROMATIC MILLING MACHINE

these three elements is necessary to appraise any milling operation and to calculate the most economical combination of feed and speed.

Tool Life. The tool-life values observed when milling the various irons are plotted in Fig. 7. In this rectangular co-ordinate chart it is seen that at a cutting speed of 1150 fpm all of the materials had a low tool life. The change of tool life with cutting speed is small at the high speeds, but the curves flatten out at the low speeds. The same data are shown on logarithmic paper in Fig. 8 where cutting speed is plotted against total volume of metal removed by one tooth before ultimate dulling. The wear on the clearance land of the tool was uniform for the E-3/4, E-1 1/4, and E-3 1/4 materials over the speed range of 1150 down to 290 fpm. However, at 210 fpm localized failures occurred at one or more points along the carbide cutting edge which resulted in the turning back of the curves at the low speed.

The tool life of the high-phosphorus "E" materials varied with the coarseness of the pearlite-graphite distribution, the coarsest (E-3 1/4) having the highest tool life, and the finest (E-3/4) producing the lowest tool life.

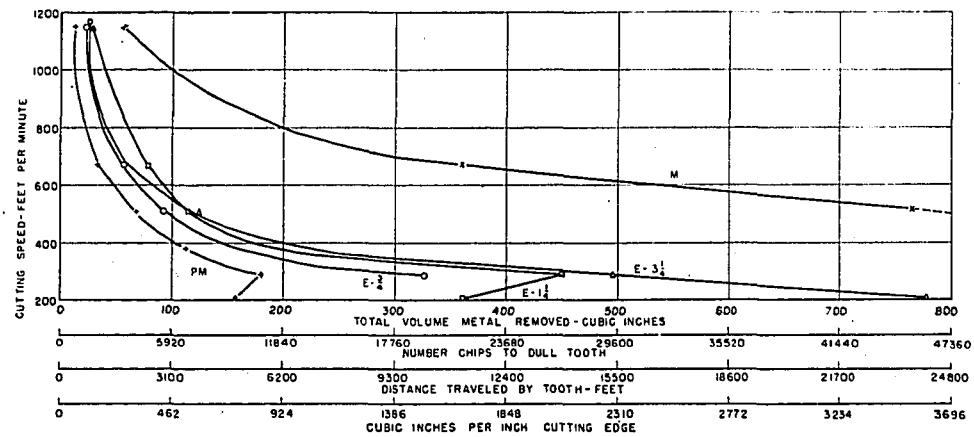

FIG. 7 CUTTING SPEED VERSUS VARIOUS TOOL-LIFE CRITERIA FOR 0.030 IN. TOOL WEAR
(Cutter: +3-deg axial rake, +3-deg radial rake, 30-deg corner angle, +4-deg resultant rake; 3/16-in. depth, 6-in. width; 0.015 in. feed per tooth.)

as described in detail in the previous paper[3] and hence will only be summarized here. The cutting tests were run on a Cincinnati 5-60 Hydromatic milling machine. A single-tooth cutter, held in a 500-lb flywheel at a 6 in. radius, was used for the tool-life and surface-finish tests. The tooth had +3 deg axial and radial rakes, a 3-deg corner angle, and a +4-deg resultant rake, Fig. 6. In all cases the cut was 3/16 in. deep, 6 in. wide, and 20 in. long with the cutter positioned centrally relative to the work. The feed per tooth was 0.015 in. Carboloy 44A was employed as the carbide and was induction-brazed to the steel shank. A 7-deg clearance angle was ground behind all cutting edges. All milling was done dry.

The test bars were stacked and clamped into a fixture to form a test block 4 1/4 in. wide, 20 in. long, and 6 in. high.

The width of the wear land on the clearance of the carbide was measured with a calibrated-eyepiece microscope after each pass. When the width of the uniform wear reached 0.030 in. the tool-life tests were stopped. However, if localized breakdown occurred on the clearance land, the tests were stopped when these grooves reached 0.040–0.050 in. in length, even though the uniform wear remained less than 0.030 in.

MACHINABILITY RESULTS

There are three important elements of machinability, namely, tool life, power requirements, and surface finish. Knowledge of

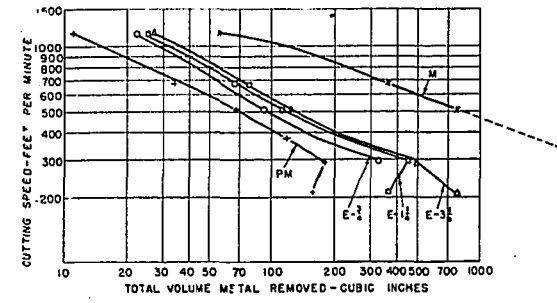

FIG. 8 CUTTING SPEED VERSUS TOTAL VOLUME METAL REMOVED TO DULL TOOTH, FOR 0.030-IN. TOOL WEAR

The pearlitic malleable (curve PM) also exhibited the break in the tool-life curve at the low speed. Hence a speed of 300 fpm appears to be the optimum for this material. The malleable iron (curve M) had such a long tool life that sufficient material was not available to obtain 0.030 in. tool wear at cutting speeds below 510 fpm. In fact 1575 cu in. were removed at 290 fpm to produce a tool wear of only 0.005 in.

The cutting-speed versus actual cutting-time curves to produce 0.030 in. wear on the clearance land are shown in Fig. 9. These curves can be represented by the following equations in the cutting-speed range of 1150 to 300 fpm:

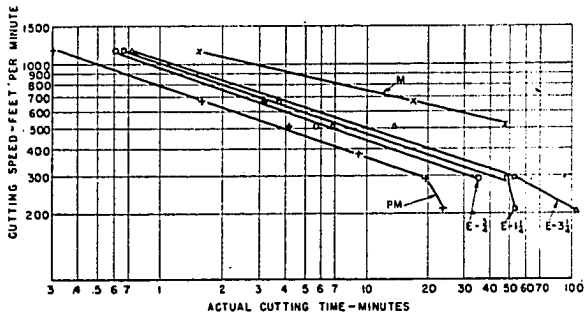

FIG. 9 CUTTING SPEED VERSUS ACTUAL CUTTING TIME, FOR 0.030-IN. TOOL WEAR

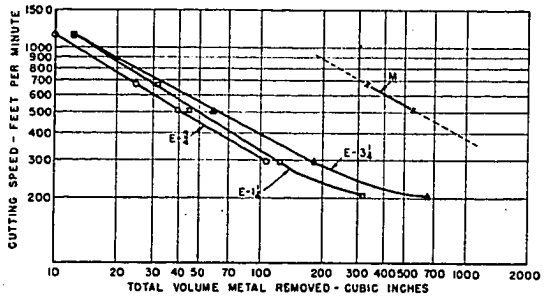

FIG. 10 CUTTING SPEED VERSUS TOTAL VOLUME METAL REMOVED TO DULL TOOTH, FOR 0.015-IN. UNIFORM TOOL WEAR

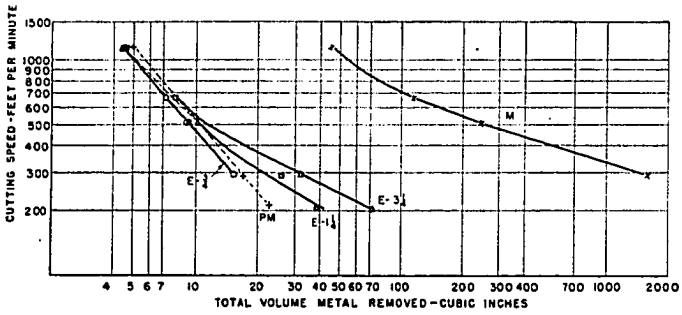

FIG. 11 CUTTING SPEED VERSUS TOTAL VOLUME METAL REMOVED TO DULL TOOTH, FOR 0.005-IN. UNIFORM TOOL WEAR

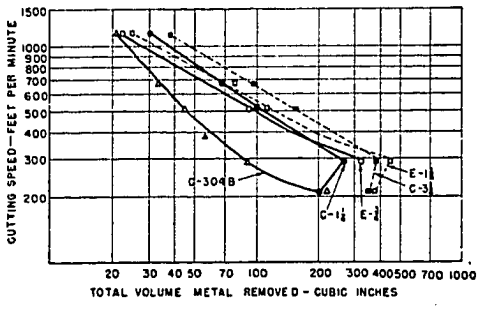

FIG. 12 CUTTING SPEED VERSUS TOTAL VOLUME METAL REMOVED TO DULL TOOTH, FOR 0.030-IN. TOOL WEAR

Material	Equation
PM	$VT^{0.333} = 790$
E-3/4	$VT^{0.342} = 960$
E-1 1/4	$VT^{0.329} = 1000$
E-3 1/4	$VT^{0.314} = 1040$
M	$VT^{0.225} = 1250$

where V = cutting speed, fpm; and T = actual cutting time, min.

A record was kept of the rate of wear on the carbide versus the volume of metal removed. By means of this record the tool life in terms of volume of metal removed could be evaluated for any tool wear. Thus the life curves corresponding to a uniform wear of 0.015 in. on the tool are shown in Fig. 10. The relative order of tool life for the various materials was the same as at 0.030 in. wear. Only two points are plotted for the malleable-iron curve. At lower speeds the tool life was so great that 0.015 in. tool wear could not be reached. At the highest speed of 1150 fpm with this same material, the carbide edge broke down locally before the 0.015-in. uniform wear was obtained. With the pearlitic malleable, the tool also exhibited this same tendency to break down suddenly before a uniform wear of 0.015 in. could be obtained so that no curve is shown for the PM material.

The tool-life curves for 0.005 in. uniform wear are shown in Fig. 11. A uniform wear of 0.005 in. was obtained for all speeds so that the curves are complete for all the materials.

The effect of the presence of steadite on tool life is shown in Fig. 12. Here the E irons of the present series are compared with the C irons discussed in the previous paper.[3] The E-3/4 material had the same pearlite-graphite size as the C-1 1/4, but the E-3/4 had approximately 5 per cent steadite in addition. The presence of the steadite reduced the tool life somewhat at speeds above 350 fpm but at lower speeds the tool life was improved by the presence of steadite. The same tendency is observed in comparing the E-1 1/4 and the C-3 1/4 materials. These two irons also had the same pearlite-graphite size. Again, it is observed that the E-1 1/4 which contained about 5 per cent steadite had a lower tool life than the C-3 1/4 at speeds above 300 fpm but had a longer tool life at the lower speeds.

TABLE 2 RELATIVE TOOL LIFE WITH FREE CARBIDES VERSUS STEADITE[a]

Cutting speed, fpm	Ratio of tool life of C-1 1/4 to C-304B (free carbides)	Ratio of tool life of C-1 1/4 to E-3/4 (steadite)
1000	1.6	1.25
700	2.2	1.21
500	2.4	1.16
300	3.0	0.80

[a] Taken from Fig. 12.
NOTE: Comparison limited to cutting speeds higher than 300 fpm because of erratic results arising from localized breakdown at lower speeds.

The effect of the hard (880 Knoop) steadite is quite different from the effect of the hard (1150 Knoop) free carbide present in the C-304 B material. (This material was discussed in detail in part I[3]). The E-3/4, C-1 1/4, and C-304B materials all had approximately the same pearlite-graphite size, with the E-3/4 containing about 5 per cent steadite and the C-340B containing about 5 per cent free carbide. From Fig. 12 and Table 2 it is seen that the presence of free carbide (curve C-304B) reduced the tool life considerably with respect to a given pearlite-graphite size (curve C-1 1/4) in the speed range of 750 to 300 fpm. On the other hand, the presence of steadite (E-3/4) decreased tool life slightly at 1000 fpm but actually increased tool life at 300 fpm.

The slight decrease in tool life at high speeds and the actual improvement in tool life at lower speeds due to the presence of steadite may possibly be explained as follows: Steadite is the iron-iron phosphide eutectic and hence is the lowest melting constituent present in the iron. The high temperature at the tool point during the milling operation should be sufficient to reduce considerably the hardness of the steadite while cutting. This reduction in hardness may even be so great as to allow the steadite to "smear" over the tool surfaces to some extent during cutting, thus in some cases protecting these surfaces instead of abrading them as the hard carbides do.

In Figs. 13 and 14 tool-life data for the C-3/4, the C-3 1/4 and the C-3 1/4 annealed irons (reported on in part I[3]) are plotted for comparison with the other irons tested in this series. Fig. 13 represents 0.030-in. tool wear, while Fig. 14 is for 0.005-in. wear.

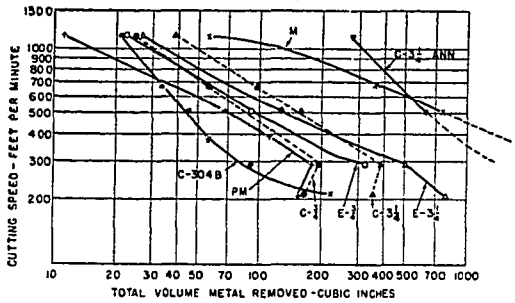

FIG. 13 CUTTING SPEED VERSUS TOTAL VOLUME METAL REMOVED TO DULL TOOTH, FOR 0.030-IN. TOOL WEAR

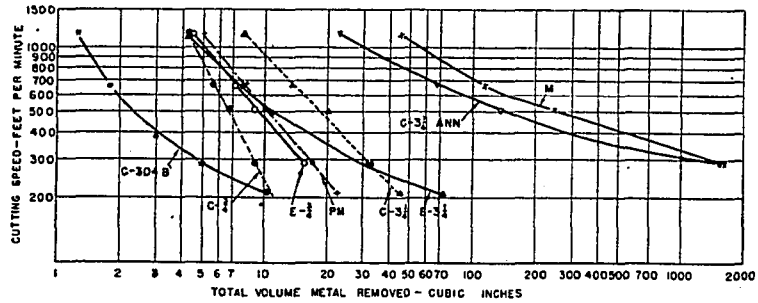

FIG. 14 CUTTING SPEED VERSUS TOTAL VOLUME METAL REMOVED TO DULL TOOTH, FOR 0.005-IN. UNIFORM TOOL WEAR

The C-3¼ annealed and the malleable-iron structures consisted only of free ferrite and free graphite, the difference between the two materials being in the form and amount of the free graphite. The graphite in the C-3¼ annealed was in the form of flakes, while the graphite in the malleable iron was in the form of nodules, see Fig. 3. The tool life for the malleable iron was practically identical with that for the C-3¼ annealed for all speeds, with the exception of the highest speed tested, i.e., 1150 fpm. The tool life for the ferritic structures, curves M and C-3¼ annealed, is seen to be at least 5 times as high as the best of the pearlitic structures at 500 fpm, and 50 times as high at 300 fpm, Fig. 14.

The pearlitic malleable which had a structure consisting of ferrite and recombined carbon with free nodular graphite gave a tool life (based on 0.030-in. tool wear) similar to that of the fine pearlite structure of the C-¾-in. material, Fig. 13. Based on 0.005-in uniform wear, the tool life was similar to the E-¾-in. material, Fig. 14. In all these tool-life comparisons it is important to keep in mind the high physical properties of the malleable irons, see Table 1.

Power Requirements. The E-¾, E-1¼, and the E-3¼ materials, as well as the pearlitic malleable iron required practically the same amount of power to remove metal at a given rate. This is shown in Fig. 15 where efficiency of metal removed in cubic inches per minute per horsepower at the spindle is plotted against feed per tooth for a sharp cutter. The efficiency varied from 1.4 at 0.002 in. feed per tooth to 2.2 at 0.030 in. feed per tooth. This power curve was determined by means of an 8-tooth cutter on the calibrated milling machine shown in Fig. 6. The sharpness of the cutter must be emphasized since it was found that a dull cutter may require as much as 3 times the power used by a sharp cutter. The efficiency curve for malleable iron is also shown in Fig. 15, the values ranging from 1.8 cu in. per min per hp at 0.002 in. feed per tooth to 2.4 cu in. per min per hp at 0.030 in. feed per tooth.

In Fig. 16 is shown a comparison of the power requirements for

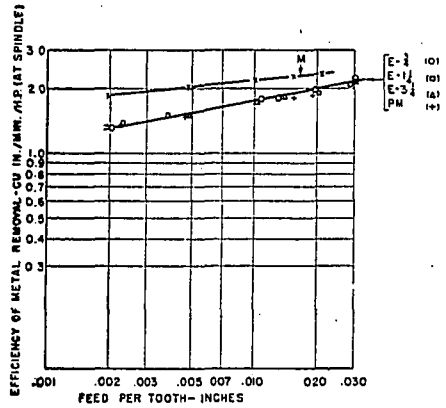

FIG. 15 EFFICIENCY OF METAL REMOVAL VERSUS FEED PER TOOTH FOR SHARP CUTTER

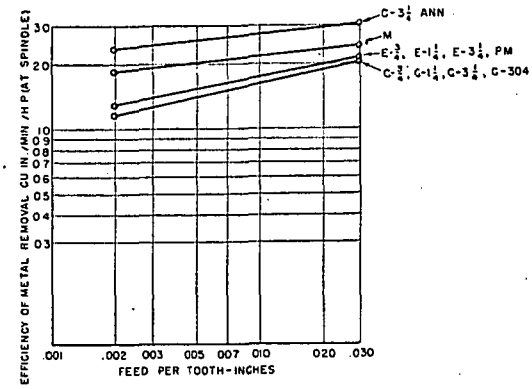

FIG. 16 EFFICIENCY OF METAL REMOVAL VERSUS FEED PER TOOTH FOR SHARP CUTTER

(Cutter: 8 teeth, 9 1/16 in. diam, +3-deg axial rake, +3-deg radial rake, 30-deg corner angle, +4-deg resultant rake; carbide: 44a. Cut dimensions: 3/16 in. depth, 6 in. width; cutting speed = 220 fpm.)

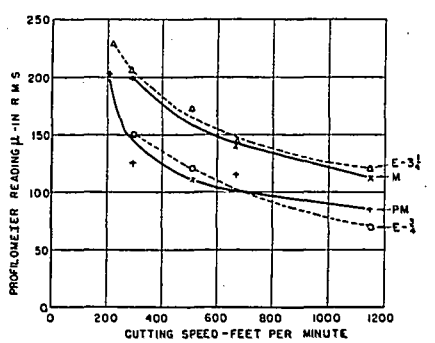

FIG. 17 PROFILOMETER READING VERSUS CUTTING SPEED

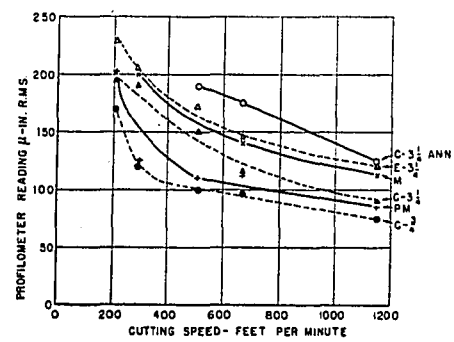

FIG. 18 PROFILOMETER READING VERSUS CUTTING SPEED

all the structures tested to date (for sharp cutters). The lowest curve is for the pearlite-graphite structures and the pearlite-graphite plus 5 per cent free-carbide structure. The next higher curve is for the pearlitic malleable iron as well as the pearlite-graphite plus 5 per cent steadite. The highest efficiency was obtained for the C-3¼ annealed iron which had a ferrite-graphite structure. The malleable iron which also had a ferrite-graphite structure had an efficiency lower than the C-3¼ annealed. The higher power requirements of the malleable iron over the C-3¼ annealed is attributed to the fact that the former material contained less free graphite, see Fig. 3.

Surface Finish. The surface finish for the E-¾, E-3¼, pearlitic malleable and malleable irons is shown in Fig. 17, where profilometer reading is plotted against cutting speed. These data are taken from the single-tooth cutting tests, using a tooth having a flat land on the face-cutting edge that was 2 to 3 times the feed per tooth. The pearlitic malleable produced a surface finish similar to the E-¾ structure, while the malleable iron and the E-3¼ surface-finish curves were likewise similar. The surface finish versus cutting-speed curves of all the representative structures are shown in Fig. 18. In general, it was observed that the surface finish was a function of the amount of free graphite present, the greater the amount of free graphite, the poorer the surface finish, see Figs. 1 and 3.

Breakout. In milling all the cast irons, the edge of the test block was broken away where the tooth left the work. For the 30-deg-corner-angle cutter feeding at 0.015 in. feed per tooth this breakout was of the order of 0.015 in. to 0.030 in., depending mainly upon the sharpness of the cutter. However, the malleable and the pearlitic malleable irons being more ductile exhibited no such breakout on the trailing edge of the test block, but on the contrary produced a small burr.

Correlation of Machinability With Physical Properties

It is not feasible to attempt to correlate machinability with tensile strength of cast iron since the tensile strength is only available from arbitration bars, whereas the tensile strength of the actual casting is rarely known.

The hardness, however, is readily determined for most castings and hence a possible correlation was investigated between tool life and Brinell hardness. It was found that a trend could be obtained between hardness and tool life if only the uniform wear on the tool is considered, i.e., if all test points are omitted for which the tool failed by localized breakdown. Thus Fig. 19 shows the Brinell hardness plotted against volume of metal removed to produce 0.030-in. uniform wear along the carbide clearance land.

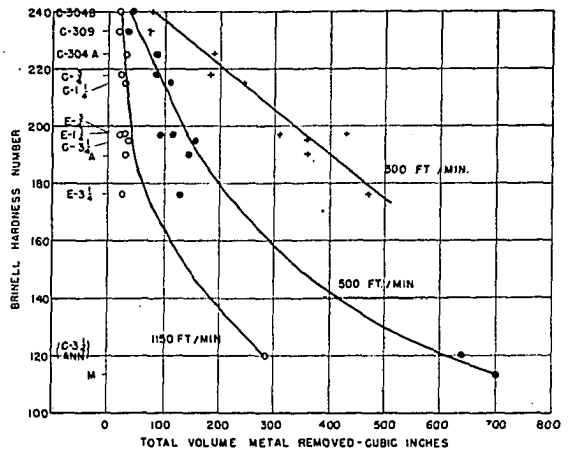

Fig. 19 Brinell Hardness Number Versus Total Volume Metal Removed, for 0.030-In. Tool Wear

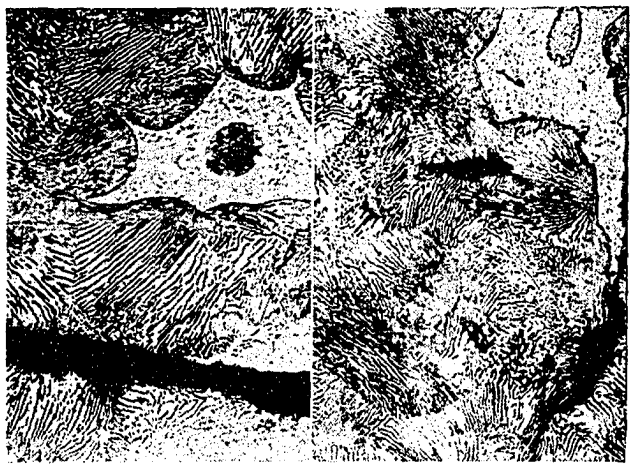

(*a*) (*b*)

Fig. 20 Photomicrographs Showing Microstructure of Analysis E-3¼

(*a*, Specimen taken from test block; *b*, chip from cut at 210 fpm; nital etch, ×375.)

The Brinell hardness of each material is indicated. It is seen that at 1150 fpm all the materials from 240 to 175 Bhn had practically the same tool-life values. At 500 fpm the change in the tool life was again small over this same hardness range. However, at 300 fpm it is observed that there is a general increase of tool life with decrease of Brinell hardness, the relation being approximately linear in the region of 175 to 240 Bhn and can be represented by the following equation

$$H + 0.78\,V = 250$$

where H = Brinell hardness number

V = Total volume of metal removed to produce 0.030-in. uniform wear on a carbide tooth at 300 fpm

This equation is intended to represent the behavior only of pearlite-graphite cast irons having a hardness range of 175 to 240 Bhn and being machined at a speed of 300 fpm. The hardness value used in the foregoing equation must be the average hardness of many readings taken over the entire surface of the casting that is to be milled.

The fact that a useful correlation between Brinell hardness and tool life was found only for a 300-fpm cutting speed confirms the conclusion presented in part I[3] of this investigation that Brinell hardness is an inadequate criterion of machinability.

Conclusions of Correlation of Microstructure With Machinability of Cast Iron

From the results of the investigations reported here and in part I, it is concluded that the microstructure of cast iron is the most reliable criterion of the three salient phases of machinability, tool life, power requirements, and surface finish. It has been shown that (1) the tool life increases as the pearlite-graphite distribution becomes coarser; (2) that the presence of approximately 5 per cent free carbide in a given pearlite-graphite distribution decreases tool life considerably; (3) that the presence of approximately 5 per cent steadite in a given pearlite-graphite distribution decreases tool life slightly at high speeds but increases tool life at low speeds; (4) that the ferrite-graphite structure improves tool life as much as 50 times over the pearlite-graphite structure at low speeds; and (5) that the form of the free graphite has no appreciable effect on tool life.

The power required to mill cast iron at a given rate of metal removal is found to be practically the same for all the pearlite-

graphite structures including the ones which contain 5 per cent free carbide or 5 per cent steadite. The ferrite-graphite structure requires less power for a given rate of metal removal than the pealitic-graphite structures. Furthermore, the power is less for the ferrite-graphite structures containing the greater amount of free graphite.

The surface finish is directly associated with the amount of free graphite present in the structure, the materials with the least amount of free graphite producing the best surface finish.

Therefore the expected machinability of a cast iron can be determined semiquantitatively by comparing its structure with those presented in this and the previous paper.[3] The tool life, power requirements, and surface finish can then be estimated from the curves corresponding to the structure involved.

The structure of the actual workpiece rather than the arbitration bar must be obtained. A sample can be cut out of the workpiece by means of a hollow mill or hacksaw and examined under the microscope. In fact the structure of the workpiece can be reliably judged from a milling chip which has been mounted in lucite or Bakelite, for it has been found that the structure of the body of the chip is not appreciably distorted in the milling of cast iron (this is not true for the milling of wrought steels). Fig. 20, for example, shows the marked similarity between the structure of the workpiece and that of the chip, the latter having been taken from a cut at 210 fpm.

This paper concludes the formal study of the effect of microstructure on the machinability. It is realized of course that other structures exist in cast irons that were not investigated here.

However, an attempt was made to cover all of the common constituents of cast irons so as to obtain an understanding of their effects on machinability.

Acknowledgments

The authors wish to thank the Dayton Malleable Iron Company, Dayton, Ohio, and the Link Belt Company, Indianapolis, Ind., for furnishing, respectively, the malleable iron and the pearlitic malleable iron used in this investigation. The authors express their appreciation to Mr. James Solsman and Mr. James Gailey, co-operative students at the University of Cincinnati. Furthermore, the authors gratefully acknowledge the aid and co-operation of Mr. Hans Ernst, research director; Dr. M. E. Merchant, research physicist, and Miss Joan Scheffel, research technician, all of the Cincinnati Milling Machine Company.

Acknowledgements

The writer wishes to acknowledge the aid and guidance rendered by Dr. H. J. Kersten, Dr. D. A. Wells, and other members of the University of Cincinnati Faculty; Dr. E. E. Stansbury now of the University of Tennessee; Mr. Hans Arhst, Dr. M. E. Merchant, Mr. N. Zlatin, Mrs. E. A. Startsman, Mrs. B. Martin and others of the Research Department of the Cincinnati Milling Machine Co.. Finally the writer wishes to express his gratitude to the Cincinnati Milling Machine Co. whose generous support made this work possible.

REFERENCES

1. H. Tresca; Bulletin de la Société d'Encouragement pour l'Industrie Nationale, 1873.

2. I. Thime; Mémoires sur le Rabotage des Métaux, St. Petersburg, Russia, 1877.

3. A. Haussner; Mitteilungen des k. k. technologischen Geiwerbemuseums in Wien II. Jahrg, 1892 Heft 4, 5, 6. pp. 117-119.

4. G. Sellergren; Zeitschrift des Oesterr, Ingenieur und Architekten Vereins, vol. 48, no. 32, 1896.

5. F. W. Taylor; "On the Art of Cutting Metals", A.S.M.E., 1906.

6. E. G. Coker; Proc. I. M.E., March 1925, pp. 357-382.

7. W. Rosenhain and A. Sturney; Proc. I. M.E., Jan. 1925, pp. 141-174.

8. E.G. Herbert; Trans. A.S.M.E., vol. 48, 1926, pp 705-748.

9. M. Kronenberg; "Grundzuge der Zerspanungslehre", Julius Springer, Berlin, 1927.

10. M. Kronenberg; Trans. A.S.M. vol. 28, No. 3, 1940 p. 277.

11. M. Okoshi; Scientific Papers of the Institute of Physical and Chemical Research, vol. 14, no. 272, 1930, pp 193-225.

12. J. Rathje; "Uber den Schnittvorgang im Sande", Doctor's Thesis, Hanover, Germany, 1931.

13. M. Okoshi and S. Fukui; Scientific Papers of the Institute of Physical and Chemical Research, vol. 22, no. 455, 1933, pp. 97-166.

14. A. Raupp; "Chip Formation of Metals", Doctor's Thesis, Hanover, Germany, 1937.

15. F. Schwerd; Zeitschrift V.D.I. 76, 1932, Heft 52 pp 1257-1265; also Zeitschrift V.D.I. 77, 1933, Heft 9, pp 211-216.

16. H. Ernst and M. Martellotti; Mech Engr., vol. 57, no. 8, Aug., 1935, pp. 487-498.

17. H. Ernst; "Machining of Metals", A.S.M; 1938 pp. 1-34.

18. M. E. Merchant; Jour App. Phy., vol. 11, no. 3, 1940, p. 230.

19. H. Ernst and M. E. Merchant, Proc. Special Summer Conference on Friction and Surface Finish, M.I.T., Cambridge, Mass. June 1940, pp. 76-101.

20. V. Piispanen; Teknillinen Aikakauslehti, no. 9, 1937, pp. 315-322.

21. M. E. Merchant; Jour App. Mech; Sept., 1944, pp. A168-A175.

22. M. E. Merchant; Jour App. Phy., vol. 16, no. 5, 1945, pp. 267-275.

23. M.E. Merchant; Jour App. Phy., vol. 16, no. 6, 1945, pp. 318-324.

24. M. E. Merchant and N. Zlatin; Experimental Stress Analysis vol. 3, no. 2, 1946.

25. P. W. Bridgman; Jour App. Phy. vol. 8, no. 5, 1937 pp. 328-336 also Rev. Modern Phy. vol. 17, no. 1, 1945, pp. 3-14.

26. P. W. Bridgman; Jour App. Phy. vol. 14, 1943 pp 273-283.

27. J. Keminy; "Torsion Compression Testing" Univ. of Cinti. Thesis, 1937.

28. N. Zlatin and M. E. Merchant; Trans ASME., 1947 (Annual Bound Volume).

29. H. C. Vacher; Jour. of Research, National Bureau of Standards, vol. 29, 1942, pp. 177-181.

30. L. Thomassen and D.M. McCutchen; Mech. Engr., vol. 56, no. 3, 1934, pp. 155-157.

31. F. Zankl, A.G. Barkow and A.O. Schmidt; Trans. A.S.M.E., vol. 69, 1937, pp. 307-317.

32. J. Wulff; Proc. Special Summer Conference on Friction and Surface Finish, M.I.T., Cambridge, Mass. June, 1940, pp. 17-20.

33. W.A. Wood; Proc. Royal Society, London, vol. A172, 1939, pp. 231-241.

34. J. O. Almen; S.A.E. Journal (Trans.) vol. 51, no. 7, pp. 249-268.

35. J. T. Norton and B.M. Loring; Welding Jour. Research Supplement, June, 1941.

36. W.T. Sproull; "X-Rays in Practice", McGraw Hill, 1946, p. 450.

37. N. P. Goss; Trans. A.S.M., vol. 23, 1935, p. 511.

38. J. L. Snoek; Z. Metallkunde, vol. 30, 1938, p. 94.

39. M. Kronenberg; Mech. Engr., vol. 65, 1943, pp. 901-904.

40. "Electropolishing Stainless Steels"; Rustless Iron and Steel Co., Baltimore, Md.

41. F. Gisen; Tech. Mitt. Krupp, Forch. Berlin, appendix 1939, pp. 35-40.

42. C.S. Barrett; "Structure of Metals"; McGraw Hill, 1943, p. 270.

43. D. E. Thomas; Jour. Sci. Inst. vol. 18, 1941, pp. 135-138.

44. G. Sachs, et. al. Welding Journal, vol. 25, 1946, pp. 405-412.

45. E. W. Milburn; Metal Treatment, vol. 12, Winter 1946, pp. 259-260.

46. M. Field; Rev. Sci. Inst. vol. 18, no. 6, 1947, pp. 451-453.

47. H. Friedman, Electronics, vol. 18, 1945, pp. 132-137.

48. F. Wever,-Trans. AIME, vol. 93, 1931, pp. 51-77.

49. C.S. Barrett; Trans. AIME, vol. 124, 1937, pp. 29-58.

50. M. Gensamer and R.F. Mehl; Trans. AIME, vol. 120, 1936, pp. 277-292.

51. B. F. Decker; Proc. ASTM, vol. 43, 1943, pp. 785-802.

52. J. K. Wood, Jr.; Trans. ASM, vol. 139, pp. 725-740.

53. B. F. Decker; E. T. Asp and D. Harker; "Preferred Orientation Determination Using a Geiger Counter X-Ray Diffraction Goniometer." Presented at the Summer, 1947 Meeting of the American Society for X-Ray and Electronic Diffraction, (unpublished).